

**THE EFFECT OF HUMAN GLUCOSYLCERAMIDASE  
ON SPHINGOLIPID LEVEL IN CELLS**



**Peeranat Jatoorathawichot**

**A thesis submitted in Partial Fulfillment of the Requirement for the  
Degree of Master of Science in Biochemistry**

**Suranaree University of Technology**

**Academic Years 2019**

การศึกษาผลจากกฏโคซิมิเดสของมนุษย์  
ต่อระดับของสฟิงโกลิพิดในเซลล์



นายพีระณัฐ จาตุรัตน์ทวิโชติ

วิทยานิพนธ์นี้เป็นส่วนหนึ่งของการศึกษาตามหลักสูตรปริญญาวิทยาศาสตรมหาบัณฑิต  
สาขาวิชาชีวเคมี  
มหาวิทยาลัยเทคโนโลยีสุรนารี  
ปีการศึกษา 2562

**THE EFFECT OF HUMAN GLUCOSYLCERAMIDASE  
ON SPHINGOLIPID LEVEL IN CELLS**

Suranaree University of Technology has approved this thesis submitted in partial fulfillment of the requirements for the Master's Degree.

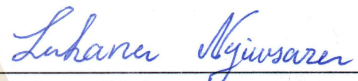
Thesis Examining committee

  
\_\_\_\_\_  
(Dr. Sakesit Chamnarnsilpa)

Chairperson

  
\_\_\_\_\_  
(Prof. Dr. James R. Ketudat-Cairns)

Member (Thesis Advisor)

  
\_\_\_\_\_  
(Dr. Lukana Ngiwsara)

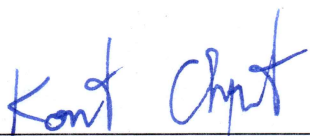
Member

  
\_\_\_\_\_  
(Asst. Prof. Dr. Chutima Talabnin)

Member

  
\_\_\_\_\_  
(Asst. Prof. Dr. Krajang Talabnin)

Member

  
\_\_\_\_\_  
(Assoc. Prof. Flt Lt Dr. Kontorn Chamniprasart)

Vice Rector for Academic Affairs  
and Internationalization

  
\_\_\_\_\_  
(Assoc. Prof. Dr. Worawat Meevasana)

Dean of Institute of Science

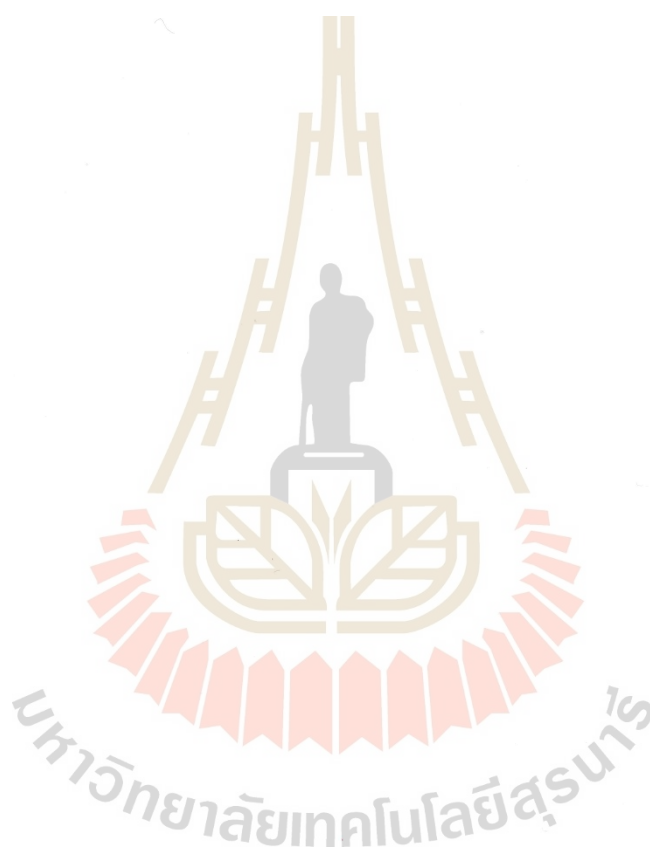
พีระณัฐ จาคูรัตน์ทวีโชติ : ผลของกลูโคซิลเซรามิเดสของมนุษย์ต่อระดับของสฟิงโก

ลิพิดในเซลล์ (THE EFFECT OF HUMAN GLUCOSYLCERAMIDASE ON

SPHINGOLIPID LEVEL IN CELLS). อาจารย์ที่ปรึกษา : ศาสตราจารย์ ดร.เจมส์ เกตุทัต-  
คาร์นส์, 154 หน้า.

กลูโคซิลเซราไมด์เป็นสารตั้งต้นในการผลิตแกงลิโอไซด์และเป็นส่วนประกอบสำคัญของเยื่อหุ้มเซลล์ ซึ่งสามารถสร้างและสลายได้อย่างต่อเนื่องในไกลโคสฟิงโกลิพิดเมตาบอลิซึม การสลายของกลูโคซิลเซราไมด์เกี่ยวข้องกับเอนไซม์ 2 ชนิด ประกอบด้วย lysosomal acid  $\beta$ -glucosidase/ $\beta$ -glucosylceramidase (GBA) และ nonlysosomal  $\beta$ -glucosidase/ $\beta$ -glucosylceramidase2 (GBA2) ความบกพร่องของเอนไซม์ GBA และ GBA2 มีผลต่อกระบวนการไกลโคสฟิงโกลิพิดเมตาบอลิซึม ซึ่งส่งผลให้เกิดโรคที่เกี่ยวข้องกับระบบประสาท ในการศึกษาี้ ผู้วิจัยแบ่งการศึกษาออกเป็น 2 ส่วนเพื่อทำการศึกษาผลของ GBA และ GBA2 ต่อระดับของสฟิงโกลิพิดภายในเซลล์ โดยเริ่มต้นทำการศึกษา GBA2 isoforms ที่มีผลกระทบต่อระดับของไกลโคสฟิงโกลิพิดใน COS-7 cells โดย 9 human GBA2 isoforms ถูกทำให้แสดงออกใน COS-7 cells จากนั้นยืนยันการแสดงออกด้วยวิธี quantitative real time-PCR และ western blotting จากนั้นตรวจสอบการทำงานของเอนไซม์โดยใช้ 4-methylumbelliferyl- $\beta$ -D-glucopyranoside (4MUG) พบว่า human GBA2 isoform 1 มีการทำงานของเอนไซม์สูงในขณะที่ isoforms อื่นๆมีการทำงานของเอนไซม์ไม่แตกต่างจากชุดควบคุม empty vector Conduiritol  $\beta$ -epoxide (CBE) ถูกใช้สำหรับยับยั้งทำงานของ GBA เพื่อยืนยันว่าการทำงานของเอนไซม์ส่วนใหญ่มาจาก GBA2 isoform 1 การศึกษาระดับของสฟิงโกลิพิดโดยใช้ shotgun direct infusion mass spectrometry ผลการทดลองแสดงให้เห็นว่าการแสดงออกของ GBA2 isoform 1 ส่งผลให้ระดับของ เซราไมด์สูงขึ้นและระดับของเฮกโซซิลเซราไมด์ลดลง จากนั้นเมื่อทำการเปรียบเทียบอัตราส่วนระหว่างกลูโคซิลเซราไมด์ที่เกี่ยวข้องกับระดับของเซราไมด์แสดงให้เห็นว่า GBA2 isoform 1 สามารถย่อยเฮกโซซิลเซราไมด์เป็นเซราไมด์ที่มีจำนวนคาร์บอนดังนี้ 34:1, 40:1, 42:1 และ 42:2 ซึ่งสนับสนุนว่าจำนวนคาร์บอนดังกล่าวเป็นมีความจำเพาะต่อการทำงานของ GBA2 ซึ่งจากการทดลองพบว่ามีเพียง GBA2 isoform 1 มีผลต่อระดับไกลโคสฟิงโกลิพิดในเซลล์ ส่งผลให้ความบกพร่องของ GBA2 isoform 1 อาจมีความเกี่ยวข้องกับโรคทางระบบประสาท ส่วนที่สองเพื่อศึกษาผลจากการกลายพันธุ์ของยีน heterozygous *GBA* และ *Parkin* ต่อระดับสฟิงโกลิพิดในเซลล์ไฟ

โอบรบลาสต์ของปวยพาร์กินสัน โดยเซลล์ไฟโอบรบลาสต์ที่มีการกลายของยีน *Parkin* และ *GBA* ถูกเลี้ยงในรูปแบบเซลล์ปฐมภูมิจากนั้นทดสอบการทำงานของเอนไซม์  $\beta$ -glucosidase และวิเคราะห์ระดับของสฟิงโกลิพิดด้วยวิธี shotgun direct infusion mass spectrometry ผลการศึกษาพบว่า *GBA* (1309delG) มีผลต่อระดับของสฟิงโกลิพิดในขณะที่การกลายของยีน *Parkin* แสดงผลที่ไม่ชัดเจนต่อระดับของสฟิงโกลิพิดในเซลล์ไฟโอบรบลาสต์ อย่างไรก็ตามการศึกษานี้มีอุปสรรคเนื่องด้วยจำนวนตัวอย่างไม่เพียงพอซึ่งส่งผลต่อการวิเคราะห์ทางสถิติและการสรุปผล



สาขาวิชาเคมี

ปีการศึกษา 2562

ลายมือชื่อนักศึกษา พริษฐ์ จาตุรงค์ไชยกุล

ลายมือชื่ออาจารย์ที่ปรึกษา James R. McG

PEERANAT JATOORATHAWEECHOT : THE EFFECT OF HUMAN  
GLUCOSYLCERAMIDASE ON SPHINGOLIPID LEVEL IN CELLS.

THESIS ADVISOR : PROF. JAMES R. KETUDAT-CAIRNS, Ph.D. 154 PP.

GLYCOSIDE HYDROLASE/GLYCOSPHINGOLIPID/GLUCOSYLCERAMIDE/  
GLUCOCEREBROSIDASE/SPLICING ISOFORMS

The membrane lipid glucosylceramide (GlcCer) is the precursor of gangliosides and is a major membrane lipid itself. It is continuously formed and degraded in glycosphingolipid metabolism. GlcCer degradation is mainly carried out by 2 enzymes, lysosomal acid  $\beta$ -glucosidase/ $\beta$ -glucosylceramidase (GBA) and nonlysosomal  $\beta$ -glucosidase/ $\beta$ -glucosylceramidase2 (GBA2). Deficiencies of GBA and GBA2 affect glycosphingolipid metabolism, resulting in neurological diseases. In this thesis, we performed two experimental parts in order to studies the effect of GBA and GBA2 on sphingolipid level in cells.

Firstly, in order to understand which GBA2 isoforms are active and how they affect glycosphingolipid levels in cells, nine human GBA2 isoforms were expressed in COS-7 cells. Expression of GBA2 isoforms were determined by quantitative RT-PCR, western blotting, and  $\beta$ -glucosidase activity assay. The human GBA2 isoform 1 showed high activity, while the other isoforms had activity similar to that in cells carrying the empty expression vector. The GBA inhibitor conduritol  $\beta$ -epoxide (CBE) was used minimize the GBA activity as well as to confirm that the activity came primarily from GBA2 isoform 1 overexpression. Sphingolipid levels were determined by shotgun direct infusion mass spectrometry. The result showed that overexpression of GBA2 isoform 1 increased ceramide but decreased hexosylceramide levels, while onther isoforms shown sphingolipid level same

as the empty vector control. Comparison of ratios of glucosylceramides to the corresponding ceramides in the extracts indicated that GBA2 isoform 1 hydrolyzes hexosylceramides with ceramide species 34:1, 40:1, 42:1 and 42:2, suggesting broad specificity for the lipid component. Therefore, among the possible human GBA2 isoforms, only isoform1 affects glycosphingolipid levels, which may be related to neurological diseases.

Secondly, we investigated whether heterozygous *GBA* mutations found in Parkinson's disease (PD) patients cause any decreases in activity or affect the sphingolipid levels in human fibroblasts. Fibroblasts from PD patients with *Parkin* mutations were tested for enzyme activity and sphingolipid level. Human fibroblasts carrying *GBA* and *Parkin* mutations were grown as primary cell lines, followed by assaying  $\beta$ -glucosidase activity and analyzing lipid profiles by shotgun direct infusion mass spectrometry. The study revealed a range of sphingolipid profiles in control and mutant human fibroblasts, and the small number of samples prevented clear conclusions as to the effects of the mutation classes. However, GBA (1309delG) was identified to have the highest glucosylceramide accumulation in the cell, while the *Parkin* mutations showed no clear affect on sphingolipid levels in fibroblasts.

School of Chemistry

Academic Year 2019

Student's signature จิระกวี นพวิฑิตวิฑิต

Advisor's signature James R. McO

## ACKNOWLEDGEMENTS

I would like to express my sincere gratitude to my thesis advisor, Prof. Dr. Jame R. Ketudat-Cairns, for providing me the opportunity to study toward my master's degree in Biochemistry, kind supervision, valuable advice and enthusiastic encouragement.

I am very grateful to Asst. Prof. Dr. Chutima Talabnin for guidance, supporting and providing knowledge on the experiment. I express my great appreciation to Dr. Lukana Ngiwsara for her encouragement, valuable suggestions, and criticism of the research. This thesis could never be done without both of them.

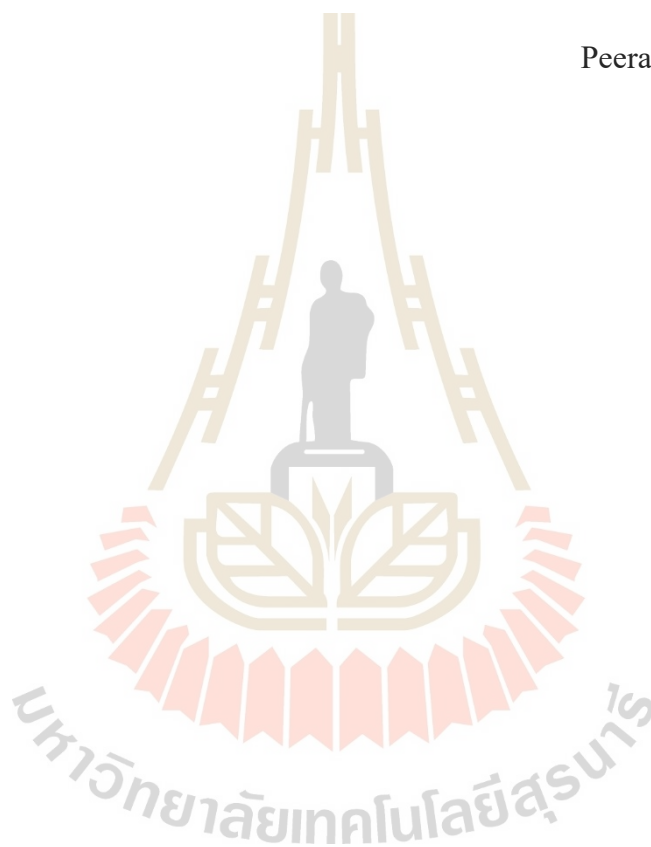
I would like to thank Prof. Gavin E. Reid for allowing me to work on mass spectroscopy and utilize the fascinating facilities in his laboratory. I would like to thank his Postdoc Dr. Vinzenz Hofferek and his PhD Students Mr Yepy Hardi Rustam, who support me for the experimental design and guidance for the programming skills so that the work can be finished sooner.

I sincerely thank to Dr. Sakesit Chumnarnsilpa for his encouragement and constructive idea. I am thank my lab members, colleagues and staff in the School of Chemistry, Suranee University of Technology for their help.

I would like to thank the Development and Promotion of Science and Technology Talents Project (DPST) for funding and opportunity.

Finally, I would like to express my deepest gratitude to my family for their love, care, support, and encouraging me and cheering me up with their best wish.

Peeranat Jatoorathawichot



# CONTENTS

	<b>Page</b>
ABSTRACT IN THAI.....	I
ABSTRACT IN ENGLISH.....	III
ACKNOWLEDGEMENT .....	V
CONTENTS .....	VII
LIST OF TABLES.....	XI
LIST OF FIGURES.....	XII
LIST OF ABBREVIATIONS .....	XVIII
<b>CHAPTER</b>	
<b>I INTRODUCTION.....</b>	<b>1</b>
1.1 General introduction.....	1
1.2 Research objective.....	4
<b>II LITERATURE REVIEW.....</b>	<b>4</b>
2.1 Lipidomics for studying metabolism.....	5
2.2 Lipid classification structures and tools.....	7
2.3 Glycolipid roles in membrane function and cellular processes.....	11
2.4 Sphingolipid synthesis and function in cellular process.....	15
2.5 Glycoside hydrolase ith GBA and GBA2.....	25
2.6 Involment of GBA and GBA2 deficiocy in human diseases.....	30
2.7 Alternative splicing and GBA2 isoforms .....	36
2.8 Protein expression systems and expression of glucosylceramidases .....	40

## CONTENTS (Continued)

	Page
<b>III MATERIALS AND METHODS.....</b>	<b>42</b>
3.1 General materials.....	42
3.1.1 Chemicals and reagents.....	42
3.1.2 Synthetic genes, plasmid and bacterial stain.....	45
3.2 General methods.....	46
3.2.1 Preparation of <i>E.coli</i> stain DH5 $\alpha$ competent cells.....	46
3.2.2 Transformation of plasmid into <i>E.coli</i> competent cells.....	46
3.2.3 Plasmid isolation by alkaline lysis.....	47
3.2.4 Vivantis plasmid miniprep.....	48
3.2.5 Agarose gel electrophoresis.....	49
3.2.6 Gel extraction and purification.....	49
3.2.7 COS-7 cell culture.....	50
3.2.8 Trypsinization.....	51
3.2.9 Protein extraction.....	51
3.2.10 Protein extraction for GBA2 activity and western blotting.....	52
3.2.11 Protein extraction for back up LC/MSMS analysis.....	52
3.2.12 BCA assay protein concentration determination.....	52
3.3 Cloning and expression.....	54
3.3.1 pcDNA 3.1 +/C-(k)-dyk empty vector production.....	54
3.3.2 Cell line confluency optimization and transfection.....	55
3.4 Gene expression analysis.....	56

## CONTENTS (Continued)

	<b>Page</b>
3.4.1 Oligonucleotide primers .....	56
3.4.2 RNA extraction .....	56
3.4.3 cDNA synthesis.....	57
3.4.4 qRT-PCR.....	58
3.5 Immunoblotting .....	59
3.5.1 Antibody design.....	59
3.5.2 Antibody optimization.....	60
3.5.3 SDS-PAGE electrophoresis.....	60
3.5.4 Western blotting.....	62
3.6 Assay of glucosylceramidase 2 activity .....	63
3.6.1 4-methylumbelliferyl- $\beta$ -D-glucoside (4MUG) standard curve .....	63
3.6.2 Activity assay by fluorescent signal determination.....	63
3.6.3 Inhibition of GBA activity by CBE (condurotol- $\beta$ -epoxide) .....	64
3.7 Glycosphingolipid level determination by LC MS/MS .....	64
3.7.1 Cell collection and lipid extraction .....	64
3.7.2 Preparation lipid extraction to Mass Spectrometer .....	65
3.7.3 Lipid data visualization .....	66
3.8 Signal peptide prediction .....	67
3.9 Statistical analysis .....	67
<b>IV RESULTS AND DISCUSSION.....</b>	<b>68</b>
4.1 Sequence analysis of GBA2 isoform.....	68

## CONTENTS (Continued)

	<b>Page</b>
4.2 Homology modeling of human GBA2 isoforms .....	70
4.3 GBA2 isoforms expression in COS-7 cells .....	72
4.4 Activity of human GBA2 isoforms in transfected COS-7 cells .....	77
4.5 Sphingolipid species level affected by overexpression of human GBA2 isoforms in transfected COS-7 cells .....	79
4.6 Sphingolipid ratios and the direction of sphingolipid flow .....	89
4.7 Lipid classes in cells .....	97
4.8 Interconnectivity of sphingolipid metabolism affected by GBA2 .....	104
4.9 Sequence analysis of novel <i>GBA</i> mutation .....	108
4.10 Structure analysis of human <i>GBA</i> mutations .....	111
4.11 Activity of human <i>GBA</i> and <i>Parkin</i> mutation .....	117
4.12 Sphingolipid species levels in fibroblasts with <i>GBA</i> or <i>Parkin</i> mutations .....	119
4.13 Sphingolipid ratio control the direction of sphingolipid connectivity .....	128
4.14 Correlation of sphingolipid ratio and its activity .....	131
<b>V CONCLUSION .....</b>	<b>133</b>
REFERENCES .....	142
APPENDIX .....	150
CURRICULUM VITAE .....	154

## LIST OF TABLES

Table	Page
2.1 Sphingolipid species and their key cellular functions .....	24
2.2 Identified <i>GBA</i> mutations .....	36
2.3 Disease-associated splicing alterations .....	39
3.1 Chemical reagent and sources .....	42
3.2 Preparation of diluted Albumin (BSA) standards .....	53
3.3 Oligonucleotide primers for <i>GBA2</i> and <i>GBA</i> gene expression .....	56
3.4 The human <i>GBA2</i> antigens used for antibody synthesis and the corresponding sequence in <i>Chlorocebus sabaues</i> <i>GBA2</i> for comparison .....	60

## LIST OF FIGURES

Figure	Page
2.1 Lipidomics for studying metabolism.....	6
2.2 Lipid building blocks .....	7
2.3 Examples of lipid categories .....	8
2.4 Lipid structure illustration .....	10
2.5 Structural similarity of phosphatidylcholine (PC) and sphingomyelin (SM) .....	11
2.6 Examples of ceramide signalling pathways and their role in stress response .....	12
2.7 Dysregulation of neuronal lipid metabolism in ALS impacts energy use .....	14
2.8 Compartmentalization of pathways of sphingolipid metabolism .....	18
2.9 Pathways of sphingolipid metabolism and key enzymes .....	19
2.10 An overview of the roles of sphingolipids in stress and growth responses .....	20
2.11 Sphingolipid metabolism .....	21
2.12 Ceramide synthesis by sphingosine salvage enzymes.....	22
2.13 Transport and transbilayer movement of bioactive sphingolipids .....	23
2.14 Structures of $\beta$ -glucosidases from different GH families .....	27
2.15 Generalized inverting mechanism for glycoside hydrolysis .....	28
2.16 Aberration of sphingolipid pathways in <i>GBA</i> deficiency .....	32
2.17 Alternative splicing and its potential effects on protein structure.....	37
4.1 Amino acid sequence alignment of human GBA2 with 9 human GBA2 isoforms in GH16 enzyme .....	69

## LIST OF FIGURES (Continued)

Figure	Page
4.2 Homology models of 9 human GBA2 isoforms based on the X-ray crystal structure of the <i>txGH116</i> $\beta$ -glucosidase (PDB code 5BVU) .....	71
4.3 A homology model human GBA2 with missing some parts .....	72
4.4 Expression of human GBA2 RNA in COS-7 cells transfected with 9 human GBA2 isoforms .....	73
4.5 Protein concentration determination of COS-7 cells transfected with 9 human GBA2 isoforms .....	74
4.6 Expression of human GBA2 protein in COS-7 cells transfected with 9 human GBA2 .....	75
4.7 Relative expression ratios of human GBA2 proteins to $\beta$ -actin in COS-7 cells transfected with 9 human GBA2 isoforms .....	76
4.8 Effect of expression of 9 human GBA2 isoforms on enzyme activity in transfected COS-7 cells .....	78
4.9 Profiles of total lipid, including phosphoglycerol lipids, glycerol lipids and sphingolipids in COS-7 cells transfected with the 9 human GBA2 isoforms .....	81
4.10 Profiles of total sphingolipids, ceramides, hexosylceramides and sphingomyelins in COS-7 cells transfected with the 9 human GBA2 isoforms at 48 hours incubation time .....	82

## LIST OF FIGURES (Continued)

<b>Figure</b>	<b>Page</b>
4.11 Profiles of total sphingolipids, ceramides, hexosylceramides and sphingomyelins in COS-7 cells transfected with the 9 human GBA2 isoforms at 72 hours incubation time .....	83
4.12 Heat map diagram of profiles of sphingolipid, ceramides, hexosylceramide and sphingomyelin in COS-7 cells transfected with the human GBA2 9 isoforms 48 hours.....	85
4.13 Heat map diagram of profiles of sphingolipid, ceramides, hexosylceramide and sphingomyelin in COS-7 cells transfected with the human GBA2 9 isoforms 72 hours.....	86
4.14 Amounts of ceramides, hexosylceramide and sphingomyelin detected in all extracts of COS-7 cells transfected with the 9 human GBA2 isoforms at 48 hours .....	87
4.15 Amounts of ceramides, hexosylceramide and sphingomyelin detected in all extracts of COS-7 cells transfected with the 9 human GBA2 isoforms at 72 hours .....	88
4.16 Effect of GBA2 isoforms on ceramide/hexosylceramide ratios of specific lipid species sphingolipid ratio in 48 hours .....	91
4.17 Effect of GBA2 isoforms on ceramide/hexosylceramide ratios of specific lipid species sphingolipid ratio in 72 hours .....	92

## LIST OF FIGURES (Continued)

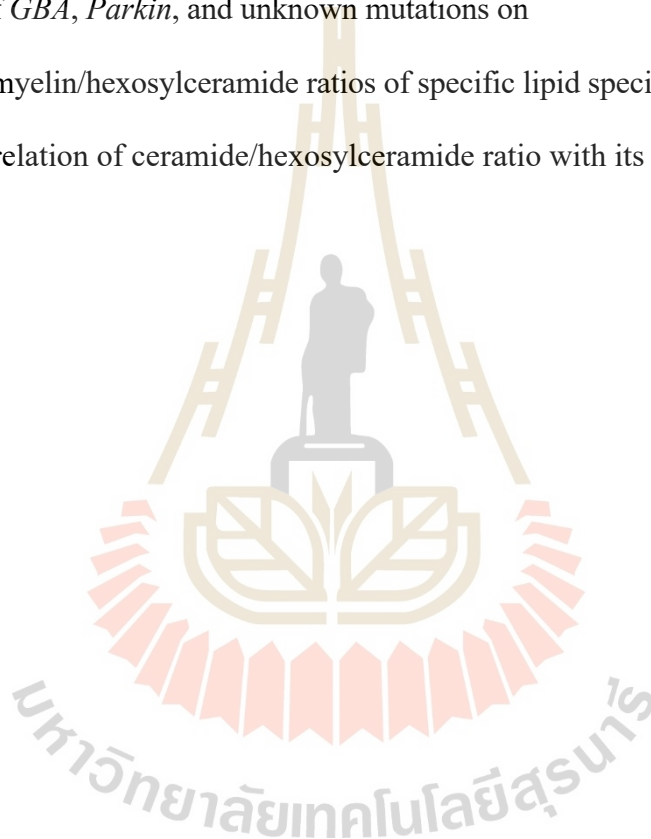
Figure	Page
4.18 Effect of GBA2 isoforms on sphingomyelin/hexosylceramide ratios of specific ceramide species 48 hours after transfection .....	93
4.19 Effect of GBA2 isoforms on sphingomyelin/hexosylceramide ratios of specific ceramide species 72 hours after transfection.....	94
4.20 Effect of GBA2 isoforms on sphingomyelin/ceramide ratios of specific lipid species sphingolipid ratio in 48 hours .....	95
4.21 Effect of GBA2 isoforms on sphingomyelin/ceramide ratios of specific lipid species sphingolipid ratio in 72 hours .....	96
4.22 Representation total of 3 lipid classes, sphingolipids, glycerophospholipids and glycerolipids, in COS-7 cells transfected with the 9 human GBA2 isoforms.....	98
4.23 The lipid distribution of 3 lipid classes .....	100
4.24 The total glycerophospholipid and glycerolipid levels in cell extracts at 48 hours after tranfection .....	102
4.25 The total glycerophospholipid and glycerolipid levels in cell extracts at 48 hours after tranfection.....	103
4.26 The changes of DAG to PC ratios upon expression of GBA2 48 hours .....	106
4.27 The changes of DAG to PC ratios upon expression of GBA2 72 hours .....	107
4.28 Amino acid sequence alignment of human GBA mutation, compared to GBA wild type.....	109
4.29 Predicted signal peptide sequence of GBA & GBA IVS2+1G>A .....	110

## LIST OF FIGURES (Continued)

Figure	Page
4.30 A homology model of the human GBA mutation N386K based on the X-ray crystal structure (PDB code 2wkl.2).....	113
4.31 A homology model human GBA mutation P428S based on the X-ray crystal structure (PDB code 2wkl.2) .....	115
4.32 A homology model human GBA mutation (1309delG) based on the X-ray crystal structure (PDB code 2wkl.2).....	116
4.33 GBA enzyme activity in Parkinson’s patient fibroblasts with GBA and Parkin mutations .....	118
4.34 Profiles of total lipid .....	120
4.35 Profiles of sterol lipid in Parkinson’s patient fibroblast with GBA and Parkin mutations .....	121
4.36 Proportions of 3 lipid classes shown as pie charts.....	122
4.37 Heat map diagram of profiles of the sphingolipids ceramides, hexosylceramides and sphingomyelins in Parkinson’s disease patient fibroblasts carrying GBA, Parkin and unknown mutations .....	124
4.38 Profiles of total ceramides, hexosylceramide and sphingomyelin, which are shown in the heat map in Parkinson’s patient fibroblasts .....	125
4.39 Profiles of totals of ceramides, hexosylceramides and sphingomyelins, detected in all control Parkinson’s patient fibroblasts with common ceramide carbon chain lengths and saturation .....	127

**LIST OF FIGURES (Continued)**

<b>Figure</b>	<b>Page</b>
4.40 Effect of <i>GBA</i> and <i>Parkin</i> on ceramide/hexosylceramide ratios of specific lipid species .....	129
4.41 Effect of <i>GBA</i> , <i>Parkin</i> , and unknown mutations on sphingomyelin/hexosylceramide ratios of specific lipid species .....	130
4.42 The correlation of ceramide/hexosylceramide ratio with its activity .....	132



## LIST OF ABBREVIATIONS

(n/μ/m)g	(nano, micro, milli) Gram
(μ/m)l	(micro, milli) Liter
(μ/m)M	(micro, milli) Molar
°C	Degree (s) Celcius
(k)bp	(kilo) Base pair DNA
bp	Base pair(s)
BSA	Bovine serum albumin
cDNA	Complementary deoxynucleic acid
CDase	Ceramidase
Cer	Ceramide
CerS	Ceramide synthase
CBE	Conduritol-β-epoxide.
DAG	Diacylglycerol
DMSO	Dimethyl sulfoxide
DNase	Deoxyribonuclease
dNTPs	Deoxynucleoside triphosphates
ER	Endoplasmic reticulum
ESI	Electrospray ionization

**LIST OF ABBREVIATIONS (Continued)**

GBA	Glucosylceramidase 1
GBA2	Glucosylceramidase 2
GSL	Glycosphingolipid
GlcCer	Glucosylceramide
GalCer	Galactosylceramide
GH	Glycoside hydrolase
HexCer	Hexosylceramide
kDa	kilo Dalton
LB	Luria-Bertani lysogeny broth
Min	Minute
MW	Molecular weight
MS	Mass spectrometry
nm	Nano meter
OD	Optical density
RNA	Ribonucleic acid
RNase	Ribonuclease
rpm	Revolutions per minute
SDS	Sodium dodecyl sulfate
PC	Phosphatidylcholine

**LIST OF ABBREVIATIONS (Continued)**

PCR	Polymerase chain reaction
PE	Phosphatidylethanolamine
PEG	Polyethylene glycol
PI	Phosphatidylinositol
PS	Phosphatidylserine
SDS-PAGE	Polyacrylamide gel electrophoresis with SDS
SPT	Serine palmitoyltransferase
SM	Sphingomyelin
SMase	Sphingomyelinase
Sph	Sphingosine
S1P	Sphingosine-1-phosphate
TEMED	Tetramethylethylenediamine
Tris	Tris-(hydroxymethyl)-aminoethane
v/v	Volume per volume
w/v	Weight per volume

# CHAPTER I

## INTRODUCTION

### 1.1 General introduction

Sphingolipid metabolism is involved in many processes in cellular biology, including apoptosis, cell- cycle arrest, differentiation, migration, proliferation, and senescence (Sakamoto, Coant et al., 2018). In addition, sphingolipids contribute to cell signaling as important components of cellular membranes, where they maintain the integrity of their structure (Zhou, Summers et al., 1998). De novo synthesis of sphingolipids begins in the endoplasmic reticulum (ER) with condensation of serine and palmitoyl-CoA by way of serine palmitoyltransferase (SPT) to make 3-keotsphingonine, which is then converted to ceramide via reduction, N-acylation and desaturation (Abdul-Hammed, Breiden et al., 2017). To synthesize GlcCer, the ceramide is transported to the cytoplasmic surface of the cis Golgi complex, where glucosylceramide synthase (GCS) converts ceramide to glucosylceramide through the addition of a glucosyl group donated by UDP-glucose (Tracey, Steyn et al., 2018). Much of the GlcCer is converted to higher complexity glycolipids in the Golgi after flipping into the luminal leaflet of the membrane. The remaining GlcCer is transferred to the plasma membrane and is ultimately fated to undergo

degradation through hydrolytic pathways. GlcCer is hydrolyzed by glucosylceramidase (GBA, E.C. 3.2.1.45) in the lysosome and glucosylceramidase2 (GBA2) on the cytoplasmic side of the ER and Golgi to release ceramide and glucose (Abdul-Hammed, Breiden et al., 2017). GBA dysfunction is the cause of Gaucher disease, which is one of the most common lysosomal storage disorders. Gaucher disease results mainly in GlcCer accumulation, particularly in the lysosome of the macrophages (Mistry, Liu et al., 2010, Burke, Rahim et al., 2013). Deficiency of GBA has also been implicated in the etiology of Parkinson's disease, for which GBA mutations are the most commonly reported genetic defect (Schöndorf, Aureli et al., 2014). In contrast, the biological significance of GBA2 is less well understood. GBA2-deficient mice present with male infertility, but humans carrying mutations in the GBA2 gene are affected with an autosomal recessive cerebellar ataxia (ARCA) with spasticity or hereditary spastic paraplegia (HSP), often involving thin corpus callosum and cognitive impairment (Online Mendelian Inheritance in Man Spastic Gait locus #46, SPG46) (Sultana, Reichbauer et al., 2015).

Alternative splicing may work as a modifier and diversifier in gene expression. It affects the expression levels, stability, half-life and localization of the messenger RNA (La Cognata, D'Agata et al., 2015). The relevance of alternative splicing to human glucocerebrosidase function is demonstrated in the point mutation g.12599C > A (c.999 + 242C > A), which was detected deep in intron 7 of the GBA gene. This mutation creates a donor splice site leading to aberrant splicing and resulting in the insertion of the first 239 nt of intron 7 (Malekkou, Sevastou et al., 2019). In contrast, the biological significance of alternative splicing of GBA2 transcripts has yet to be linked to human disease.

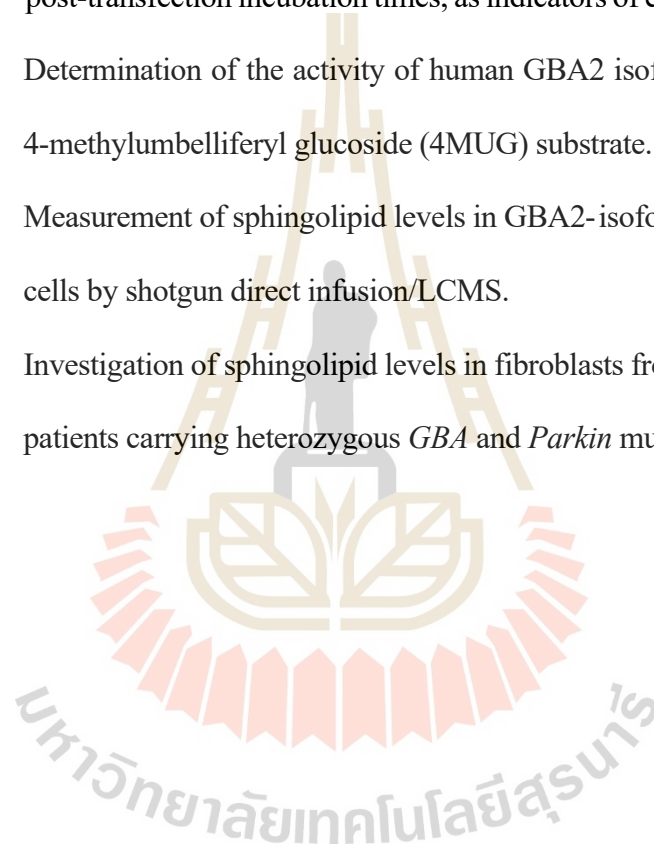
A recent study revealed 5 novel putative GBA mutations in Thai PD patients, including 1275C>A (N386K), 1399C>T (P428S), 1309delG, IVS9+3G>C and IVS10-9\_10GT>AG (Teeratom Pulkes et al., 2014). Two common mutations, L444P and IVS2+1G>A, were also found, and the authors suggested that 1309delG, IVS9+3G>C and IVS10-9\_10GT>AG are critical mutations causing GBA deficiency. The 1309delG mutation is in exon 9 and was predicted to result in valine substitution by serine at amino acid residue 437, followed by a frame shift resulting in a premature stop codon at codon 443. This leads to translation into an abnormal shorter protein product (442 instead of the normal 536 amino acid residues). IVS9+3G>C and IVS10-9\_10GT>AG may cause missplicing that results in reading frame shifts that translate to truncated protein products. That first study provided evidence of GBA mutations as an important risk of PD in Thailand and suggested that the L444P mutation is common in Thai PD patients having GBA mutations. However, it lacked information on the relation between GBA mutation and sphingolipid profiles in Thai PD patients. Therefore, this study aimed to identify the correlation of sphingolipid levels in patient fibroblasts with heterozygous GBA mutations and Parkin mutations in PD.

In order to understand the biological significance of GBA2 isoforms and their effect on sphingolipid levels, we studied extracts of cells over expressing GBA2 isoforms using biochemical assays and mass- spectrometry. We assessed GBA2 isoforms activity with the artificial substrate (4MUG) and natural substrates (GlcCer) found in the cells in which they were expressed. In addition, we analyzed human fibroblasts carrying GBA mutation and Parkin mutations by shotgun mass spectroscopy to identify any features of the sphingolipid profile associated with the GBA and Parkin mutations.

## 1.2 Research objectives

To achieve the aims of the thesis, the following specific objectives were investigated.

- 1.2.1 Expression of the predicted splice variants of the human GBA2 gene in COS-7 cells.
- 1.2.2 Investigation of the human GBA2 RNA and protein levels at 48 and 72 hr post-transfection incubation times, as indicators of expression and stability.
- 1.2.3 Determination of the activity of human GBA2 isoforms for hydrolysis of 4-methylumbelliferyl glucoside (4MUG) substrate.
- 1.2.4 Measurement of sphingolipid levels in GBA2-isoform-transfected COS-7 cells by shotgun direct infusion/LCMS.
- 1.2.5 Investigation of sphingolipid levels in fibroblasts from Parkinson's disease patients carrying heterozygous *GBA* and *Parkin* mutations.



## **CHAPTER II**

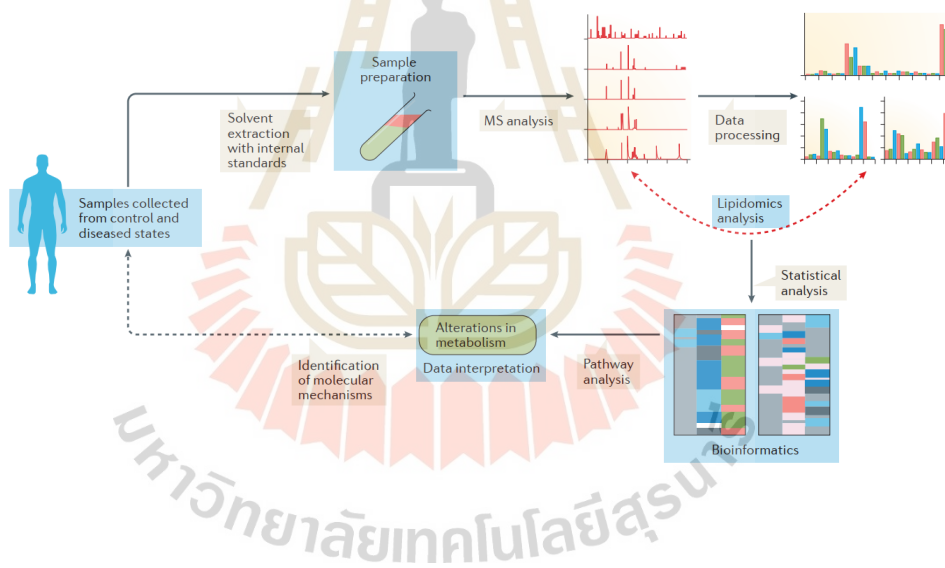
### **LITERATURE REVIEW**

#### **2.1 Lipidomics for studying metabolism**

Lipids are essential metabolites that have several pivotal cellular functions and can provide a direct readout of cellular metabolic status. Lipidomics is the investigation of lipidomes, the total lipid contents of cells or tissues, using the principles and techniques of analytical chemistry (Kishimoto, Urade et al., 2001). The lipidome of a cell is predicted to be inside the scope of tens of thousands to hundreds of thousands of lipids at concentrations of between  $\mu\text{mol}/\text{mg}$  and  $\text{nmol}/\text{mg}$  of protein. Lipidomics constitutes a comprehensive evaluation of lipid molecules in the context of genomics and proteomics, and vital to understanding cellular physiology and pathology.

Lipidomics emerged in 2003 as an approach to study the metabolism of the cellular lipids (Han and Gross, 2003). Lipidomics is a relatively recent research discipline that has been driven by rapid advances in a number of analytical technologies, in particular mass spectrometry (MS), and computational methods, coupled with the recognition of the function of lipids in many metabolic diseases along with obesity, atherosclerosis, stroke, hypertension and diabetes (Watson, 2006, Orešič, Hänninen et al., 2008). The analytical

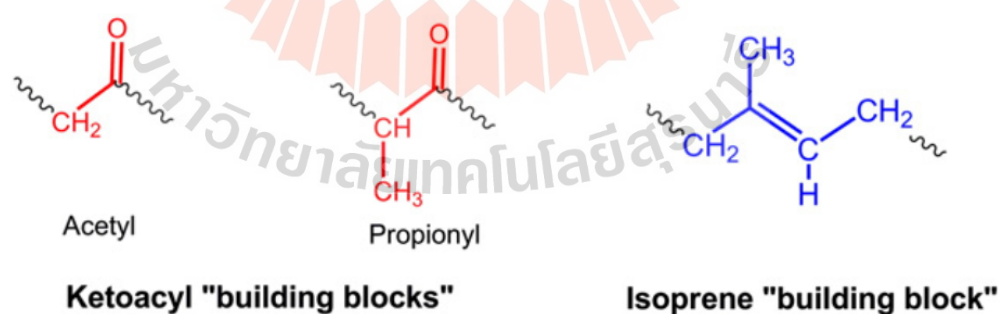
power of new and improved mass spectrometry (MS) instruments and methods have quickened the adoption of this developing discipline (Blanksby and Mitchell 2010, Han, Yang et al., 2012). Lipidomics provides a powerful tool for the discovery and development of lipid biomarkers for ailment states. Importantly, this approach enables us to contemplate cellular metabolism by evaluating the changes of individual lipid classes, subclasses and molecular species that reflect metabolic processes. Since the pathways and networks of lipid metabolism have been widely studied (Vance and Vance, 1996), any changes in lipid amounts can simultaneously reveal variations in several enzymatic levels, activities and/or gene expression patterns, as shown in Figure 2.1.



**Figure 2.1** Lipidomics for studying metabolism. Human samples are prepared for mass spectrometry (MS) analysis. The MS and information processing constitute the lipidomics analysis. Bioinformatic analysis identifies changes in cellular metabolism, and ultimately the biochemical mechanisms underpinning the pathogenesis of the illness (Han, 2016).

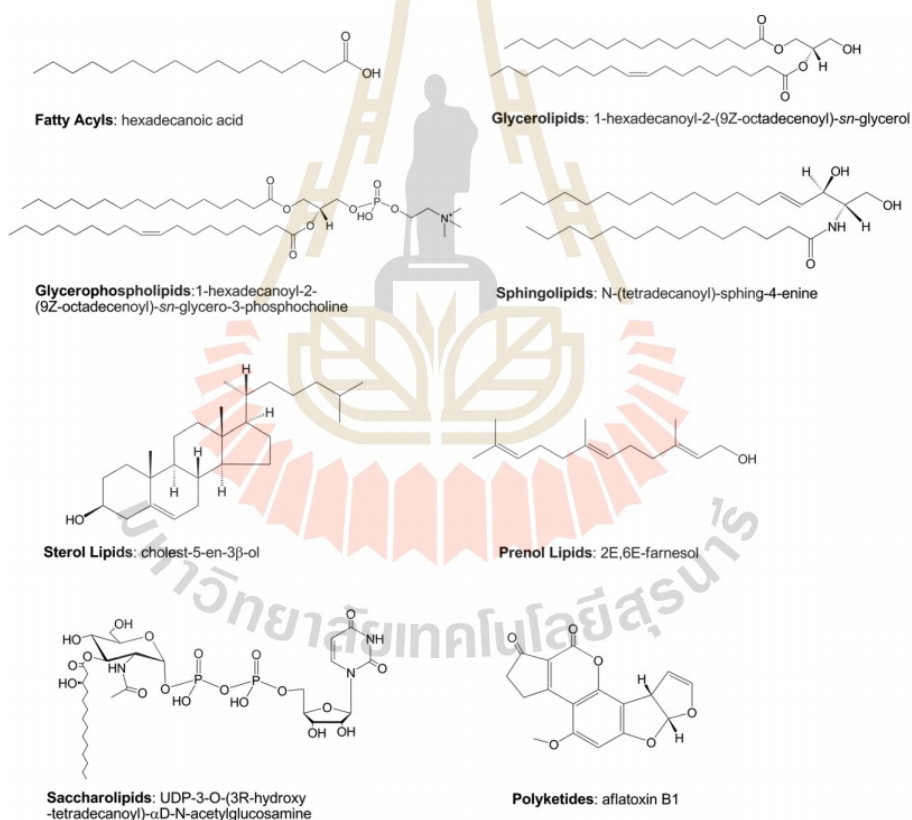
## 2.2 Lipid classification structures and tools

Lipids are a various and ubiquitous group of compounds that have many key biological functions, such as serving as energy storage compounds, structural components of cell membranes, and components and modifiers in signaling pathways. The variety in lipid characteristics reflects the enormous variation in the structures of lipid molecules. Unlike the case of genes and proteins, which are ordinarily composed of linear combinations of 4 nucleic acids and 20 amino acids, respectively, lipid structures are usually much more complex because of the number of different biochemical changes that arise at some point of their biosynthesis. This level of diversity makes it vital to develop a comprehensive classification, nomenclature, and chemical representation system to accommodate the large variety of lipids that exist in nature. The LIPID MAPS (<https://www.lipidmaps.org>) classification system is based on the concept of 2 fundamental “building blocks”: ketoacyl groups and isoprene groups as shown in Figure 2.2.



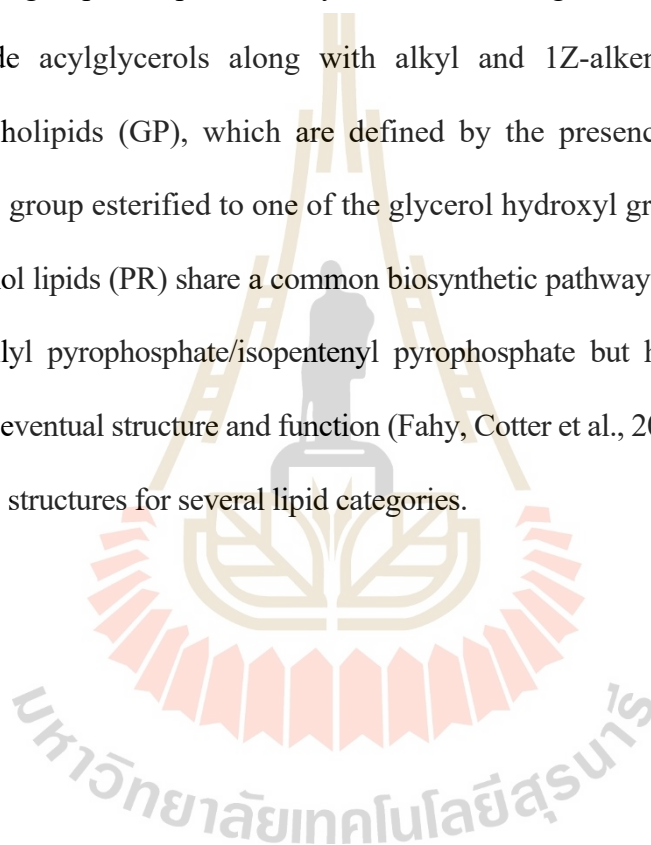
**Figure 2.2** Lipid building blocks. The LIPID MAPS classification system is based on the concept of 2 fundamental biosynthetic “building blocks”: ketoacyl groups and isoprene groups (Fahy, Cotter et al., 2011).

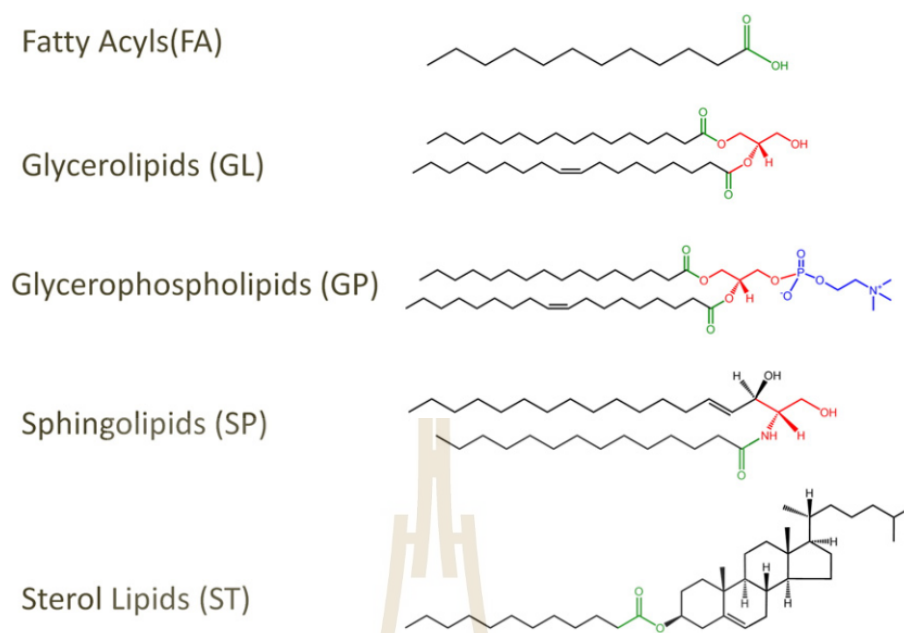
In this context, lipids are defined as hydrophobic or amphipathic molecules part or all of which can be synthesized by carbanion based condensations of ketoacyl thioesters and/or by carbocation based condensations of isoprene units (Fahy, Cotter et al., 2011). Based on this classification system, lipids are divided into 8 categories: fatty acyls, glycerolipids, glycerophospholipids, sphingolipids, saccharolipids and polyketides (derived from the condensation of ketoacyl subunits); and sterol lipids and prenol lipids (derived from the condensation of isoprene subunits), as shown in Figure 2.3



**Figure 2.3** Examples of lipid categories. Representative structures from each of the 8 LIPID MAPS lipid categories (Fahy, Cotter et al., 2011).

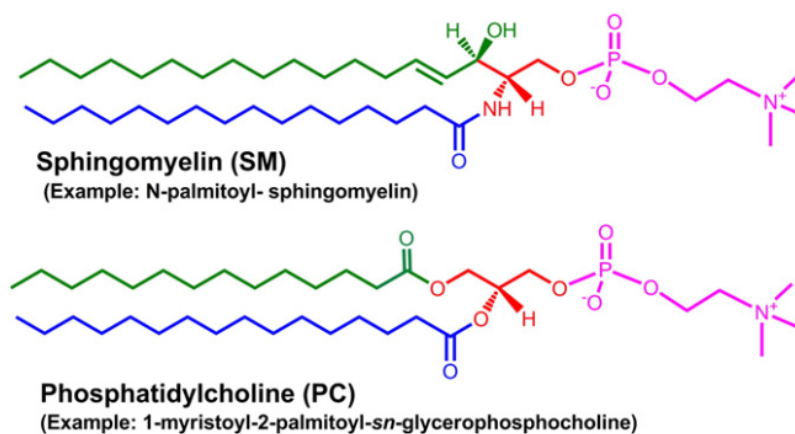
The fatty acyls (FA) are a various group of molecules synthesized via chain elongation of an acetyl-CoA primer with malonyl-CoA (or methylmalonyl-CoA) groups that may include a cyclic capability and/or be substituted with heteroatoms. It is notable that, in addition to fatty acids, this category contains several different functional group variants, such as alcohols, aldehydes, amines and esters. Structures with a glycerol group are represented by two distinct categories: the glycerolipids (GL), which include acylglycerols along with alkyl and 1Z-alkenyl variants, and the glycerophospholipids (GP), which are defined by the presence of a phosphate (or phosphonate) group esterified to one of the glycerol hydroxyl groups. The sterol lipids (ST) and prenol lipids (PR) share a common biosynthetic pathway via the polymerization of dimethylallyl pyrophosphate/isopentenyl pyrophosphate but have key variations in terms of their eventual structure and function (Fahy, Cotter et al., 2011). Figure 2.4 shows representative structures for several lipid categories.





**Figure 2.4** Lipid structure illustration. Examples of structures from variety lipid classes, within which acyl or prenyl chains are oriented horizontally with the terminal functional group (in green) on the right and the unsubstituted “tail” on the left (Fahy, Cotter et al., 2011).

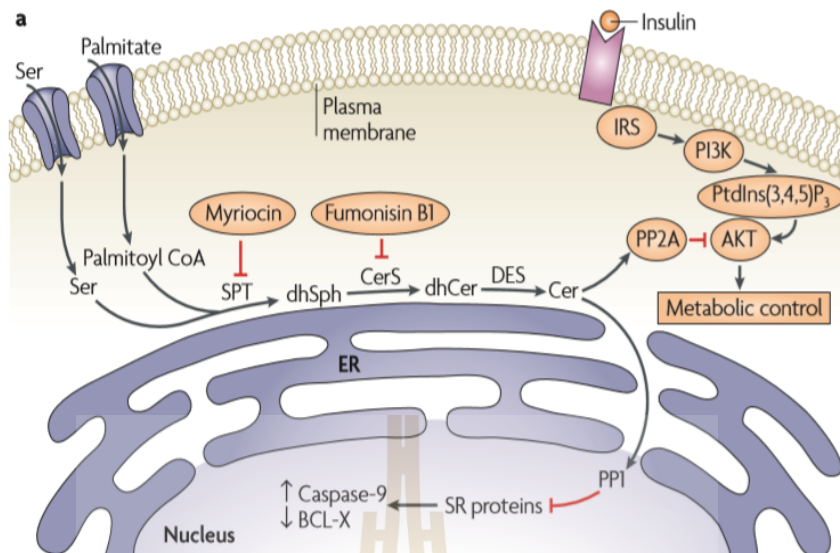
This approach of classification has the advantage of facilitating recognition of lipids within a category or class, and additionally allowing one to focus on structural similarities between categories. For instance, the glycerophosphocholines (PC) and sphingomyelins (SM) have different biosynthetic origins, but their structural similarities as amphipathic membrane lipids are evident once displayed, as shown in Figure 2.5.



**Figure 2.5** Structural similarity of PC and SM. Orientation of examples of phosphatidylcholine (PC) and sphingomyelin (SM) structures highlights their similarity. The sphingosine “backbone” of SM is biosynthetically derived from palmitoyl-CoA (green) and serine (red), whereas PC contains a glycerol core (red) with an additional acyl chain (green). Both molecules contain a phosphocholine (pink) head group (Fahy, Cotter et al., 2011).

### 2.3 Glycolipid roles in membrane function and cellular processes

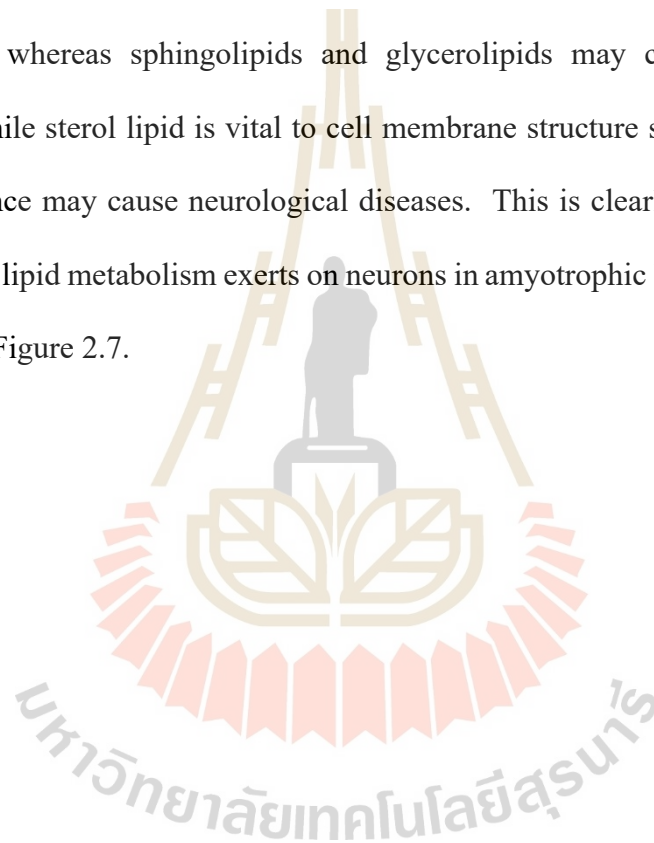
The eukaryotic plasma membrane consists largely of glycerolipids, sterols and sphingolipids. These lipids play a vital role to maintain the physiological turnover of cellular membrane organelles in a specific pattern (Marques, Mirzaian et al., 2016), as well as serving as bioactive molecules that act as communication transducers and communication molecules (Bartke and Hannun, 2009). Examples of how ceramide modulates signaling pathways are shown in Figure 2.6.



**Figure 2.6** Examples of ceramide signaling pathways and their role in stress response, the *de novo* pathway in palmitate signaling and insulin resistance. Extracellular palmitate is taken up by cells where it is acylated to make palmitoyl CoA, which along with serine, serve as the initial substrates for sphingolipid synthesis. Excess palmitate increases *de novo* synthesis, which might lead to higher ceramide (Cer) levels. Accumulation of Cer has been shown to activate protein phosphatase-2A (PP2A), resulting in inhibition of AKT, a key mediator of the metabolic effects of insulin. Excessive Cer also activates PP1 phosphatase, and activation of both PP1 and PP2A can enhance cytotoxic and apoptotic responses (Hannun and Obeid, 2008).

Both lipid-lipid and lipid-protein interactions promote the formation of raft domains, which is driven chiefly by preferential binding of cholesterol to sphingolipids (Ramstedt and Slotte, 1999). Presumably, other lipids, such as gangliosides, as well as variations in lipid composition are actually key drivers of lipid membrane heterogeneity (Lozano, Hovis et al., 2016). In order to maintain homeostasis in the cells, lipids are constantly metabolized and targeting lipid metabolism could improve symptoms of

diseases affected by defects in their pathways (Bdira, Artola et al., 2018). Glycoconjugate compose of sphingolipids, glycerophospholipids and glycerolipids can play important roles in biological processes in the cells and have been linked to multiple pathologies (Bdira, Artola et al., 2018). Lipid metabolism also provides the cross link between the 3 lipid classes (Hannun and Obeid, 2008). Glycerophospholipids comprise the most abundant lipid class in the cell, which can help to maintain the lipid consistency, whereas sphingolipids and glycerolipids may contribute to the cell activities, while sterol lipid is vital to cell membrane structure such as cholesterol, so their imbalance may cause neurological diseases. This is clearly shown in the effect dysregulated lipid metabolism exerts on neurons in amyotrophic lateral sclerosis (ALS) as shown in Figure 2.7.



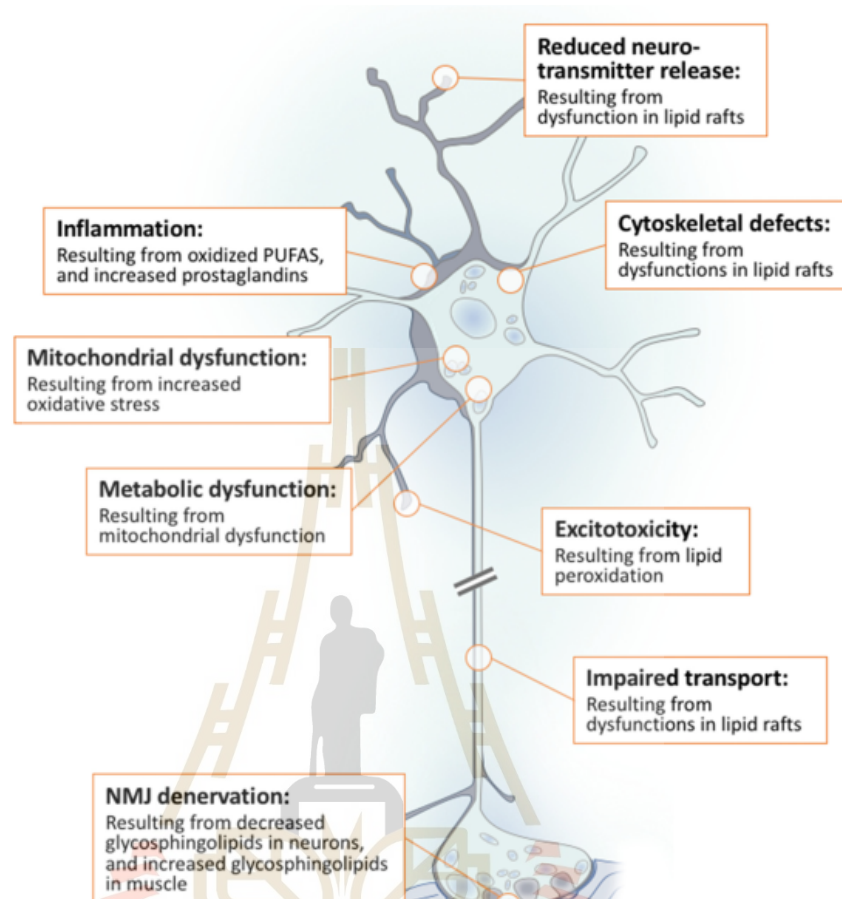


**Figure 2.7** Dysregulation of neuronal lipid metabolism in ALS impacts energy use, structural integrity and signaling processes. Increased use of lipids as an energy associated substrate leads to increased oxidative stress. Altered lipid metabolism conjointly disrupts intracellular lipids leading to cytoskeletal defects and the denervation of neuromuscular junctions. Finally, changes in lipid metabolism impact the composition of lipid rafts. This disrupts signaling processes that are crucial in control neurotransmitter synthesis and unleash, cytoskeletal integrity and intracellular transport (Tracey, Steyn et al., 2018).

## 2.4 Sphingolipid synthesis and function in cellular processes

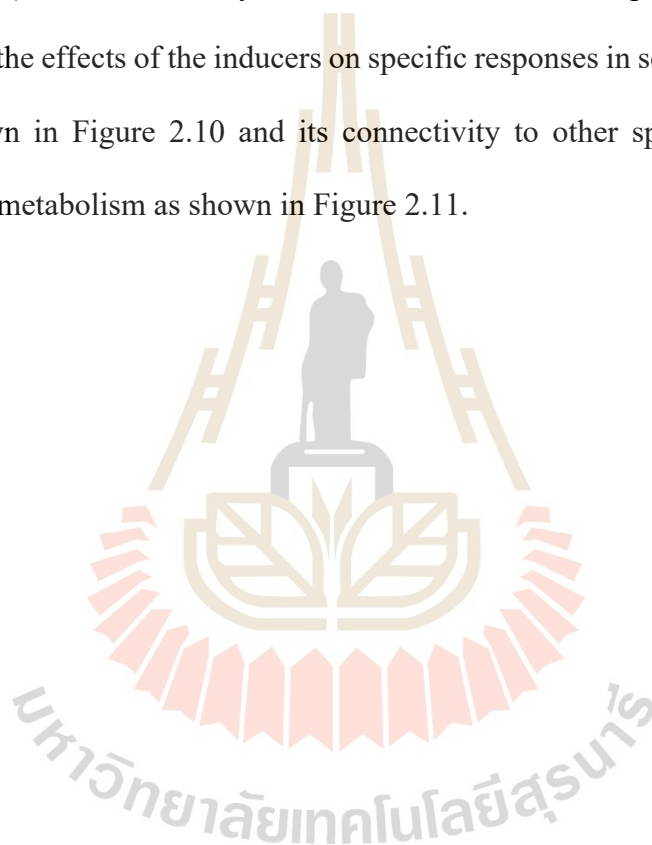
Sphingolipid metabolism is involved with several processes in cellular biology, including apoptosis, cell-cycle arrest, differentiation, migration, proliferation, and senescence (Sakamoto, Coant et al., 2018). Additionally, sphingolipids contribute to cell signaling as a vital component of cellular membranes, where they help maintain the integrity of the structure (Zhou, Summers et al., 1998) and organization. Sphingolipids are implicated in neurodevelopment, inflammation, cancer, and a number of other physiological and pathological processes (Ogretmen and Hannun 2004, Yoshida, Furuya et al., 2004, Maceyka and Spiegel, 2014). Sphingolipid *de novo* synthesis begins in the endoplasmic reticulum (ER) with condensation of serine and palmitoyl-CoA catalyzed by serine palmitoyltransferase (SPT) to make 3-ketosphingonine, which is reduced to dihydrosphingonine. Then, it is converted to ceramide by N-acylation and desaturation of bond between carbons 4 and 5, and ceramide is transported to the Golgi.

The Golgi apparatus is the site of synthesis of sphingomyelin (SM) and glucosylceramide (GlcCer), with the latter serving as the precursor for many more complicated glycosphingolipids (GSLs). The transport of Cer to the Golgi happens either through the action of the transfer protein CERT, which specifically delivers Cer for SM synthesis, or through vesicular transport, which delivers Cer for the synthesis of GlcCer. In turn, transfer of GlcCer for GSL synthesis requires the action of the recently described transport protein phosphatidylinositol-four-phosphate adapter protein 2 (FAPP2), which transports GlcCer back to the ER (Yamaji, Kumagai et al., 2008). GlcCer is synthesized on the cytosolic side of the Golgi and is moved to the luminal leaflet by a GlcCer flippase found in ER and Golgi membranes before further

saccharides can be added in complex GSL synthesis in the Golgi. Delivery of SM and complex GSLs to the cell membrane appears to occur by vesicular transport, which help to move SM to the outer membrane leaflet.

These membrane lipids can be converted back to ceramide, either for metabolic or signaling purposes. For instance, acid sphingomyelinase (SMase) that is present in the outer membrane leaflet or neutral SMases in the inner leaflet of the bilayer can metabolize SM to Cer and subsequently other bioactive lipids (Hannun and Obeid, 2008). This metabolic network additionally extends to the circulatory system, where several of the enzymes (acid SMase, neutral ceramidase (CDase) and sphingosine kinase (SK) have been detected, usually in association with lipoproteins that are rich in SM and Cer. Internalization of membrane sphingolipids proceeds through the endosomal pathway by which SM and GlcCer may reach the lysosomal compartment, where they are degraded by the actions of SMases and acid glucosidase (GBA) to form Cer. Cer is hydrolysed by acid CDase to form sphingosine (Sph). Sph may exit the lysosome, although its ionizable positive charge favors partitioning in lysosomes. Therefore, it is postulated that the action of SK1 at or close to the lysosome may be required to 'trap' Sph through phosphorylation. Following retrograde transport, dephosphorylation by S1P phosphatases in the ER would recycle the salvaged Sph to Cer. A similar role for SK in delivering exogenous sphingoid bases to internal metabolic pathways has been demonstrated in yeast. Sph formed from this salvage pathway is sufficiently soluble in the cytosol to move among membranes. A summary of sphingolipid related compartmentalization in the cell is shown in Figure 2.8. (Hannun and Obeid, 2008, Abdul-Hammed, Breiden et al., 2017).

Studies in the mid-1980s defined bioactive functions for sphingosine, followed by ceramide, sphingomyelin, and glucosylceramide. These emerging functions act in various aspects of cellular processes, as shown in a summary of sphingolipid metabolism in Figure 2.9. As mentioned above, sphingolipid metabolites interact with specific protein targets, such as phosphatases, kinases and G protein coupled receptors (S1P receptors), that successively mediate the effects of these lipids and, at least in part, also mediate the effects of the inducers on specific responses in several processes in the cell, as shown in Figure 2.10 and its connectivity to other sphingolipid species in sphingolipid metabolism as shown in Figure 2.11.



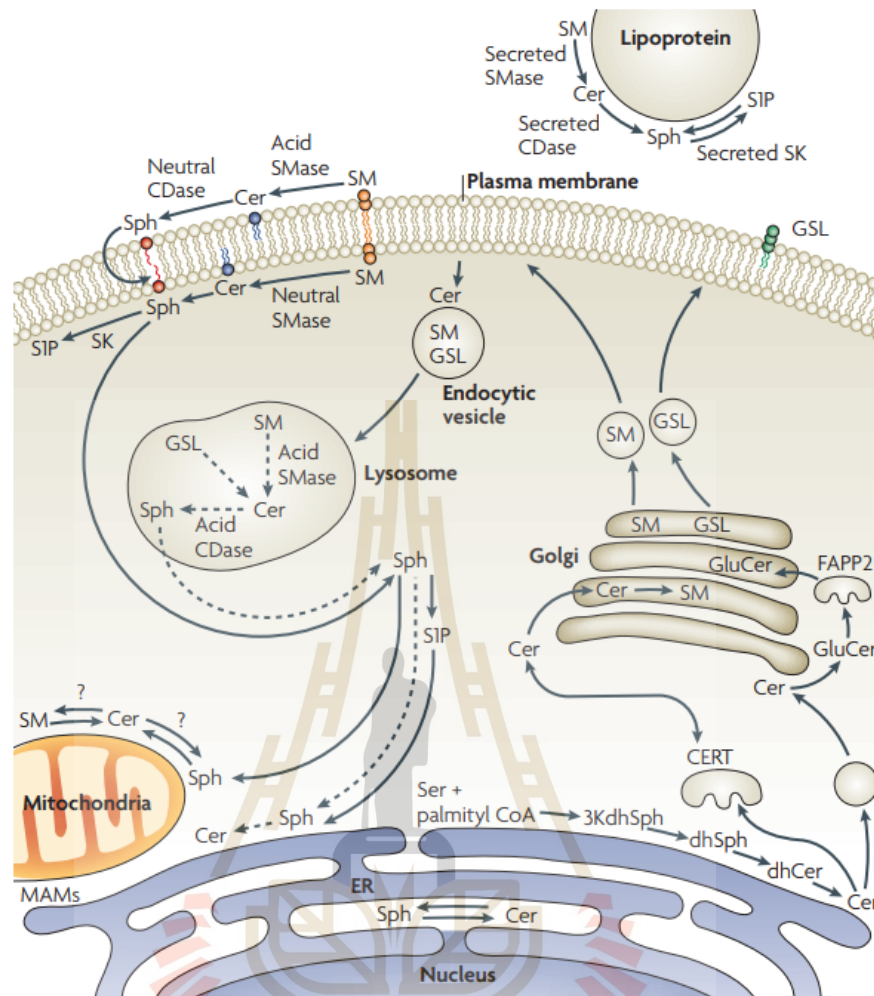


**Figure 2.8** Compartmentalization of pathways of sphingolipid metabolism (Hannun and Obeid, 2008).

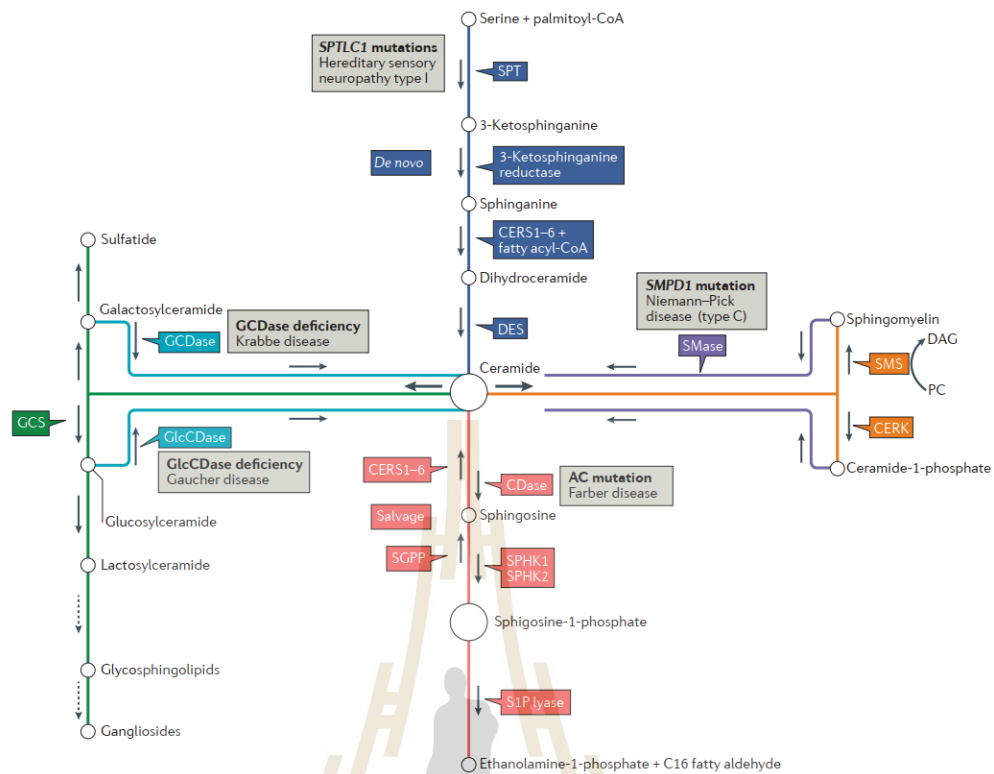


**Figure 2.9** Pathways of sphingolipid metabolism and key enzymes. Ceramide is the central molecule in sphingolipid metabolism and can be synthesized *de novo* (dark blue boxes) by the functions of serine palmitoyl-transferase (SPT), 3-ketosphinganine reductase, (dihydro) ceramide synthases (CERS1–6) and dihydroceramide desaturase (DES). Ceramide can also be generated by the hydrolysis of complex sphingolipids, such as sphingomyelin (SM) by the action of sphingomyelinases (SMases) (purple box). Synthesis of complex sphingolipids, such as glycosphingolipids or gangliosides, requires the synthesis of glucosylceramide (GlcCer) by glucosylceramide synthase (GCS) (green box), and GlcCer is a precursor for the synthesis of complex sphingolipids (dotted arrows) (Ogretmen, 2018).

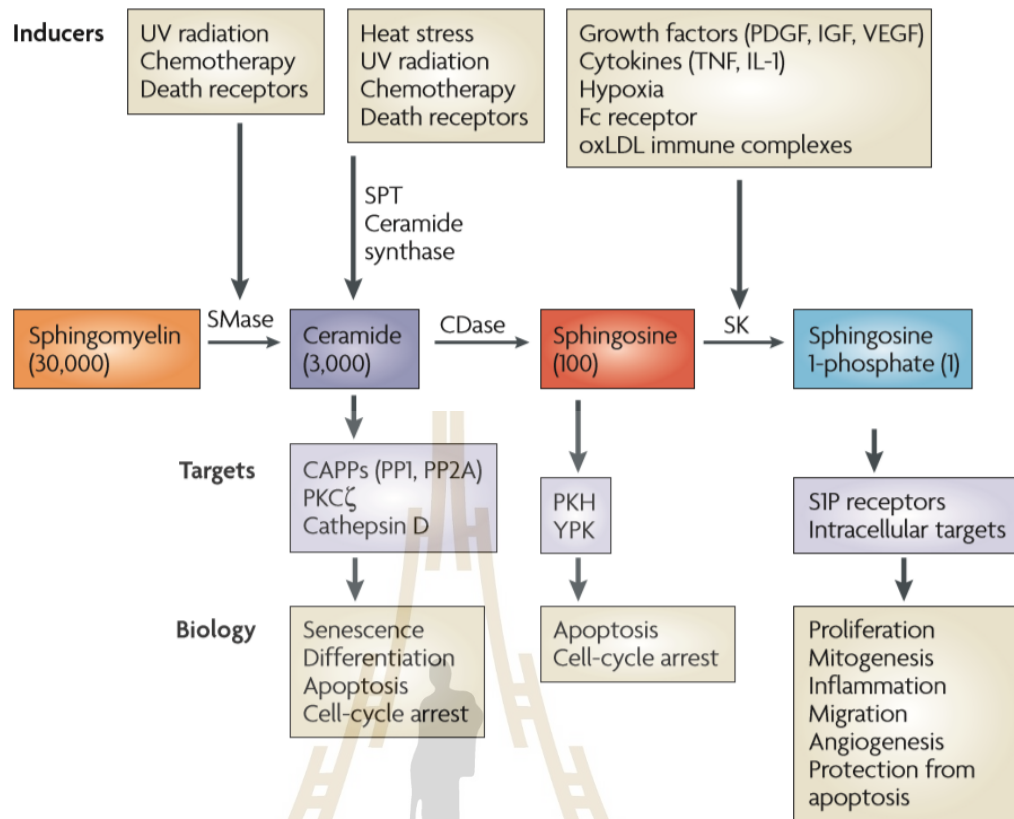


**Figure 2.10** An overview of the roles of sphingolipids in stress and growth responses (Hannun and Obeid, 2008).

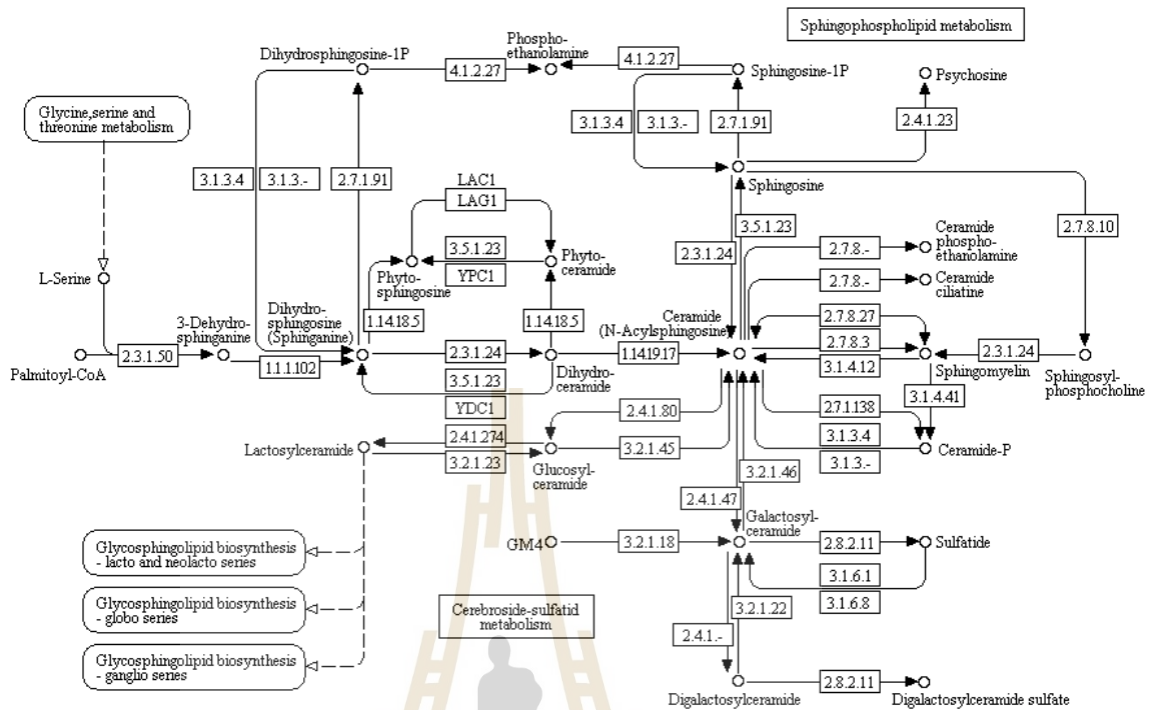


**Figure 2.11** Sphingolipid metabolism showing the position of glucosylceramide breakdown by GBA and GBA2 as highlight in the red box to hydrolyze glucosylceramide releasing glucose and ceramide as well as sphingolipid can connect to glycerophospholipid via sphingosine- 1- phosphate to phosphoethanolamine.

(<https://www.genome.jp/kegg/pathway/map/map00600.html>).

To synthesize ceramide from Sph, specific (dihydro)-ceramide synthase (also known as Lass or CerS) enzymes function to catalyze the formation of distinct ceramides that are distinguished by their N-linked fatty acyl groups. As an example, CerS1 catalyzes the synthesis of C18-ceramide, whereas CerS5 and CerS6 result in the preferential formation of C16-ceramide, as shown in Figure 2.12. Studies based on overexpression of CerS isoenzymes suggest that they are localized to the endoplasmic

reticulum (ER); however, interpreting localization based on the overexpression of hydrophobic proteins should be done with caution.

As noted earlier, some of the sphingolipids act as the signaling molecules. Their role in signaling usually involves moving across the membrane and between membranes, as shown the detail in Figure 2.13.

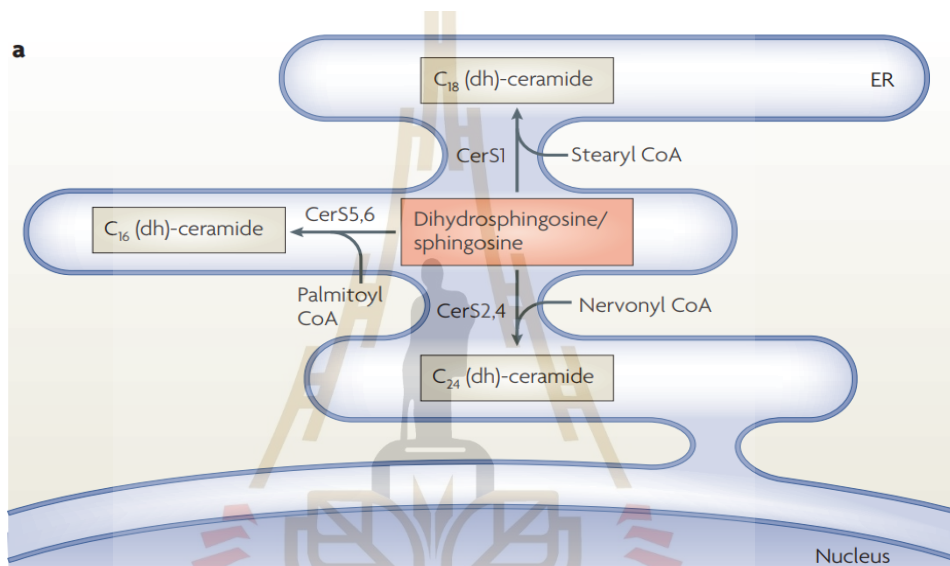


**Figure 2.12** Ceramide synthesis by sphingosine salvage enzymes (Hannun and Obeid, 2008).

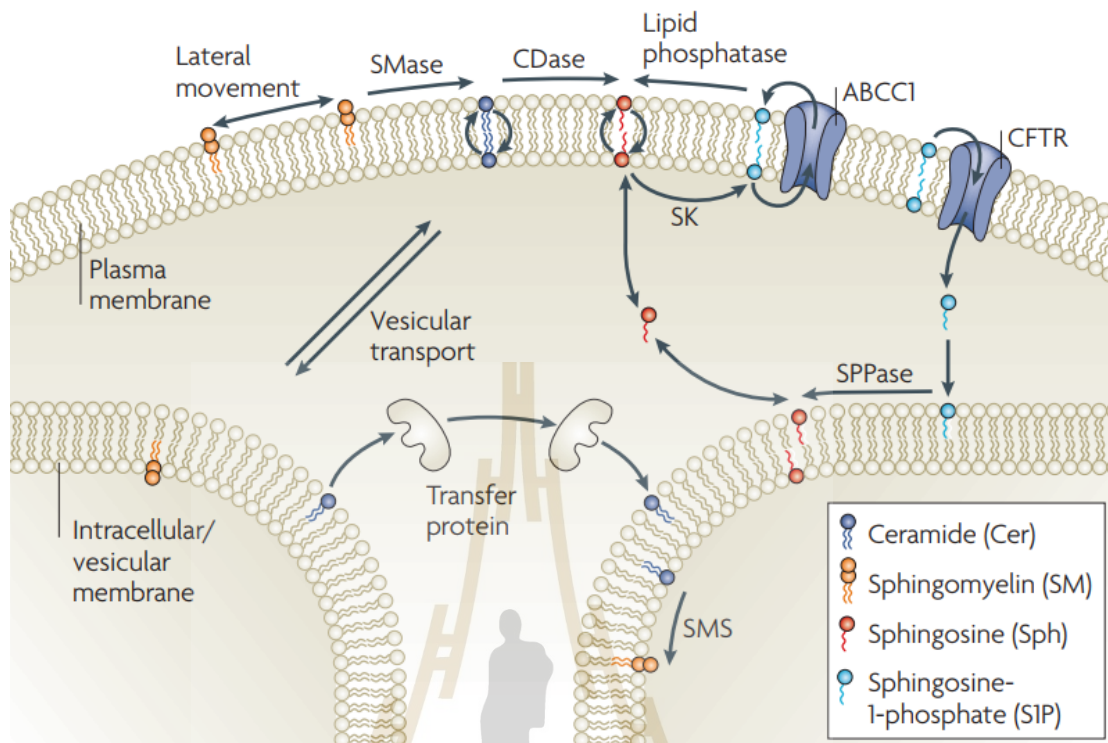


**Figure 2.13** Transport and transbilayer movement of bioactive sphingolipids. Shown are model membranes that represent the plasma membrane, vesicular membranes and intracellular membranes, and the mechanisms by which sphingolipids may be transported between and across them. Sphingomyelin (SM) has two aliphatic chains and a zwitterionic head group. Therefore, it only occasionally (if at all) flip-flops across bilayers and has negligible aqueous solubility, but may have significant lateral movement. Ceramide (Cer) contains two aliphatic chains, but has a neutral head group, so it exhibits less aqueous solubility than SM, but is readily able to flip-flop in model membranes (Bdira, Artola et al., 2018).

**Table 2.1** Sphingolipid species and their key cellular functions (Hannun and Obeid, 2018).

<b>Sphingomyelin</b>	
Cell growth	<ul style="list-style-type: none"> <li>↑ Sphingomyelin via SMS1 overexpression exogenous sphingomyelin</li> <li>↑ Sphingomyelin via basic fibroblast growth factor-dependent stimulation of SMS</li> </ul>
Cell adhesion	<ul style="list-style-type: none"> <li>↑ Sphingomyelin in cells treated with phorbol ester stimulated cell adhesion</li> <li>↑ Sphingomyelin induced by nSMase treatment caused detachment</li> </ul>
<b>Galactosylceramide</b>	
Inflammation	<ul style="list-style-type: none"> <li>↑ Galactosylceramides in GALC mutant mice</li> <li>Exogenous galactosylceramide treatment stimulates natural killer T cells</li> </ul>
HIV-1 infection	<ul style="list-style-type: none"> <li>Binding of HIV-1 gp120 to GalCer</li> <li>HIV-1 infection in CD4-GalCer+ T lymphocytes</li> </ul>
<b>Glucosylceramid</b>	
Multidrug resistance in cancer cells	<ul style="list-style-type: none"> <li>↑ Glucosylceramides via GCS overexpression in multiple multidrug-resistant tumours and cancer cell lines</li> </ul>
Inflammation	<ul style="list-style-type: none"> <li>↑ Glucosylceramides induced by mutations in the <math>\beta</math>-glucosylceramidase beta gene (Gaucher disease)</li> </ul>
Cell adhesion	<ul style="list-style-type: none"> <li>↑ Glucosylceramides via GCS overexpression</li> <li>↑ Glucosylceramides in cells treated with 12-O-tetradecanoylphorbol-13-acetate</li> </ul>
Cell differentiation	<ul style="list-style-type: none"> <li>↑ Glucosylceramides in cells treated with 12-O-tetradecanoylphorbol-13-acetate</li> </ul>
<b>Ceramide</b>	
Cell death	<ul style="list-style-type: none"> <li>↑ C18 ceramide in chemotherapy-induced cell death in human HNSCCs</li> <li>↑ C16 ceramide via CerS activation induced by a variety of cell stressors</li> </ul>
Cell differentiation	<ul style="list-style-type: none"> <li>↑ Total ceramides</li> </ul>
Cell proliferation	<ul style="list-style-type: none"> <li>↑ C24 and C24:1 ceramide via overexpression of CerS2</li> </ul>
Cell cycle arrest	<ul style="list-style-type: none"> <li>Exogenous C2 or C6 ceramide</li> </ul>
Senescence	<ul style="list-style-type: none"> <li>↑ Total ceramides</li> <li>Exogenous C8 ceramide</li> </ul>
Necrosis	<ul style="list-style-type: none"> <li>↑ Total ceramides</li> <li>Exogenous C2 or C6 ceramide</li> </ul>
Necroptosis	<ul style="list-style-type: none"> <li>Exogenous C16 ceramide</li> <li>↑ C16 ceramide in TNF<math>\alpha</math>-treated cells</li> </ul>

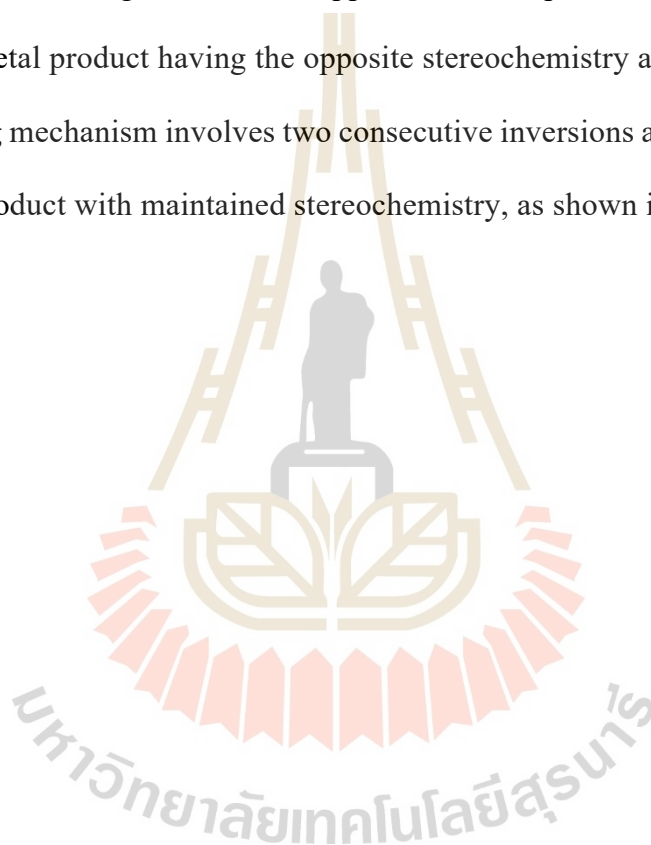
## 2.5 Glycoside hydrolases, including GBA and GBA2

Henrissat developed an alternative classification system for glycoside hydrolases based on amino acid sequence and structural similarity with members in animals, plants, fungi, archaea, and eubacteria (Lombard, Golaconda Ramulu et al., 2014). In this system, those enzymes with overall amino acid sequence similarity and well-conserved sequence motifs are grouped into the same family. At this writing, 115 glycoside hydrolase families are listed in the frequently updated Carbohydrate Active enZYme (CAZY) Web site (<http://www.cazy.org>).

$\beta$ -Glucosidases have various structures, but the overall fold of the catalytic domain is similar in each GH family. The families GH1, GH5, and GH30 belong to the Clan GH-A, and they all have similar (b/a)<sub>8</sub>-barrel domains that contain their active site. GH9 enzymes have (a/a)<sub>6</sub>-barrel structures, while the GBA2 family shows weak homology to proteins with this (a/a)<sub>6</sub> structure as shown in Figure 2.14. The clan GH-A enzymes of families GH1, GH5, and GH30 all have a common (b/a)<sub>8</sub>-barrel structure and their active sites contain two conserved carboxylic acid residues on b-strands 4 and 7, serving as the catalytic acid/base and nucleophile, respectively (Cairns and Esen, 2010).

In addition, the human bile acid  $\beta$ -glucosidase/GBA2 glucocerebrosidase and its relatives were assigned to a family GH116. The families that have similar catalytic domain structures and conserved catalytic amino acids, suggestive of a common ancestry and catalytic mechanism, are grouped into clans (Cairns and Esen, 2010). The GH30 human acid b-glucosidase (GBA) and the bile acid  $\beta$ -glucosidase or GBA2, these enzymes are thought to play roles in metabolism of glycolipids and dietary glucosides (Cairns and Esen, 2010).

Glycoside hydrolases (GH, O-glycoside hydrolases, EC 3.2.1) are enzymes that catalyze hydrolysis at the anomeric carbon of glycosides, resulting in formation of a hemiacetal or hemiketal and the corresponding free aglycon or reducing end saccharide. Hydrolysis can proceed with either net retention or inversion of stereochemistry at the anomeric center. Most often, two active site carboxyl residues are responsible for catalysis. The inverting mechanism happens in one step via a single displacement to get a hemiacetal product having the opposite stereochemistry at the anomeric center. The retaining mechanism involves two consecutive inversions at the anomeric center, yielding a product with maintained stereochemistry, as shown in Figure 2.15.



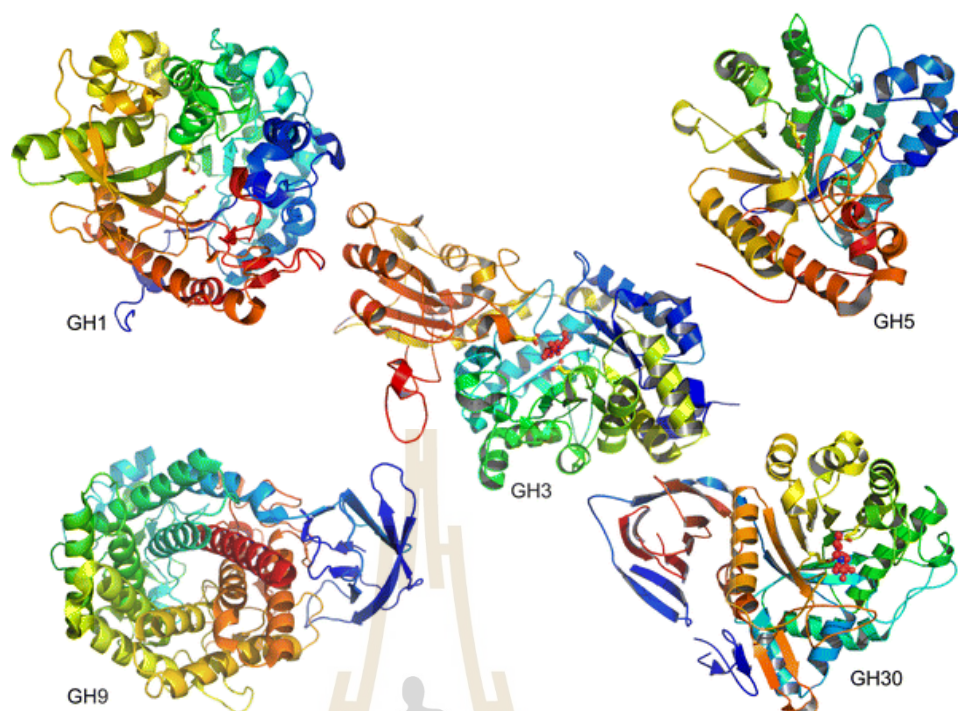


**Figure 2.14** Structures of  $\beta$ -glucosidases from different GH families. These include  $\beta$ -glucosidases or related enzymes from GH1 (*Zea mays* ZmGlu1, PDB code 1E1E), GH3 (*Hordeum vulgare* Exo I  $\beta$ -glucan glucohydrolase, PDB code 1EX1), GH5 (*Candida albicans* exo- $\beta$ -(1,3)-glucanase Exg exoglucanase, PDB code 1CZ1), GH30 (*Homo sapiens*, acid  $\beta$ -glucosidase/glucoocerebrosidase GBA, PDB code 2V3D), and GH9 (*Vibrio parahaemolyticus*, putative exoglucanase, PDB code 3H7L). The ligands shown are glucose in the GH3 barley ExoI and N-butyl-deoxynojirimycin in the GH30 human GBA, both of which are shown with carbons in pink. The human GBA2 (bile acid  $\beta$ -glucosidase) shows low levels of sequence similarity to ( $\alpha/\alpha$ )<sub>6</sub> enzymes, (Cairns and Esen, 2010).

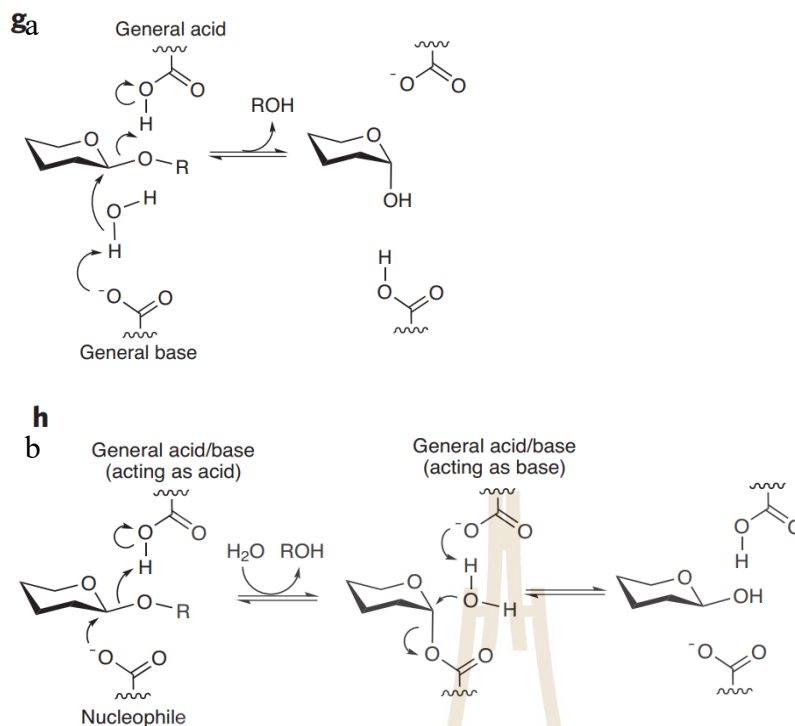


**Figure 2.15** Generalized inverting mechanism for glycoside hydrolysis (a) and generalized retaining mechanism for glycoside hydrolysis (b).

Glucosylceramide is degraded to ceramide and glucose by a class of  $\beta$ -glucosidases called glucosylceramidases (EC 3.2.1.45), lysosomal acid  $\beta$ -glucosidase (GBA), localized in the lysosome, while  $\beta$ -glucosidase 2 (GBA2), which was originally thought to associate with the plasma membrane, but was later shown to be found on the cytoplasmic face of the endoplasmic reticulum and Golgi (Kallemeijn, Witte et al., 2014, Sultana, Reichbauer et al., 2015). GBA and GBA2 are members of glycoside hydrolase families GH30 and GH116 family, respectively, based on amino acid sequence similarity.

The GBA open reading frame (ORF) nucleotide sequence is 1611 nucleotides, which is contained in 11 exons of the GBA gene on the human chromosome 1 reverse strand. The ATG codons are in exon 1 and 2, respectively; while coding of the mature

protein begins in exon 3 (deduced based on the human GBA sequence) (Stratil, Wagenknecht et al., 2004). The exon sequences coding for the signal peptide contain 117 nt (long form ATGGAGTTT.....GGGCATCAG) to yield a 39-amino acid residue signal sequence to target the protein into the lysosome and sequences for mature protein 1491 nt (stop codon is not included) (Stratil, Wagenknecht et al. 2004). GBA protein contains 536 amino acid residues with predicted molecular weight of 59.72 kDa. GBA protein has four glycosylation sites at p.Asn58, p.Asn98, p.Asn185, and p.Asn309 (N19, N59, N146, and N270, respectively), and its catalytic residues are located at p.Glu274 and p.Glu379 (E235 and E340, respectively, in the mature protein) (Hruska, LaMarca et al., 2008).

The human GBA2 ORF nucleotide sequence comprises 2784 nucleotides, which are contained in the 17 exons of its gene located on chromosome 9. GBA2 protein contains 927 amino acid residues with a predicted molecular weight of 104 kDa. Fortunately, our lab's previous study from (Charoenwattanasatien, Pengthaisong et al., 2016) generated a human GBA2 structural model that, when superimposed with the *TxGH116* complex with glucose X-ray crystal structure, identified active site residues of human GBA2 and the *TxGH116* (Charoenwattanasatien, Pengthaisong et al., 2016). All of the sugar binding residues are conserved between *TxGH116* and GBA2, as well as the aspartate (D508) that interacts with H507 in *TxGH116* (Charoenwattanasatien, Pengthaisong et al., 2016).

The first indication of GBA2 that it was involved in glucosylceramide metabolism by using mice deficient in GBA2 and found that these animals had normal bile acid metabolism, suggesting that GBA2 hydrolyzed glucosylceramide to glucose and ceramide; the same reaction catalyzed by the  $\beta$ -glucosidase acid (GBA) (Yildiz,

Matern et al., 2006). Then, the non-lysosomal glucosylceramidase was identical to the earlier described bile acid  $\beta$ -glucosidase, being  $\beta$ -glucosidase 2 (GBA2) as well as in mice pharmacological inhibition of GBA2 activity is associated with impaired spermatogenesis, a phenomenon also very recently reported for GBA2 knock-out mice (Boot, Verhoek et al., 2007).

One of the study has provide that glucosylceramide accumulation in GBA2 knockout-mice alters cytoskeletal dynamics due to a more ordered lipid organization in the plasma membrane (Raju, Schonauer et al., 2015). Thus, this result can concluded that glucosylceramide regulates cytoskeletal dynamics as the first indication that it was involved in glucosylceramide metabolism (Raju, Schonauer et al., 2015).

## **2.6 Involment of GBA and GBA2 deficiocy in human diseases**

### **2.6.1 Complete deficiency effects**

Gaucher disease (GD) is an autosomal recessive disorder caused by the deficiency of GBA leads to accumulation of glucosylceramide in the lysosome (Hruska, LaMarca et al., 2008) as well as cumulative evidence from previous studies suggests that GBA2 could play a role in the pathogenesis of GD and potentially interacts with GBA (Yildiz, Hoffmann et al., 2013). Three major clinical types of GD have been described, Types 1, 2, and 3. GD type 1 is characterized by the presence of clinical or radiographic evidence of bone disease and the absence of primary central nervous system disease (Pastores and Hughes, 2018). GD types 2 and 3 are characterized by the presence of primary neurologic disease (Pastores and Hughes, 2018). Moreover, the 3 types of Gaucher disease have different severity of symptoms and GBA mutations (Pastores and Hughes, 2018). Lysosomal storage of the substrate GlcCer in cells of the

reticuloendothelial system leads to multisystemic effects, including involvement of the liver, spleen, bone marrow, lungs, and nervous system. Almost 300 unique mutations have been reported in the GBA gene, with a distribution that spans the gene. These include 203 missense mutations, 18 nonsense mutations, 36 small insertions or deletions that lead to either frameshifts or in-frame alterations, 14 splice junction mutations, and 13 complex alleles carrying two or more mutations in cis (Hruska, LaMarca et al., 2008). One study showed that homozygosity for L444P GBA results in type 3 GD, albeit with remarkable variability in severity (Ferraz, Kallemeijn et al., 2014).

A previous study showed that the deletion of GBA2 in Gaucher disease (GD) model mice, considerably rescued the clinical phenotype, suggesting that the two enzymes interact through the accumulation of their common substrates, glucosylceramide (GlcCer) and possibly glucosylsphingosine (GlcSph), as shown in Figure 2.16 (Mistry, Liu et al., 2014).

As mentioned, besides lysosomal GBA, cells also contain a non-lysosomal glucosylceramidase (GBA2), given that the two  $\beta$ -glucosidases share substrates. Thus, speculated that over-activity of GBA2 during severe GBA impairment might influence neuropathology (Marques, Aten et al., 2015).

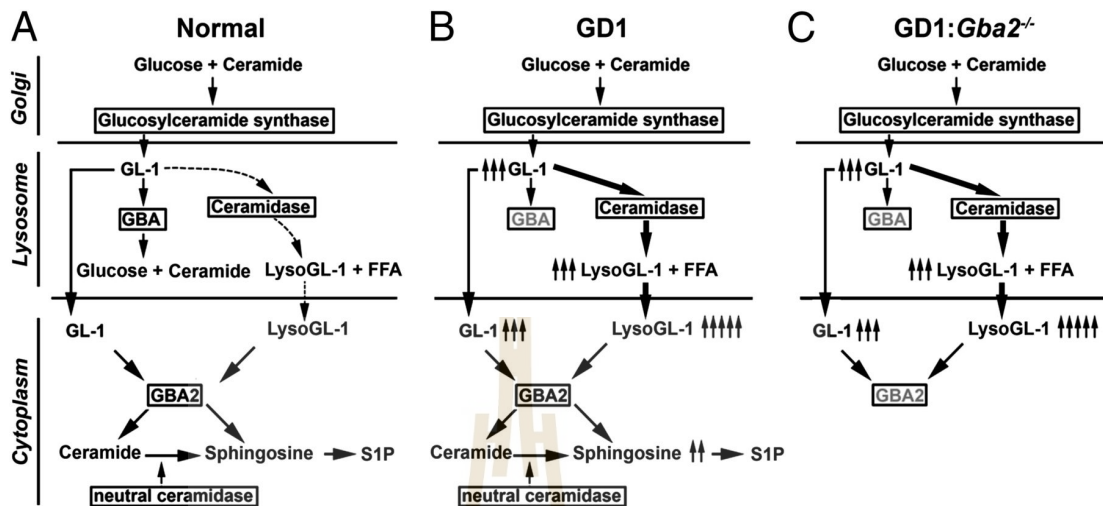


**Figure 2.16** Aberration of sphingolipid pathways in GBA deficiency.

Therefore, it appears that GBA2 may contribute to GD. Moreover, reduced GBA activity primarily results in accumulation of two substrates, GlcCer and GlcSph, which are likely to be present in GD, and may also contribute to Parkinson's disease. It was demonstrated that GlcSph is a more selective biomarker than GlcCer for neuronopathic GD (Hamler, Brignol et al., 2017). The role of GBA2 in Gaucher disease pathology and its relationship to GBA is not well understood. A recent report, investigated a possible feedback loop involving GBA2. The results showed that sphingosine, a cytotoxic metabolite accumulating in Gaucher cells through the action of GBA2, directly binds to GBA2 and inhibits its activity. Therefore, sphingosine, the product of breaking down GlcSph (glucosylsphingosine), can inhibit GBA2 activity. GlcSph can be easily measured in GD patient plasma and it is useful as a diagnostic marker for GD. GlcSph can be measured from a single-phase total lipid extraction of plasma by liquid

chromatography–electrospray ionization–tandem mass spectrometry (Fuller, Szer et al., 2015).

Loss of GBA2 function also results in accumulation of glucosylceramide, but with different clinical manifestations (Woeste and Wachten, 2017). Mutations in the human GBA2 gene have been associated with hereditary spastic paraplegia (HSP), autosomal-recessive cerebellar ataxia (ARCA) and Marinesco-Sjögren-like syndrome (Woeste and Wachten, 2017). The discovery that GBA2 mutations can lead to HSP and ARCA with spasticity, suggests a role for GBA2 in cerebral neuron maintenance (Martin, Schüle et al., 2013, Hamler, Brignol et al., 2017). Lack of GBA2 activity is associated with a specific hereditary spastic paraplegia/cerebellar ataxia complementation group called SPG46, which constitute a group of clinically and genetically heterogeneous neurodegenerative diseases characterized by progressive spasticity and weakness of the lower limbs (Sultana, Reichbauer et al., 2015). The genomic sequencing study of HSP patients found that four different GBA2 mutations (three variants causing truncations of the protein and one missense variant), which were found to co segregate with the disease (Martin, Schüle et al., 2013). It was later found that GBA2 mutations can also cause a Marinesco-Sjögren-like Syndrome (Haugarvoll, Johansson et al., 2017). Furthermore, these investigators found that leukocytes seem to be an acceptable enzyme source for *in vitro* analysis of GBA2 activity that may correlate with phenotypic variability associated with GBA2 mutations, and suggested that patients with Marinesco-Sjögren-like syndrome should be tested for mutations in this gene. Since there are relatively few ARCA, HSP and Marinesco-Sjögren-like syndrome patients with GBA2 mutations, the role of GBA2 in these syndromes is not well understood.

### 2.6.2 GBA mutation involvement in Parkinson's disease

In recent years, it has been recognized that carriers of a mutant GBA gene are at about 20-fold increased risk for developing Parkinson disease (PD) compared to general population (Siebert, Sidransky et al., 2014). In addition, a previous study has showed that a significant reduction of GBA activity was associated with increased total alpha-synuclein accumulation (Taguchi, Liu et al., 2017). Furthermore, PD patients had significantly higher odds for carrying the common GBA mutations than patients having Alzheimer's disease and healthy subjects (Aerts, Kuo et al., 2019). Thus, heterozygous GBA mutations were identified as risk factors for PD in about 3-9% of the patients (Aerts, Kuo et al., 2019).

Subsequence studies in various ethnicities including Chinese, Caucasians of multiple origins, and Japanese have consistently confirmed the correlation, especially in individuals with early onset PD. In such patients, GBA mutations such as L444P, N370S, R120W and IVS2+1G>A, were common among multiple ethnicities. Furthermore, homozygous L444P mutation is almost invariably associated with nervous system disorders, whereas the N970S mutation is less related to neurological symptoms (Aerts, Kuo et al., 2019).

A recent study by Teeratom Pulkes et al (Pulkes, Choubtum et al., 2014) revealed 5 novel putative GBA mutations in Thai PD patients, including 1275C>A (N386K), 1399C>T (P428S), 1309delG, IVS9+3G>C and IVS10-9\_10GT>AG, as shown in Table 2.2, along with 2 common mutations, L444P and IVS2+1G>A. Their results suggested that 1309delG, IVS9+3G>C and IVS10-9\_10GT>AG are mutations that likely lead to GBA deficiency and loss of function. The 1309delG mutation is in exon 9 and was predicted to result in substitution of valine by serine at the codon 437, and a frameshift leading to a premature stop codon at codon 443, leading to translation of an abnormal shorter protein product (442 instead of the normal 536 amino acid residues). IVS9+3G>C and IVS10-9\_10GT>AG are also

thought to result in abnormal splicing that leads to frame shifts and translation to truncated protein products. These results provided evidence that GBA mutations are important risk factors for PD in Thailand and that the L444P mutation is common in Thai PD patients having GBA mutations (Pulkes, Choubtum et al., 2014).



**Table 2.2** GBA mutations identified in Thai PD patients (Pulkes, Choubtum et al., 2014).

Nucleotide substitution	Protein	Allele name	Location	EOPD		AAO > 50y-PD		All PD		Controls	
				N	%	N	%	N	%	N	%
<b>Known mutation</b>											
C. 1448T < C	p.Leu483Pro	L444P	Exon 10	8	7.4	7	1.9	15	3.1	1	0.3
IVS2+1G > A	Skipping of exon 2		Intron 2	1	0.9	0	0	1	0.2	0	0
<b>Novel mutations</b>											
c.1275C > A	p.Asn425Lys	N386K	Exon 9	1	0.9	0	0	1	0.2	0	0
c.1399C > T	p.Pro467Ser	P428S	Exon 10	1	0.9	1	0.3	2	0.4	1	0.3
c.1309delG	Premature stop at condon 443	V398fsX404	Exon 9	1	0.9	0	0	1	0.2	0	0
IVS9+3G > C	Possible truncated protein		Intron 9	1	0.9	0	0	1	0.2	0	0
IVS10-9_10GT > AG	Possible truncated protein		Intron 10	1	0.9	2	0.5	3	0.6	0	0
<b>Total</b>				14	12.8	10	2.7	24	5.0	2	0.5

Abbreviations are as follow: PD = Parkinson's disease; EOPD = early-onset Parkinson's disease;

AAO > 50y-PD = Parkinson's disease with age at onset over 50 years. <sup>a</sup>The cDNA sequence numbering is from GenBank reference sequence NM\_001005741.2 <sup>b</sup>Protein names are based on the primary translation precursor protein, including the 39-residue signal peptide. <sup>c</sup>Allele names use the common published nomenclature, which do not include the 39-residue signal peptide.

As mentioned above, the previous study provides the GBA mutation associated with PD, but the relation between heterozygous GBA mutations and sphingolipid profiles in Thai PD patients has yet to be investigated. Therefore, I studied the sphingolipid levels in Thai PD patients with heterozygous GBA and Parkin mutations to see if there is a correlation of mutations with GlcCer and other sphingolipid levels.

## 2.7 Alternative splicing and GBA2 isoforms

One important process to regulate gene function in the eukaryotic cell after transcription is alternative splicing of pre-mRNA to generate two or more mature mRNAs, which leads to greater protein diversity (Breitbart, Andreadis et al., 1987). It means that a single gene can translate into many proteins, which are called protein isoforms, as shown in Figure 2.17.

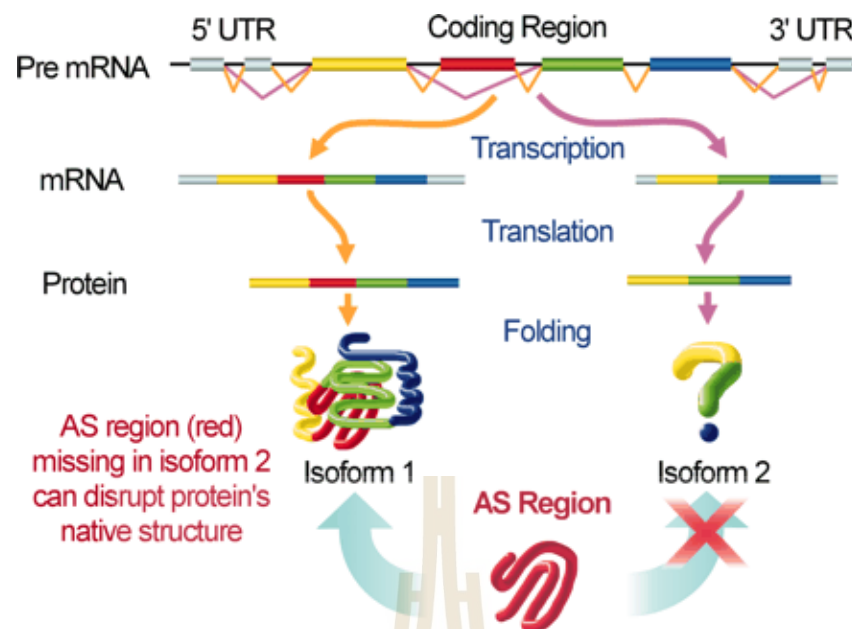


**Figure 2.17** Alternative splicing and its potential effects on protein structure (Romero, Zaidi et al., 2006).

In a previous report, the authors investigated whether alternative splicing can contribute to disease by setting up the hypothesis that polypeptide segments affected by alternative splicing are most often intrinsically disordered (Romero, Zaidi et al., 2006).

In such a case, alternative splicing would enable functional and regulatory diversity while avoiding structural complications. During transcription, RNA is generated from a gene and processed to form the mRNA that will be translated into protein, hence the designation 'pre-mRNA'. The mRNA to be translated is assembled from pre-mRNA by splicing the introns away, so that only the exons remain. They developed a machine-learning technique that scores how strongly genetic variants affect RNA splicing, the alteration of which contributes to many diseases. They analyzed more than 650,000 intronic variants, which revealed intronic disease mutations that are more than 30 nucleotides from any splice site alter splicing nine times

as often as common variants, and that missense exonic disease mutations that have the least impact on the protein structure and derived function are five times as likely as others to alter splicing (Xiong, Alipanahi et al., 2015). This complexity makes splicing susceptible to sequence polymorphisms and deleterious mutations. Indeed, RNA mis-splicing underlies many human diseases, which can have serious consequences for our society (Scotti and Swanson, 2016).

For neurological disease, some research groups have investigated the role of alternative splicing in the regulation of diverse biological processes and provided evidence that alternative splicing plays a particularly important role in neurological disease, as shown in Table 2.3 (Van Cauwenberghe, Van Broeckhoven et al., 2016). Therefore, alternative splicing of the GBA and GBA2 RNA may occur in their gene mutations, which can thereby may affect glycosphingolipid levels and GD, HSP or PD symptoms.

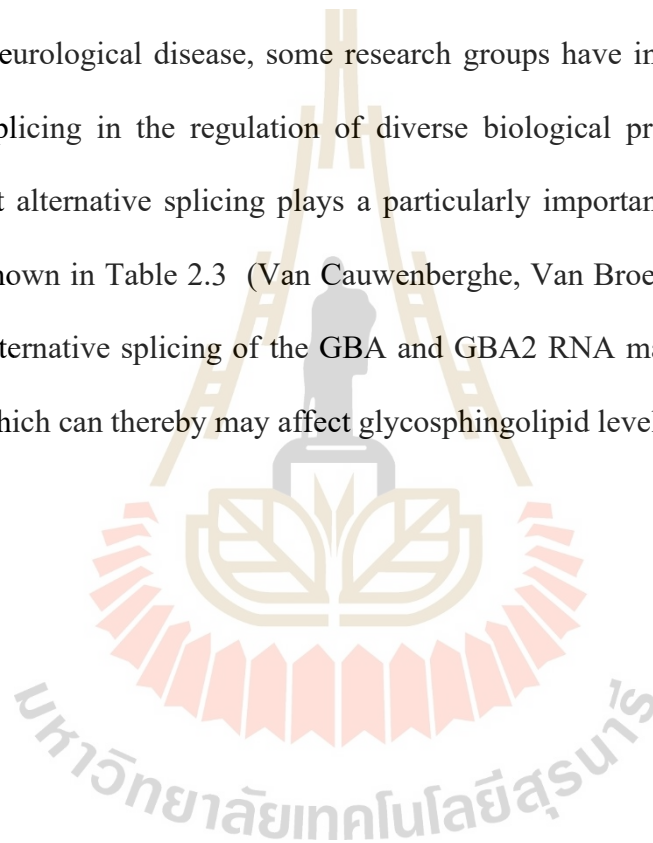


**Table 2.3** Disease-associated splicing alterations (Scotti and Swanson, 2016).

Disease	Gene (mutation)	Mechanism	Splicing effect	Inheritance
Cis				
Limb girdle muscular dystrophy type 1B (LGMD1B)	LMNA <sup>2+</sup> (c.1608+5G>C)	5'ss mutaion	Intron 9 retention resutling in NMD	Dominant
Familial partial lipodystrophy type 2 (FPLD2)	LMNA <sup>25</sup> (c.1488+5G>C)	5'ss mutation	Intron 8 retention resutling in NMD	Dominant
Hutchinson-Gilford progeria syndrome (HGPS)	LMNA <sup>26</sup> (c.1824C>T)	Alternative 5'ss	150 nt deletion in exon 11, resulting in progerin generation	Dominant
Dilated cardiomyopathy (DCM)	LMNA <sup>28</sup> (c.640-10A>G)	Alternative 3'ss	Extension of exon 4 adding 3 amino acids to lamin A/C	Dominant
Familial dysautonomia (FD)	IKBKAP <sup>128</sup> (c.2204+6T>C)	Decreased U1 recruitment	Exon 20 skipping	Recessive
Duchenne muscular dystrophy (DMD)	DMD <sup>129</sup> Exon 45-55 deletions are common	Exon deletions and skipping	Framshift resulting in NMD	X-linked
Becker muscular dystrophy	DMD <sup>130</sup> (c.4250T>A)	ESS creation	Exon31 partial in-frame skipping	X-linked
Early-onset Parkinson disease (PD)	<i>PINK1</i> (REF.131)(c.1488+1G>A)	U1 5'ss mutation	Cryptic splice site usage, resulting in exon7 skipping	Recessive
Frontotemporal dementia with parkinsonism chromosome17 (FTDP-17)	MAPT <sup>132</sup> (c.892A>G)	ESS mutation	Increased exon 10 inclusion	Dominant
X-linked parkinsonism with spasticity (XPDS)	ATP6AP2 (REF. 133)(c.345C>T)	Novel ESS creation	Increased exon4 exclusion	X-linked

A BLASTp search of human proteins with GBA2-related protein sequences results in 14 protein isoforms, including isoform1, isoform2, isoformX1, isoformX2, isoformX3, isoformX4, isoformX6, isoformX7, isoformX8, isoformX9, isoformX10, isoformX11, isoformX12 and isoformX13. All of these isoforms show 97-100% identity compared with isoform1, which matches the translation from the original cloned cDNA, but some are missing some part of the sequence and/or have additional sequence inserted into it.

Charoenwattanasatien et al. solved the X-ray crystal structure of the first family GH116 member, *Thermoanaerobacterium xylanolyticum* TxGH116  $\beta$ -glucosidase, and predicted the structure of human GBA2  $\beta$ -glucosidase. It contains N-terminal  $\beta$ -

sandwich and C-terminal solenoid domains. The catalytic site is found in the C-terminal domain. They also predicted a very similar structure for the human GBA2 enzyme and explained the effect of disease causing GBA2 mutants on the protein structure and activity. Therefore, it should be possible to predict the structures of the additional 13 observed or predicted amino isoforms from the TxGH116 structure and predict which are likely to form a similar stable structure (Charoenwattanasatien, Pengthaisong et al., 2016). Therefore, we conducted this study in order to solve the question of which of the GBA2 isoforms form active structures and are likely to be biologically significant.

## **2.8 Protein expression systems and expression of glucosylceramidases**

To achieve human GBA2 expression in animal cell line systems, IMR-32 and SH-SY5Y (human neuroblastomas), RAW264/7 (murine monocyte/macrophage), THP-1 (human monocyte), and COS-7 cells (African green monkey kidney) were transfected with a protein expression plasmid containing a cDNA-encoding human GBA2 (C-terminally DYK- and Myc-tagged) in the pCMV6-NeoR mammalian expression vector (Ridley, Thur et al., 2013). In order to study effect of GBA and GBA2 on glycosphingolipid levels in cells, the experiments have been performed by using animal cell lines, including mouse embryonic fibroblast from wild-type and GBA- or GBA2-knockout mice, human fibroblasts, HAP1, Human embryonic kidney 293 (HEK293) cells, and HeLa delta SGPL1 (Sphingosine-1-Phosphate Lyase 1) were culture in cell culture media, then cellular glycosphingolipid levels were quantified by mass spectrometry (Schonauer, Körschen et al., 2017). However, no previous publications have reported the effect of expression of GBA2 in animal cell lines on

sphingolipid levels in the cells or the expression of different GBA2 isoforms. Utilization of the eukaryotic cell system allows evaluation of the levels of glycosphingolipids that are affected by GBA2 activity and may act as biomarkers for neurological disease.



# CHAPTER III

## MATERIALS AND METHOD

### 3.1 General materials

#### 3.1.1 Chemicals and reagents

Chemical reagents used in this work and their sources are shown in Table 3.1

**Table 3.1** Chemical reagent and sources.

Reagent	Source
Acetic acid	Carlo Erba
Ammonium sulfate	
Chloroform	
Citric acid	
Calcium chloride	
Di-sodium hydrogen phosphate	
Di-sodium hydrogen phosphate anhydrous	
Ethylenediaminetetraacetic acid disodium salt (EDTA)	
Ethanol	
Formic acid	

**Table 3.1** Chemical reagent and sources (Continued).

<b>Reagent</b>	<b>Source</b>
Glycerol	Carlo Erba
Hydrochloric acid	
Isopropanol	
Methanol	
Sodium acetate anhydrous	
Sodium carbonate anhydrous	
Sodium dodecyl sulfate (SDS)	
Sodium chloride	
Tris (hydroxymethyl)-aminomethane	
Calcium chloride	
Coomassie brilliant blue R250	Acros Organics
Dithiothreitol (DTT)	
Ethidium bromide (EtBr)	
2-Mercaptoethanol	
Triton X-100	
QIAQuick gel purification kit	QIAGEN
QIAQuick PCR purification kit	

**Table 3.1** Chemical reagent and sources (Continued).

<b>Reagent</b>	<b>Source</b>
Vivantis plasmid miniprep	Vivantis
Agarose	
<i>Taq</i> DNA polymerase	
Protein marker	
GeneJET Gel Extraction kit	ThermoFisher
Pierce™ BCA Protein Assay Kit	Scientific
Dulbecco's Modified Eagle Medium	
Penicillin streptomycin	
Trypsin/EDTA	
fetal bovine serum (FBS)	
<i>Pfu</i> DNA polymerase	Promega
Deoxyribonucleotide triphosphates (dATP, dGTP, dCTP, and dTTP)	
T4-DNA ligase	
Dimethyl sulfoxide (DMSO)	Sigma
Glass beads 500-700 um	
Sodium hydroxide	Merck

**Table 3.1** Chemical reagent and sources (Continued).

<b>Reagent</b>	<b>Source</b>
Bacto-agar	HiMedia
Peptone	
Yeast extract	
Skim milk	
Restriction enzymes: <i>EcoRI</i> , <i>NotI</i> , <i>XhoI</i> , <i>Sall</i> , <i>XbaI</i> , <i>NheI</i>	New England Biolabs
HPLC grade water	Labscan
Acetonitrile	

### 3.1.2 Synthetic genes, plasmid and bacterial stain

In the Genbank non-redundant protein database, in addition to the primary human GBA2 isoform, isoform1, 13 predicted splice variant isoforms were found. However, in this study we focused on 9 isoforms, the human GBA2 major transcript (isoform1, NM\_001330660.1), isoform2 (NM\_001330660.2), isoform X1 (XM\_006716809.3), isoform X2 (XM\_005251526.4), isoform X3 (XM\_017014937.1), isoform X4 (XM\_017014938.1), isoform X6 (XM\_017014939.1), isoform X7 (XM\_017014940.1), and isoform X8 (XM\_017014941.1). The corresponding cDNAs were synthesized and inserted into the pcDNA3.1+/c-(k)-dyk expression vector for mammalian cells by GenScript Corporation (Piscataway, NJ USA). *E.coli* strain DH5 $\alpha$  was used for cloning to increase the amount of recombinant plasmid for cell line transfection.

## 3.2 General methods

### 3.2.1 Preparation of *E. coli* strain DH5 $\alpha$ competent cells

*E. coli* strain DH5 $\alpha$  glycerol stock was streaked on LB plates without antibiotic and incubated at 37 °C for 16-18 h until colonies were visible. A single colony was picked and inoculated into 5 mL of LB broth without antibiotic and grown with shaking at 37 °C, 200 rpm for 16-18 h. Then, 100  $\mu$ L of starter culture was moved to 100 mL of LB broth in a 250 mL Erlenmeyer flask, which was then shaken at 37 °C, 200 rpm until the optical density at 600 nm (OD<sub>600</sub>) reached 0.4-0.6. The cell culture was chilled on ice for 5 min and collected at 4,000 rpm at 4 °C for 10 min, then the cell pellet was resuspended in 10 mL of ice-cold, sterile 0.1 M CaCl<sub>2</sub> and centrifuged to collect the pellets. Finally, the pellets were resuspended with 1 mL of 0.1 M CaCl<sub>2</sub>, containing 15% glycerol and 50  $\mu$ L aliquots were stored at -80 °C until use.

### 3.2.2 Transformation of plasmid into competent *E. coli* cells

A 50  $\mu$ L of aliquot frozen competent cells was thawed for 5 min on ice, then 1-10  $\mu$ L containing 20-100 ng of cloning or expression plasmids or ligation reactions were mixed with the thawed competent cells. The mixture was incubated on ice for 30 min, then the cells were transformed with plasmid by heat shocking at 42 °C for 1 min and quickly chilling on ice for 5 min. Then, 200  $\mu$ L of LB broth were added to the mixtures, which were then incubated at 37 °C, 200 rpm for 1 h. The transformed cells were spread on LB agar, which was contained ampicillin 100  $\mu$ g/mL and incubated at 37 °C overnight.

### 3.2.3 Plasmid isolation by alkaline lysis

A single colony that contain recombinant plasmid was picked into 5 mL of LB broth, followed by incubation at 37 °C with shaking at 200 rpm for 16- 18 h, then the cultures were moved to 1.5 mL tubes and were collected by centrifugation at 12,000 rpm, for 1 min, then removed the supernatant. Cell pellets were resuspended by pipetting with 100 µL of ice-cold lysis buffer I, which contained 50 mM glucose, 10 mM EDTA, 50 mM Tris-HCl, pH 8.0, followed by adding 200 µL of freshly prepared lysis buffer II, contained 0.2 N NaOH, 1% (w/v SDS) and the tubes were inverted by hand for 5-10 times until completely mixed. After that, 150 µL of ice-cold lysis buffer III, containing 3 M potassium acetate, pH 4.8, was added and the tubes were inverted 5- 10 times, until they were completely mixed. The alkaline lysis reactions were incubated in ice for 5 min, then centrifuged at 13,000 rpm for 10 min at 4 °C. The clear supernatant solution was transferred without disturbing the pellet to a 1.5 mL tube. One volume of phenol: chloroform: isoamyl alcohol (25: 24: 1) was added into the tube, which was then inverted 10 times. The mixture was centrifuged at 13,000 rpm for 10 min at room temperature, then the upper layer was transferred to a new 1.5 mL microcentrifuge tube without disturbing lower layer. Two volumes of absolute ethanol were added to the tube, and it was then incubated on ice for 30 min to overnight. The precipitated DNA pellet was collected by centrifugation at 13,000 rpm for 10 min. The leftover ethanol was removed by speed vacuum. Then, the DNA pellet was resuspended in 100 µL of TE buffer, pH 8.0, containing 2 µL of 1 mg/mL RNase A, then incubated at 37 °C for 10 min. After that, 70 µL of cold 20% PEG 6000/2.5 M NaCl was added and the tube incubated on ice for 1 hour. Centrifugation at 12,000 rpm for 10 min pelleted the DNA and the supernatant was removed. After that, the pellet

was washed with 500  $\mu$ L 70% ethanol and centrifuged at 14,000 rpm 4  $^{\circ}$ C for 10 minutes to remove the remaining PEG and NaCl. The pellet was dried at 50  $^{\circ}$ C in an oven, then dissolved in 50  $\mu$ L TE buffer. Finally, the DNA solution was kept in -80  $^{\circ}$ C until use.

### 3.2.4 Vivantis plasmid miniprep

The *GF1* plasmid DNA extraction kit was used for plasmid DNA extraction from *E. coli* strain DH5 $\alpha$  according to the manufacturer's instructions. Each single colony was picked into 5 mL LB broth with 50  $\mu$ g/mL of ampicillin, to select for the *pcdna3.1+/-c-(k)dyk* plasmid, which contains the ampicillin resistance gene. The culture was grown overnight for 16 hours at 37  $^{\circ}$ C with agitation. Cell pellets from 1.5-5 mL of bacterial culture were collected by centrifugation at 6,000 x g for 2 min at room temperature, and the medium was completely removed and discarded. The pellet was resuspended in 250  $\mu$ L of S1 reagent by pipetting. Then, 250  $\mu$ L of S2 reagent was added into the suspension and the tube was gently mixed by inverting for 4-6 times. To neutralize the lysate, 400  $\mu$ L of NB buffer was added, then gently mixed by inverting the tube for 6-10 times until a white precipitate formed. The tube was centrifuged at 14,000 x g for 10 min. The supernatant was transferred into a column assembled in a clean collection tube, then centrifuged at 10,000 x g for 1 min, and the flow through was discarded. Then, 700  $\mu$ L of wash buffer was added into the column, which was then centrifuged at 10,000 x g for 1 min, and the flow through was discarded. The empty column was centrifuged at 10,000 x g for 1 min to remove residual ethanol, then the column was placed into a sterile 1.5 mL tube. Then, 50  $\mu$ L of elution buffer was added directly onto the column membrane and the column was left to stand for 1 min.

Finally, the column was centrifuged at 10,000 x g for 1 min to elute the DNA. The DNA sample was stored at -40 °C or -20 °C until use.

### **3.2.5 Agarose gel electrophoresis**

DNA samples were checked by agarose gel electrophoresis through 1-2% agarose gels (depending on the DNA size, below 500 bp in 2% agarose, and more than 500 bp in 1% agarose) prepared in 1X TAE (40 mM Tris HCl, pH 8.0, 40 mM acetic acid, 1 mM EDTA, pH 8.0) or TBE buffer (90 mM Tris HCl, pH 8.0, 89 mM boric acid, 2.5 mM EDTA, pH 8.0). The DNA samples were mixed 5:1 with 6X NEB DNA loading dye (0.025% (w/v) bromophenol blue, 0.025% (w/v) xylene cyanol, 30% (v/v) sterilized glycerol, New England BioLabs). Agarose gel electrophoresis was performed in a gel electrophoresis apparatus (Bio-Rad) at a constant voltage of 100-120 V for 22-35 min. The DNA bands in the agarose gel were detected by staining with ethidium bromide (0.1 µg/mL) for 1 min, then de-staining in distilled water for 5-10 min or until sharp bands were visualized by UV irradiation on a transilluminator (Bio-Rad). The size of the DNA in the bands was estimated by comparing their migration with those of known bands in 100 bp or 1 kb DNA ladder.

### **3.2.6 Gel extraction and purification**

The target DNA bands with the expected size that were separated on agarose gel electrophoresis were purified with the GeneJET Gel Extraction kit (ThermoFisher Scientific). The agarose gel band containing the target DNA band was excised with a blade cutter, then transferred to a 1.5 mL tube and weighed. An equal volume of binding buffer was added to the gel slice (volume: gel weight = 1), and the gel mixture was incubated at 50-60 °C for 10 min or until the gel was completely dissolved. Up to 800 µL of solubilized gel solution was transferred to the GeneJET purification column,

which was then centrifuged for 1 min at 10,000 rpm. The flow-through solution was discarded and column reassembled. Then, 700  $\mu$ L wash buffer (3M sodium acetate in 75% ethanol solution) was added to the column, which was then centrifuged for 1 min at 10,000 rpm, and the flow-through was discarded. The empty column was centrifuged for an additional 1 min to completely remove the residual wash buffer. The GeneJET column was moved into a clean 1.5 mL tube, then 50  $\mu$ L of elution buffer (TE buffer was composed of 1 M of tris base pH 10-11 and 0.5 M of EDTA) was added, and the tube was centrifuged for 1 min at 10,000 rpm. Finally, the purity and concentration of the DNA solution was assessed by absorbance at 260 nm and 280 nm in a nanodrop spectrophotometer. A 260/280 absorbance ratio of  $\sim$ 1.8 is generally accepted as “pure” for DNA; a ratio of  $\sim$ 2.0 is generally accepted as “pure” for RNA and the DNA quality and quantity were estimated by gel electrophoresis. The remaining purified DNA was stored at -20 °C until use.

### **3.2.7 COS-7 cell culture**

The Gibco DMEM used for COS-7 cell medium was prepared according to the manufacturer’s instructions, procedure D (prepare powdered medium), as described in the appendix. COS-7 cells were obtained from Aj. Lukana Ngiwsara, Chulabhorn Research Institute, Bangkok, and seeded into 75 cm<sup>2</sup> cell culture flask with DMEM containing 10% Pen-Strep.

### 3.2.8 Trypsynization

COS-7 cells were cultured in DMEM at 37 °C, 5% CO<sub>2</sub> until the percent confluency reached 80-90%. The medium was removed and washed 1 time with sterile 1X PBS, which was then discarded. One milliliter of trypsin/EDTA solution was added into cell culture flask to ensure that the volume covered the entire flask surface on which cells are adherent. The plate was incubated at 37 °C for 3-5 min or until the cells were completely removed from the flask surface. 5 mL of complete medium (DMEM containing 10% FBS) was added to suspend the cells, then the cell suspension was transferred to a 15 mL tube, and centrifuged at 1,200 rpm for 2 min. The supernatant was removed, complete medium was added and the cells were resuspended. A 10 µL aliquot of the cell suspension was mixed with 0.4% trypan blue at the ratio 1:1, and these cells were counted in a TC20™ Automated Cell Counter. Finally, the 2×10<sup>5</sup> cells of cell suspension were seeded into the new cell culture flask with 5 mL complete medium for the next cell passage.

### 3.2.9 Protein extraction

COS-7 cells were cultured on 6 cm<sup>2</sup> cell culture plates for 48 hr and 72 hr incubation times. After trypsinization, 10 µL of cell suspension was counted with a TC20™ Automated Cell Counter as well as confirmed by hemocytometer. The medium was removed and washed 2 times with ice-cold 1X PBS, then the COS-7 cells were collected in 1 mL of ice-cold 1X PBS by scraping, then the cell suspension was transferred to a 1.5 mL tube on ice. The cell suspension was centrifuged at 4000 rpm at 4 °C for 10 min, and the supernatant was removed. One hundred microliters of sterile 1X PBS was added to the cell pellets, and the tubes were then vortexed for 10 s. The

cell suspension was used for protein extraction for protein assay, GBA2 activity, and western blotting analysis, and lipid extraction for analysis by LC/MSMS.

### **3.2.10 Protein extraction for GBA2 activity and western blotting**

The cell suspension was sonicated on ice at 30% amplitude for 12 cycles with 5 s sonication and 5 s stop with a Q2000 SONICATOR. Extracted cells were diluted to 1:20 in 1X PBS and stored in -80 °C until measurement of the protein concentration by BCA assay.

### **3.2.11 Protein extraction for back up LC/MSMS analysis**

The human fibroblast and human GBA2 transfected COS-7 cells was took to university of Melbourne. The remaining solution in the cell pellets was evaporated in a speed vacuum (speedyVap) for 2 min. Then, 200 µL of 2% SDS in 1X PBS (w/v) was added to the cell pellets obtained from approximately  $1 \times 10^6$  cells. The cell suspension was homogenized with a bullet blender after adding approximately 100 µL of beads, then 50 µL of 10% SDS was added, and the tube was incubated at 95 °C for 10 min or longer, until the pellet was dissolved. Extracted cells were stored in -80 °C until measurement of the protein concentration by BCA assay.

### **3.2.12 BCA assay protein concentration determination**

The Pierce™ BCA Protein Assay Kit (Thermo Scientific) was used for protein concentration determination, according to the manufacturer's instructions and the BSA protein standard concentrations were as shown in Table 3.2. Reagents A and B were mixed together at the ratio 100:3 (v/v) to make the working solution. Ten microliters of either sample or BSA standard were added to triplicate wells of a 96 well plate, followed by adding 160 µL of working solution, then the plate was shaken for 30 s, covered and incubated at 37 °C for 30 min. The plate was cooled to room temperature. The

absorbance at 562 nm was measured with the microplate reader spectrophotometer (BIO-RAD Benchmark Plus).

**Table 3.2** Preparation of diluted Albumin (BSA) standards.

<b>Vial</b>	<b>Volume of Dilution (<math>\mu\text{L}</math>)</b>	<b>Volume and Source of BSA (<math>\mu\text{L}</math>)</b>	<b>Final BSA concentration (<math>\mu\text{g/mL}</math>)</b>
<b>A</b>	0	300 of stock	2000
<b>B</b>	125	375 of stock	1500
<b>C</b>	325	325 of stock	1000
<b>D</b>	175	175 of vial B dilution	750
<b>E</b>	325	325 of vial C dilution	500
<b>F</b>	325	325 of vial E dilution	250
<b>G</b>	325	325 of vial F dilution	125
<b>H</b>	400	100 of vial G dilution	25
<b>I</b>	400	0	0 = Blank

### 3.3 Cloning and expression

#### 3.3.1 pcDNA 3.1 +/C-(k)-dyk empty vector production

In order to produce a control plasmid for COS-7 cell transfection, the human GBA2 cDNA was excised from the recombinant pcDNA 3.1 +/C-(k)-dyk/hGBA2-isoform-1 plasmid that was obtained from Genscript Corp (NJ, USA). The plasmid (100 ng) was cut with 5 units each of *Xba*I and *Nhe*I restriction endonucleases (10,000 units/mL), in 1X NEBuffer™ 2.1. The reaction was incubated at 37 °C overnight. Then, the mixture was run in agarose gel electrophoresis to isolate the target band with 5,444 bp expected size, which was extracted from the gel and purified as described in Section 3.2.5. The absorbance of the DNA solution was measured by nanodrop spectrophotometer to determine the DNA concentration. Then, the linear DNA was ligated by T4 ligase (Promega Corporation), then transformed into *E.coli* DH5 $\alpha$ . A single colony was picked and cultured in LB broth with 50  $\mu$ g/mL ampicillin overnight. The bacterial culture was collected, and the plasmid DNA purified via the Vivantis plasmid miniprep kit (Section 3.2.3). The absorbance of the DNA solution was measured to determine the concentration and an aliquot was run on agarose gel electrophoresis to check that it had the correct size.

### 3.3.2 Cell line confluency optimization and transfection

One million COS-7 cells were seeded into a 6 cm<sup>2</sup> plate with DMEM medium, then cultured to 80-90% overnight. The medium was removed, and the plate washed 1 time with sterile 1X PBS, then 2 mL of opti-mem was added into the plate. Firstly, 240  $\mu$ L of opti-mem was mixed with 10  $\mu$ L of lipofectamine 2000 and a second aliquot of 230-240  $\mu$ L of opti-mem was mixed with 10-20  $\mu$ L containing 2  $\mu$ g total plasmid including either GBA2 isoform 1, isoform2, isoformX1, isoformX2, isoformX3, isoformX4, isoformX6, isoformX7 or isoformX8 cDNA or no insert and let to stand for 5 min at room temperature. The two solutions were mixed together (to give a total volume of 500  $\mu$ L), then incubated for 20 min at room temperature. The mixture was gently added drop by drop into the cell culture plate containing the cells in opti mem with gentle shaking, followed by incubation at 37 °C, 5% CO<sub>2</sub> for 6 hours. After 6 hours, the opti-mem was removed, and replaced by DMEM complete medium with antibiotics. Finally, the COS-7 cells were incubated for 48 hours and 72 hours, then collected for analysis.

### 3.4 Gene expression analysis

#### 3.4.1 Oligonucleotide primers

Custom oligonucleotides were purchased from Pacific Science (Thailand) and are shown in Table 3.3.

**Table 3.3** Oligonucleotide primers for GBA2 and GBA gene expression.

Primer name	Sequence (5'-3')
<b>GBA2 cDNA forward</b>	CCACTACAGGCGGTATACAA
<b>GBA2 cDNA reverse</b>	GATCTGTCATCCAATACCGG
<b>GBA cDNA check forward</b>	GTTCCAGAAAGTGAAGGGAT
<b>GBA cDNA check reverse</b>	TTCTCTGAAGAAGGAATCGG

#### 3.4.2 RNA extraction

COS-7 cells transiently transfected with the vectors for human GBA2 isoform expression or empty vector were collected after 48 hr and 72 hr incubation. Firstly, the media was removed, then washed with sterile 1X PBS for 5 mL. After that, 1 mL of Trizol reagent was added, then pipetted up and down to mix and lyse the cells. The suspension was moved to a 1.5 mL tube and 200  $\mu$ L of chloroform were added and mixed by tube inversion by hand 10 times. The suspension was centrifuged at 12,000 xg at 4 °C for 15 min, then of the upper layer was transferred to a new tube. Five hundred microliters of isopropanol was added to this tube and it was inverted 10 times and incubated at room temperature for 10 min, then centrifuged at 12,000 xg at 4 °C for 30 min. The supernatant was discarded, then 1 mL of 75% of ethanol was added to wash the pellet. The tube was centrifuged at 7,500 xg at 4 °C, the supernatant discarded,

and the pellet dried at room temperature. The pellet was then dissolved in 30  $\mu\text{L}$  RNase free water. The RNA concentration was determined by measuring the absorbance at 260 nm ( $1 A_{260} = 40 \mu\text{g/mL RNA}$ ) and 260/280 nm on a nano drop spectrophotometer to check the RNA purity and RNA quality was checked by 0.8% agarose gel electrophoresis to expect 2 bands, including 28S and 18S rRNA.

### 3.4.3 cDNA synthesis

The cDNA was synthesized with SuperScript III reverse transcriptase (Invitrogen, Thermo Fischer), according to the manufacturer's instructions. In order to make the RNA/primer mixture, the RNA extracted in Section 3.4.1 (2  $\mu\text{g}$ ) was mixed with 1  $\mu\text{L}$  of 50  $\mu\text{M}$  oligo(dT) primer and 1  $\mu\text{L}$  of 10 mM dNTP mix, then the final volume was adjusted up to 10  $\mu\text{L}$  with RNase free water. The tube was incubated at 65  $^{\circ}\text{C}$  for 5 min, then placed on ice for at least 1 min. The cDNA synthesis mixture (for 1 reaction) was prepared by mixing 2  $\mu\text{L}$  10X RT buffer, 4  $\mu\text{L}$  of 25 mM  $\text{MgCl}_2$ , 2  $\mu\text{L}$  of 0.1 M DTT, 1  $\mu\text{L}$  of RNaseOUT<sup>yh</sup> (40 U/ $\mu\text{L}$ ) and 1  $\mu\text{L}$  of SuperScript III RT (200 U/ $\mu\text{L}$ ). Then, 10  $\mu\text{L}$  of cDNA synthesis mix was added to each RNA/primer mixture, the solutions were mixed gently and collected by brief centrifugation. Then, the mixture was incubated 50 min at 50  $^{\circ}\text{C}$ , and the reaction was terminated by incubating at 85  $^{\circ}\text{C}$  for 5 min, then chilled on ice. The reactions were collected by brief centrifugation, then 1  $\mu\text{L}$  of RNaseH was added to each tube and the tubes were incubated for 20 min at 37  $^{\circ}\text{C}$ . In order to dilute the reaction mixture to 10 ng/ $\mu\text{L}$  of cDNA, 180  $\mu\text{L}$  of RNase free water was added to the reaction, and the synthesized cDNA was stored in -20  $^{\circ}\text{C}$  until use.

### 3.4.4 qRT-PCR

To optimize the PCR reaction condition, 10  $\mu\text{L}$  of cDNA aliquot was used for PCR. Five microliters of 10 ng/ $\mu\text{L}$  cDNA was added to 0.25  $\mu\text{L}$  of 10  $\mu\text{M}$  *GBA2* forward and reverse primer, 0.25  $\mu\text{L}$  of 0.25 mM dNTP mix, 1.25  $\mu\text{L}$  of 10X *Taq* DNA polymerase buffer, 0.25  $\mu\text{L}$  of *Taq* DNA polymerase and 5.25  $\mu\text{L}$  of sterile water, to give a final volume of 12.5  $\mu\text{L}$ . The PCR thermocycler was set up with initial denaturation at 95  $^{\circ}\text{C}$  for 5 min, denaturation at 95  $^{\circ}\text{C}$  for 30 s, annealing at 58  $^{\circ}\text{C}$  or 60  $^{\circ}\text{C}$  for 30 s, extension at 72  $^{\circ}\text{C}$  for 30 s and final extension at 72  $^{\circ}\text{C}$  for 5 min.

Real-time PCR was done with the gene-specific primers described above and listed in Table 3.2. Each qRT-PCR reaction mixture was composed of 10  $\mu\text{L}$  of 2X SYBR Green Master Mix, 1  $\mu\text{L}$  of 10  $\mu\text{M}$  Forward and reverse primers, 5  $\mu\text{L}$  containing 10  $\mu\text{g}$  cDNA and 4  $\mu\text{L}$  of sterile water (total volume 20  $\mu\text{L}$ ). The PCR thermocycling was the same as described for optimization in the preceding paragraph. The expression level of human *GBA2* isoforms was quantified and normalized against the expression of a housekeeping gene,  $\beta$ -actin as well as the internal control. The expression of the genes was calculated by the  $2^{-\Delta\text{CT}}$  equation, as described by Rao et al., 2013.

### 3.5 Immunoblotting

#### 3.5.1 Antibody design

The amino acid sequences of all the human non-lysosomal glucosylceramidase isoforms in this study were aligned by the MUSCLE algorithm in the MEGA X program, to see which sequences were found with all isoforms, then 3 representative peptide sequences (12-15 amino acids) were selected as antigens for the antibody production. The antigen sequences were compared to green monkey (*Chlorocebus sabaesus*) non-lysosomal glucosylceramidase isoform1 amino acid (NP\_065995.1) to check how similar the amino acid sequence is to that which might be expressed in the COS-7 cells, to assess whether this could be a source of non-specific bands. All antibodies were produced in rabbits by Genscript Corporation (Piscataway, NJ USA), as described the detail in the appendix Figure A1. All the peptide antigen sequences are shown in Table 3.4.

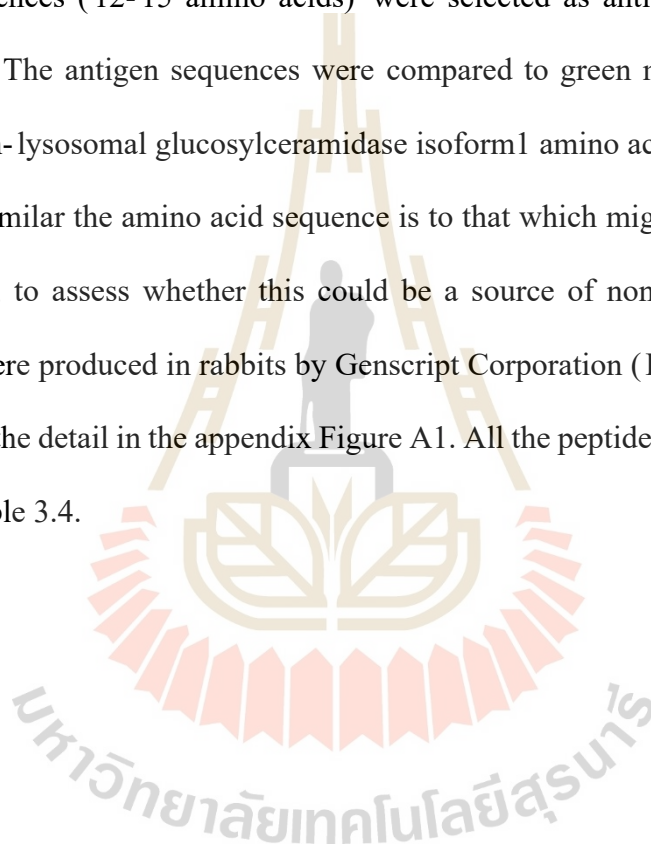


**Table 3.4** The human GBA2 antigens used for antibody synthesis and the corresponding sequence in *Chlorocebus sabaesus* GBA2 for comparison.

Name	Sequences	Position	Number of Differences
<b>GBA2-1</b>	KSPEDSRPPKETDC	46-59	3
<i>C. sabaesus</i>	KSPEDNRPQKETGC		
<b>GBA2-2</b>	CGQLDSPTGQSTPTQ	372-384	1 (2)*
<i>C. sabaesus</i>	DGQLDSPAGQSTPTQ		
<b>GBA2-3</b>	CRRNVIPHDIGDPDD	587-596	0 (1)*
<i>C. sabaesus</i>	KRRNVIPHDIGDPDD		

\***Note:** The N-terminal cysteines on the GBA2-2 and GBA2-3 peptides were added to couple the peptides to the carrier protein and are not part of the natural protein sequence. The number in parentheses includes this unnatural residue as a difference.

### 3.5.2 Antibody optimization

Peptide (antigen), BSA and antibody that were obtained from the company were dissolved in sterile water with 1 g/mL. The protocol and result was described in the Appendix Figure A2

### 3.5.3 SDS-PAGE electrophoresis

Proteins were extracted as described in section 3.2.10. Polyacrylamide gels were prepared from 5 mL of 10% separating gel consisting of 2 mL of distilled water (DW), 1.25 mL of 1.5 M Tris-HCl pH 8.8, 1.65 mL of 30% acrylamide, 50  $\mu$ L of 10% SDS, 25  $\mu$ L of 10% ammonium persulfate (APS) and 5  $\mu$ L of TEMED. The 2.5 mL of 4% stacking gel consisted of 1.5 mL of DW, 625  $\mu$ L of 0.5 M Tris-HCl pH 6.8, 332.5  $\mu$ L

of 30% acrylamide, 25  $\mu$ L of 10% SDS, 12.5  $\mu$ L of 10% APS and 5  $\mu$ L of TEMED. After adding the APS and TEMED, the separating gel was poured into the gel plates, covered with butanol and left to harden for 20-30 min for setting. Similarly, the stacking gel was poured on top of the rinsed stacking gel, the comb added, and the gel left to harden.

Four volumes of 20  $\mu$ g of total protein was homogeneously mixed with one volume of 5X sample loading buffer (50 mM Tris-HCl, pH 6.8, 10% SDS, 0.2 mg/mL bromophenol blue, 50% glycerol, 20% of  $\beta$ -mercaptoethanol), then the mixture was boiled at 95  $^{\circ}$ C for 5 min to denatured protein, followed by cooled and centrifuged briefly. The protein sample was loaded into the individual well and 3  $\mu$ L of pre-stained protein ladder was loaded into the gel as well. The loaded gel was electrophoresed in Tris-glycine electrode buffer (50 mM Tris base, 125 mM glycine and 0.1% SDS, pH 8.3) at a constant voltage of 80 volt for 15 min until the dye front entered the resolving gel, then turned the current was increased to 100 volts for 1.30-2 hours or until the tracking dye front reached the bottom of the gel plate. The gels were move to the western blotting step in 3.5.5, after that gels were subsequently stained in staining solution containing 0.1% (w/v) Coomassie Brilliant Blue R250, 40% (v/v) methanol, and 10% (v/v) acetic acid in water for 1-2 hours and destained with destaining solution (40% (v/v) methanol and 10% (v/v) acetic acid in water) for 1-2 h. The molecular masses of protein bands were determined by comparison to standard low molecular weight protein markers (BLUeye Prestained Protein ladder), which consist of 11-245 kDa of protein makers.

### 3.5.4 Western blotting

After the SDS-PAGE gel was finished running, the stacking gel was cut off, then the separating gel was transferred to the western blotting module (Black side, sponge > filter paper > gel > nitrocellulose membrane > filter paper > sponge, red side). The module was closed, and the module was filled with 1X blotting buffer (25 mM Tris, 192 mM glycine and 20% methanol). The proteins were transferred to the nitrocellulose membrane by electro-blotting in a wet-blot apparatus at 100 volts for 1 hour. The nitrocellulose membrane was blocked by 5% skimmed milk in 0.05% PBST (5  $\mu$ L of tween 20 in 100 mL of 1X PBS) at room temperature for 1 hour, then the membrane was washed by 0.05% PBST 2 times for 15 min each with gentle agitation. Then, the membrane was incubated with human GBA2-2 antibody at a dilution 1:200, primary FLAG tag antibody at a dilution 1:1000 or primary  $\beta$ -actin antibody at a dilution 1:1000 with 1% skimmed milk in 0.05% PBST, pH 7.2, then agitating at 4 °C overnight. The membrane was washed with 0.05% PBST 3 times for 10 min each while gently agitating, followed by incubating with anti-mouse/HRP (horse-radish-peroxidase-conjugated) secondary antibody for anti-GBA2 and FLAG-tag primary antibodies and anti-rabbit/HRP secondary antibody for  $\beta$ -actin primary antibody at a dilution 1:2,000 in 1% skimmed milk in 0.05% PBST, pH 7.2, at 4 °C for 1 hour. The membrane was washed with 0.05% PBST 3 times for 10 min each with gentle agitation. The antibodies were detected by ECL (Thermo Scientific: Super Signal West Pico) for 5 min at room temperature, then the membrane was transferred to the film cassette. Finally, the film was exposed on top the membrane in a film cassette in the darkroom for 1-10 min, followed by film development in fixer and developer for 30 s each.

## 3.6 Assay of glucosylceramidase 2 activity

### 3.6.1 4-methylumbelliferyl- $\beta$ -D-glucoside (4MUG) standard curve

4MU and 4MUG were dissolved in the 0.1 M citric acid and 0.2 M sodium phosphate pH 5.8, 4MU standard concentrations, including 1, 0.9, 0.8, 0.7, 0.6, 0.5, 0.4, 0.3, 0.2, 0.1 and 0 nmole of 4MU were prepared. Then, 100  $\mu$ L of each 4MU solution was transferred to a 96 well black microtiterplate in 3 replicates, followed by adding the 200  $\mu$ L of glycine/NaOH (pH 10.6), then centrifuged at 4,000 rpm for 2 min to remove cell debris in the reactions. Then, 200  $\mu$ L of the supernatant to pipetted to a 96 well plate for detection of the fluorescent signal by fluorescent microplate reader at excitation 355 nm and emission. 460 nm. The result was demonstrated by result = (fluorescent signal x 3)/2 as described in 3.6.2.

### 3.6.2 Activity assay by fluorescent signal determination

The cell lysate protein extracts described in Section 3.2.10 were assayed for GBA2 activity, in aliquots of cell lysate containing 20  $\mu$ g total protein. The cell equivalent cell lysate volume was adjusted to 10  $\mu$ L with 1X PBS in a 1.5 mL tube, which was incubated on ice for 5 min. Then, 55  $\mu$ L of buffer (0.1 M citric acid and 0.2 M sodium phosphate pH 5.8) was added, followed by 35  $\mu$ L of 10 mM 4-methylumbelliferyl- $\beta$ -D-glucoside (4MUG) to give 3.5 mM final concentration. The reaction mixture was incubated at 37 °C for 30 min and the reaction stopped by adding 200  $\mu$ L of glycine/NaOH (pH 10.6), then centrifuged at 4,000 rpm for 2 min to remove cell debris in the reactions. Then, 200  $\mu$ L of the supernatant to pipetted to a 96 well plate for detection of the fluorescent signal by fluorescent microplate reader with the excitation at 355 nm and emission. 460 at nm. The result was demonstrated by result =

(fluorescent signal $\times 3$ )/2. Because 300  $\mu\text{L}$  of total reaction but only 200  $\mu\text{L}$  of reactions were transferred to microplate. Thus, the results were expressed by the above equation.

### 3.6.3 Inhibition of GBA activity by CBE (conduritol- $\beta$ -epoxide)

20 of total protein in 10  $\mu\text{L}$  final volume was pre-incubated with 1  $\mu\text{L}$  of 1 mM CBE for 10 min on ice. The activity in this protein was then assayed following the protocol in Section 3.6.2.

## 3.7 Glycosphingolipid level determination by LC MS/MS

### 3.7.1 Cell collection and lipid extraction

The cells were collected by adding 200  $\mu\text{L}$  1X PBS, then scraping the cells from the plate and moving them to a 1.5 mL tube with safety lock. The cell suspension was centrifuged at 4,000 rpm at 4  $^{\circ}\text{C}$ , and the supernatant was removed. Cell pellets and extraction blank (contained 200  $\mu\text{L}$  of 1XPBS) were dried by speed vacuum, then samples were stored in -80  $^{\circ}\text{C}$  until use.

Two hundred microliters of ice-cold 60% methanol containing 0.01% butylated hydroxytoluence (BHT) per  $1 \times 10^6$  cells was added to blanks and samples, then 39  $\mu\text{L}$  of internal standards as shown in the appendix. Working solution was added into all samples and extraction blanks. One scoop (using a 100  $\mu\text{L}$  of white plastic scoop) of Zirconium oxide bead (0.15 mm) was added to each 1.5 mL tube. Cell pellets were homogenized on a bullet blender at speed 8 for  $6 \times 30$  s (samples were cooled on dry ice in between homogenization for at least 15 s). One hundred and twenty microliters of Milli-Q water was added into the tube, followed by 394  $\mu\text{L}$  methanol (containing 0.01% BHT, butylated hydroxytoluene) and 257  $\mu\text{L}$  of  $\text{CHCl}_3$  (containing 0.01% BHT),

and the tube was vortexed vigorously for 1 min. Samples were incubated on a ThermoMix at 1,000 rpm for 15 min at room temperature, then centrifuged at 14,000 rpm for 15 min. The supernatant (organic phase) was transferred to a 2 mL tube. The remaining pellet was re-extracted by adding 100  $\mu$ L of milli-Q water, then vortexing for 10 s, followed by adding 400  $\mu$ L of  $\text{CHCl}_3$ : MeOH (1:2, v/v, containing 0.01% BHT), then vortexing for 10 s. Samples were incubated on a ThermoMix at 1,000 rpm for 5 min at room temperature. All samples were centrifuged at 14,000 rpm for 15 min to collect the supernatant, then the supernatant was transferred to the tube containing the first extraction. The pooled supernatant was dried by speedvap rotary vacuum evaporator for 1-3 hours. Lipid pellets were resuspended in isopropanol: methanol: chloroform (4:2:1, v:v:v, containing 0.01% BHT) at the final concentration of 250  $\mu$ L per  $10^6$  cells, then vortexed for 10 s, followed by mixing on a ThermoMix at 1,000 rpm for 3 min. The lipid extracts were centrifuged at 14,000 rpm for 15 min at room temperature to precipitate any residual solids. Finally, the supernatant was transferred to a 2 mL sample vial and stored at  $-80\text{ }^\circ\text{C}$  until use.

### **3.7.2 Preparation lipid extraction to Mass Spectrometer**

Ten microliters of lipid extracts were evaporated, then washed with 10 mM  $\text{NH}_3\text{HCO}_3$ , followed by reconstitution in 40  $\mu$ L of isopropanol: methanol: chloroform (4:2:1, v: v: v, containing 20 mM ammonium formate. The solutions were then placed into the wells of an Eppendorf twin-tec 96-well PCR plate, and the plate was sealed with sealing tape. Two microliters of each derivatized lipid sample was aspirated via nano liquid chromatography electrospray ionization (nanoESI) to a high resolution/accurate mass Thermo Scientific model Orbitrap Fusion™ Lumos™ Tribrid™ Mass Spectrometer with an Advion Triversa Nanomate nESI source (Advion, Ithaca, NY),

operating with a spray voltage of 1.2 kV in positive mode and 1.4 kV in negative mode, and a gas pressure of 0.3 psi.

### 3.7.3 Lipid data visualization

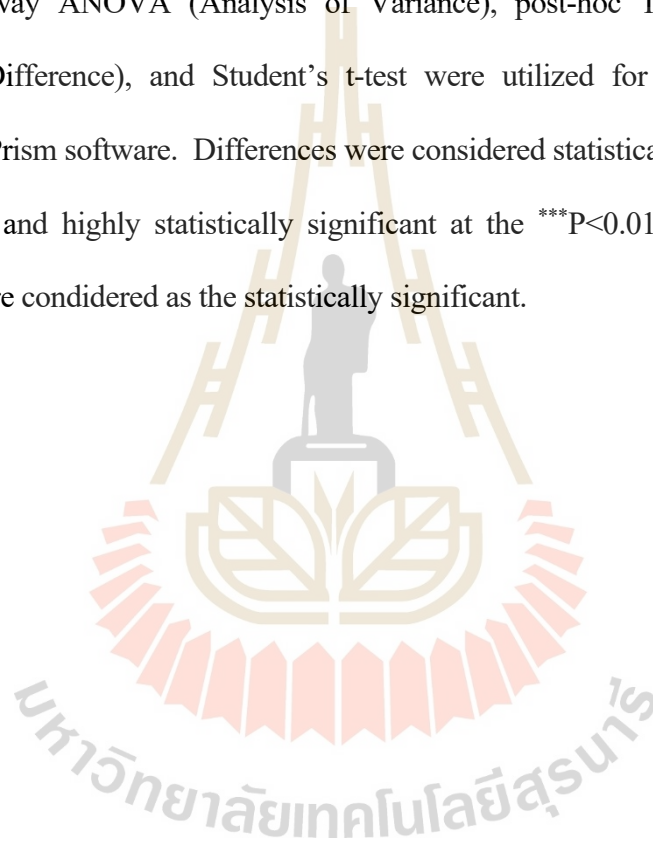
Peaks corresponding to the target analytes and internal standards (ISs) were measured and processed with the Xcalibur software system and lipid search software. The lipid levels were normalized to total protein ( $\mu\text{g}$ ). The output data was visualized via R Core Team (2019; R: A language and environment for statistical computing. R Foundation for Statistical Computing, Vienna, Austria. URL <https://www.R-project.org/>) order script, `setwd('')` to create the file directory, `Lipid <- read.csv('filename.CSV', row.name = 1)` to import the .CSV file to R, `library("pheatmap")` to download the library algorithm from the database, `pheatmap(Lipid, cutree_rows = 4)` to generate the heat map with clustering analysis to group similarities in the heat map. All values were expressed as Z-score (the position of a raw score in terms of its distance from the mean,  $z = (x-\mu)/\sigma$ , where  $x$  is the mean value for samples of the same isoform,  $\mu$  is the mean of the values of all isoforms and  $\sigma$  is the standard deviation between the means of all isoforms)

### 3.8 Signal peptide prediction

The protein sequences were subjected to online signal peptide prediction by using SignalP-5.0 (<http://www.cbs.dtu.dk/services/SignalP>).

### 3.9 Statistical analysis

One-way ANOVA (Analysis of Variance), post-hoc Tukey HSD (Honestly Significant Difference), and Student's t-test were utilized for statistical analysis in GraphPad 5 Prism software. Differences were considered statistically significant at the \*P < 0.05 level and highly statistically significant at the \*\*\*P<0.01 level. The difference alphabets were considered as the statistically significant.



## CHAPTER IV

### RESULTS AND DISCUSSION

#### 4.1 Sequence analysis of GBA2 isoforms

Fourteen putative GBA2 isoforms are listed in the National Center for Biotechnology Information (NCBI) Gene database entry 57704. Experimentally determined cDNA sequences for only two of these, isoform1 and isoform X1, are found in the database, while the rest are supported by high throughput mRNA sequencing data (RNASeq). We have evaluated functionality of 9 of these GBA2 isoforms that cover most of the gene and do not contain other start codons before their putative start codons by sequence analysis and homology modeling. GBA2 isoform protein sequences are aligned in Figure. 4.1. Isoform 1 is the well-characterized standard form of GBA2 with 927 amino acid residues, while isoform X1, for which a cDNA has been isolated from *Substantia nigra* (AK295967.1), differs only by the insertion of 6 amino acid residues in the N-terminal domain. Isoforms X2 and X4 share this same insertion. Isoforms X2, X4, X6 and X8 have an alternative C-terminus, which is shorter than that found in isoform 1. Isoforms X2, X3 and X6 are missing 22 amino acid residues that contribute to two helices and a loop around the active site in the model of the human GBA2 structure. Isoforms X7 and X8 are missing 79 amino acid residues, which comprise 5  $\beta$ - strands in the N-terminal domain lead to proteins with slightly to moderately modified.



## 4.2 Homology modeling of human GBA2 isoforms

The 14 GBA2 protein isoforms show 97-100% identity compared with isoform 1, but some are missing some part of the sequence and/or have additional sequence inserted into it. Therefore, the human GBA2 enzyme isoforms were predicted that it may have very similar structures and the differences may help explain the effects of disease causing GBA2 mutants on the protein structure and activity. Therefore, it should be possible to predict the structures of the additional 9 observed or predicted amino isoforms from the TxGH116 structure (Charoenwattanasatien et al., 2016) and predict which are likely to form a similar stable structure, as shown in Figure 4.2.

The predicted GBA2 structures from homology modeling show the missing some part of the sequence and/or have additional sequence inserted into isoforms as shown in Figure 4.3. Isoform X1, Isoform X2 and Isoform X4 show additional 6 amino acid sequence at Q191 to add small loop between Q191 and F198, whereas Isoform X2 is missing 22 amino acid residues at Q633 and Isoform X3 and isoform X6 are also missing those 22 amino acid residues relative to isoform 1, causing loss of 2 small  $\beta$ -stands. The missing part due to deletion of 79 amino acid at Q189 in isoform X7 and isoform X8, corresponds to 5  $\beta$ -sheets in the N-terminal domain. We also found the 28-amino-acid and 18-amino-acid segments missing in Isoform 2, Isoform X4, Isoform X6 and Isoform X8, correspond to 1  $\beta$ -stand and 3  $\beta$ -sheets in the C-terminal domain that might contribute to the catalytic site, so we hypothesized that these deletions may cause enzyme dysfunction, as may the big deletion of 79 amino acid residues in the N-terminal domain. However, it is possible that the structures may adjust with relatively small changes and these isoforms may be active isoforms that hydrolyze glucosylceramide and affect sphingolipid metabolism, perhaps with different properties.

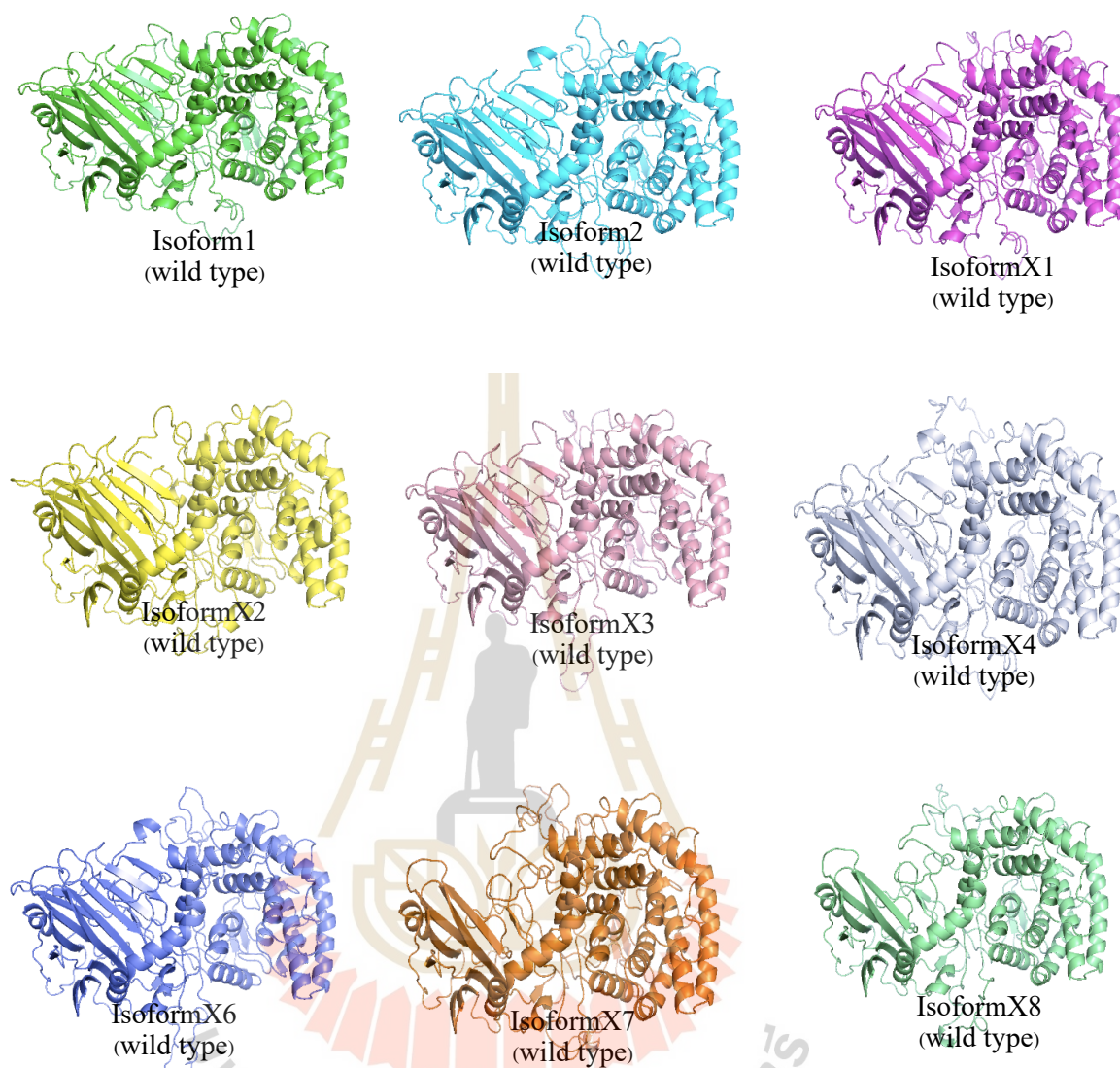


**Figure 4.2** Homology models of 9 human GBA2 isoforms based on the X-ray crystal structure of the txGH116  $\beta$ -glucosidase (PDB code 5BVU).

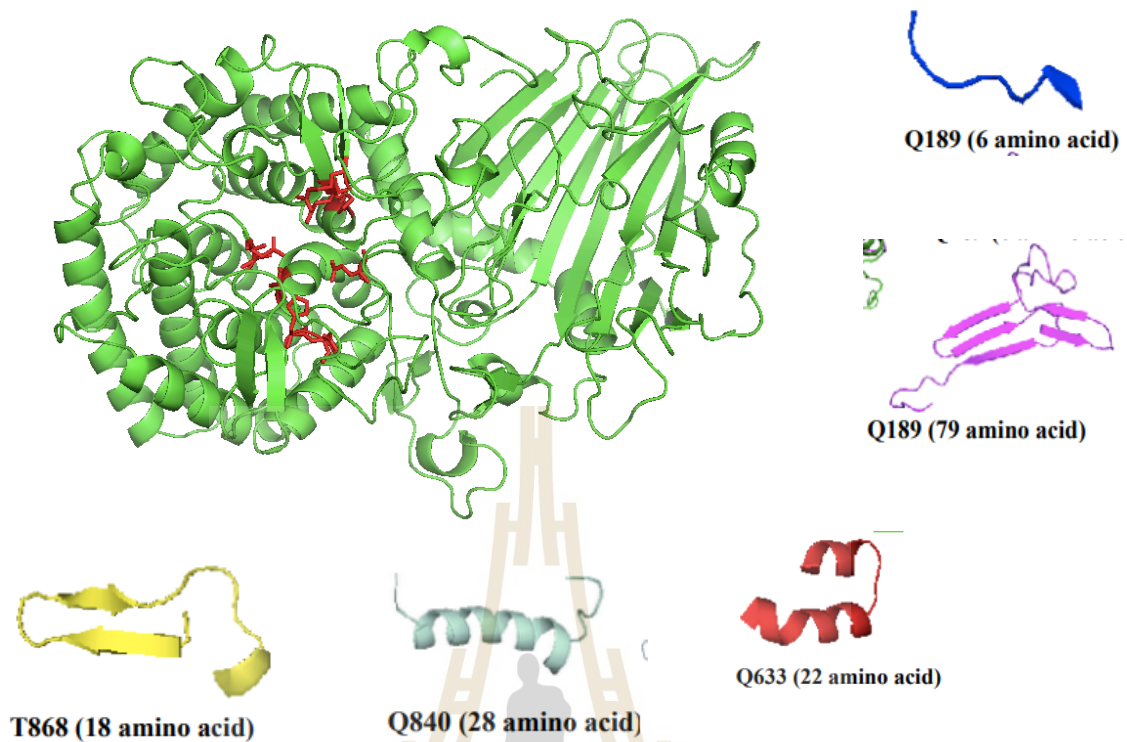


**Figure 4.3** A homology model human GBA2 showing the parts missing and/or added in the uncharacterized isoforms compared to GBA2 isoform 1. The model was based on the X-ray crystal structure of the *TxGH116*  $\beta$ -glucosidase (PDB code 5BVU). All of the sugar binding residues are conserved between *TxGH116* and GBA2, as well as the aspartate (D508) that interacts with H507 in *TxGH116* as shown in the red residues sticks.

### 4.3 GBA2 isoforms expression in COS-7 cells

GBA2 was expressed in COS-7 cells, which is essentially the same system previously utilized such as 363C > A, 518G > A, 700C > T, 1018C > T, 1255T > G (Sultana, Reichbauer et al., 2015 and Marques, Mirzaian et al., 2016) to study effects of GBA2 mutations on its activity. Expression analysis by qRT-PCR confirmed that mRNA levels of all human GBA2 isoforms were not significantly different at the same incubation time, but were significantly different between 48 and 72 hours, as shown

in Figure 4.4. Then, proteins were extracted and the total protein concentrations measured were not significantly different in the extracts from cells expressing different isoforms at both 48 and 72 hours, excepted the non-transfection condition had higher protein, as shown in Figure 4.5. After that, the soluble crude protein extract was observed by SDS-PAGE, followed by confirmation of the expression of each human GBA2 isoform by western blotting using anti-GBA2 and anti-FLAG-tag antibodies, as shown in Figure 4.6. The western blot showed that all the human GBA2 isoforms were expressed at the protein level with a band ~104 kDa, or somewhat smaller, depending on the expected mass of the isoform.

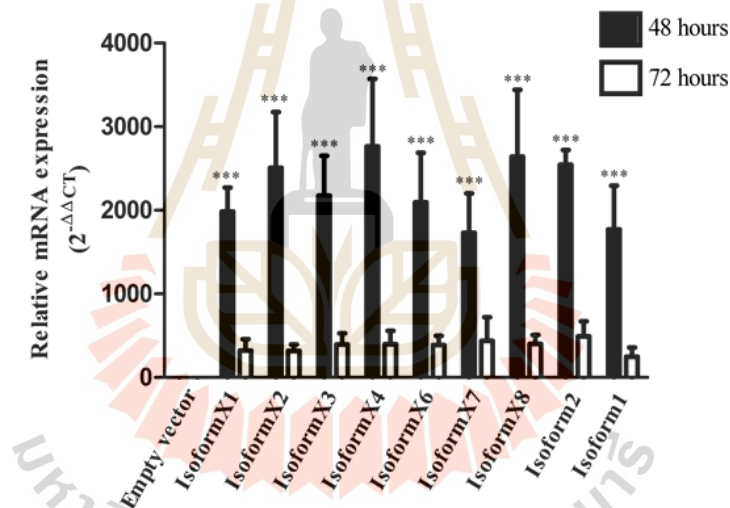


**Figure 4.4** Expression of human GBA2 RNA in COS-7 cells transfected with 9 human GBA2 isoforms. The RNA expression levels of human GBA2 isoforms in transfected COS-7-cells are shown at 48 and 72 hours after transfection. Data are expressed as mean of three independent replicates  $\pm$  SD, \*\*\* $p$ <0.01.

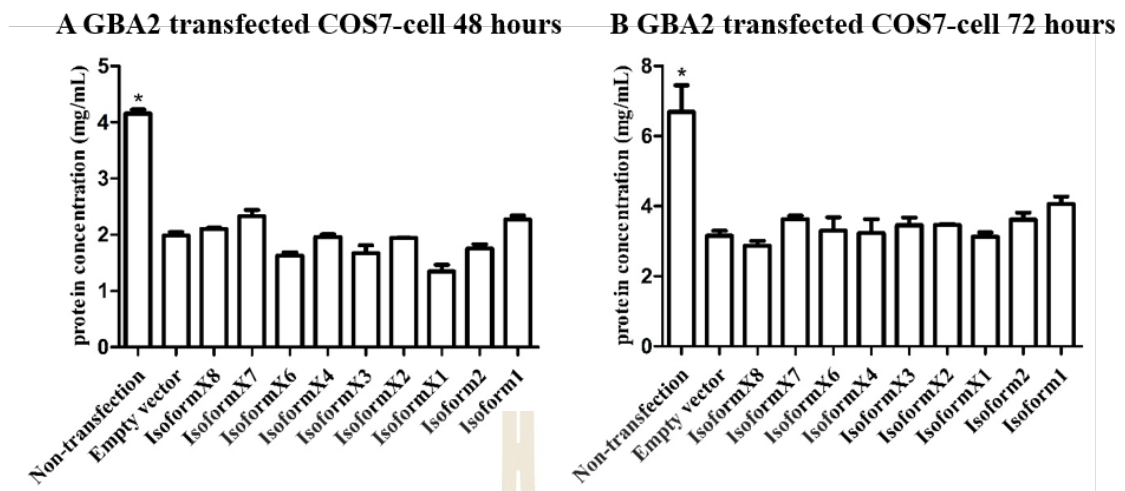


**Figure 4.5** Protein concentration in COS-7 cells transfected with 9 human GBA2 isoforms. (A) protein concentration of GBA2 isoforms at 48 hours. (B) protein concentration of GBA2 isoforms at 48 hours. Data are expressed as mean of three independent replicates  $\pm$  SD, \* $p < 0.05$ .

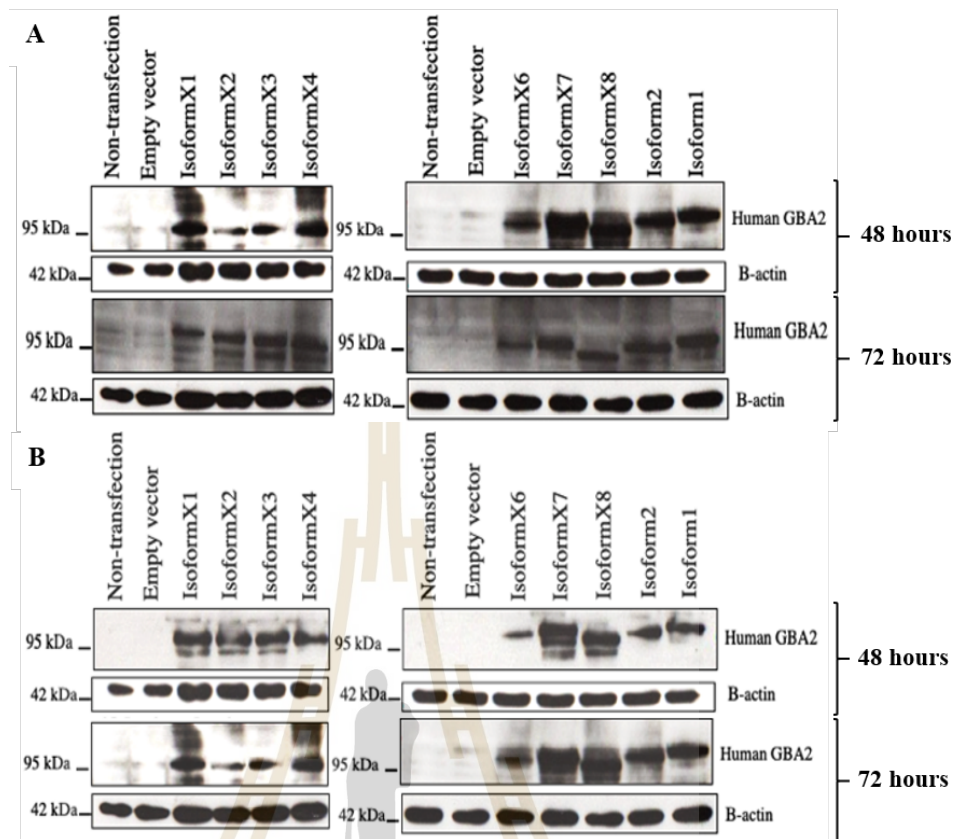


**Figure 4.6** Expression of human GBA2 protein in COS-7 cells transfected with 9 human GBA2 isoforms. Protein expression of human GBA2 in transfected COS-7 cells was detected by western blot with anti-human GBA2 (A) and anti-FLAG-tag (B) antibodies.

In order to clarify the relative expression levels of human GBA2 isoforms expressed in COS-7 cells, western blotting bands were quantified and the ratio between each human GBA2 isoform band to that of  $\beta$ -actin band calculated by image J. The resulting bar graph in Figure 4.7 shows that GBA2 expression levels were significantly different in cells transfected with GBA2 expression vectors compared to the control at both 48 and 72 hours, but were relatively similar to each other.

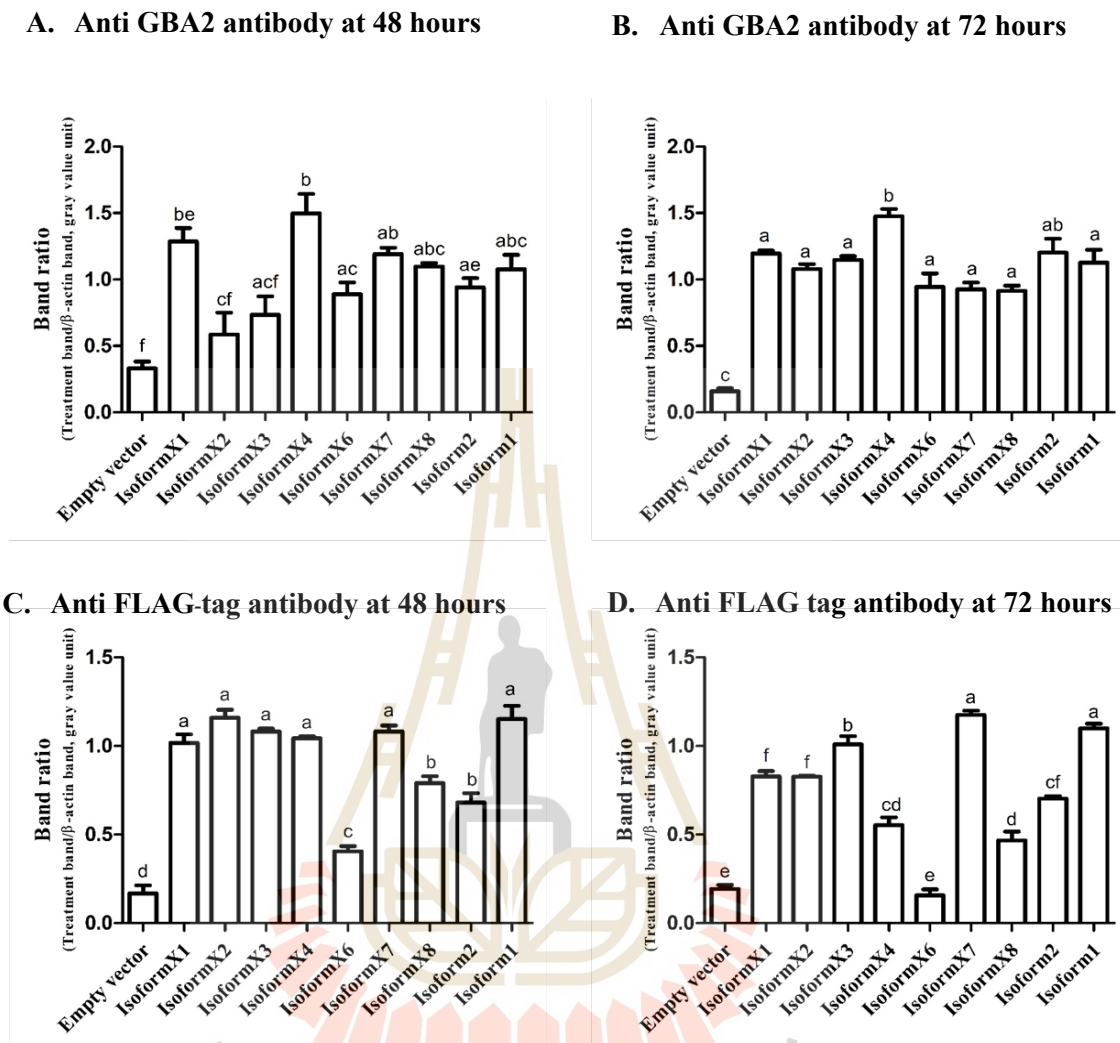


**Figure 4.7** Relative expression ratios of human GBA2 proteins to  $\beta$ -actin in COS-7 cells transfected with 9 human GBA2 isoforms. GBA2 proteins in western blots of cell lysates detected with anti-GBA2 antibodies (A) and (B) in 48 and 72 hours, and anti-FLAG-tag antibodies (C) and (D) in 48 and 72 hours, respectively. Data are expressed as mean of three independent replicates  $\pm$  SD, \* $p < 0.05$ . The difference alphabets were considered as the statistically significant.

#### 4.4 Activity of human GBA2 isoforms in transfected COS-7-cells

In order to confirm which isoforms are active, human GBA2 activity was measured in lysates from transfected COS-7 cells (at 48 or 72) against the fluorescent substrate 4-methylumbelliferyl  $\beta$ -D-glucoside (4MUG). CBE was added as a GBA inhibitor to one set of assays, although it also exhibits weaker inhibition of GBA2. After 48 hours of transfection, we found that human GBA2 activity of cells transformed with GBA2 isoform 1 (isoform 1) was significantly higher than cells transformed with empty vector as a negative control, while cells with other isoforms were similar to the negative control, as shown in Figure 4.8. Furthermore, GBA2 activity decreased about 25% upon addition of CBE, confirming that most of the activity resulted from GBA2 rather than endogenous GBA activity. Thus, all human GBA2 isoforms were expressed but only isoform 1 clearly hydrolyzed MUG substrate. These results suggest that none of the deletion or insertions shown in the protein sequence alignment Figure 1 can be accepted and still form an active 4MUG hydrolase. Missing a large or a small part of beta-strand and loop in either the N-terminal or C-terminal domains disrupt activity. Surprisingly, isoform X1, which has an insertion of 6 amino acid between residues 189 and 190 in a beta-strand of the N-terminal non-catalytic domain compared to isoform 1, showed no significant activity, suggesting that the structural integrity of the N-terminal domain is also critical to the activity. This data to improves the understanding of enzyme dysfunction gained from previous work that expressed GBA2 in cells, including looking at the effects of mutations such as 363C > A, 518G > A, 700C > T, 1018C > T, 1255T > G, 1780 G > C, 1888C > T, 2048G > C, 2608C > T and 2618G > A (Sultana, Reichbauer et al., 2015).

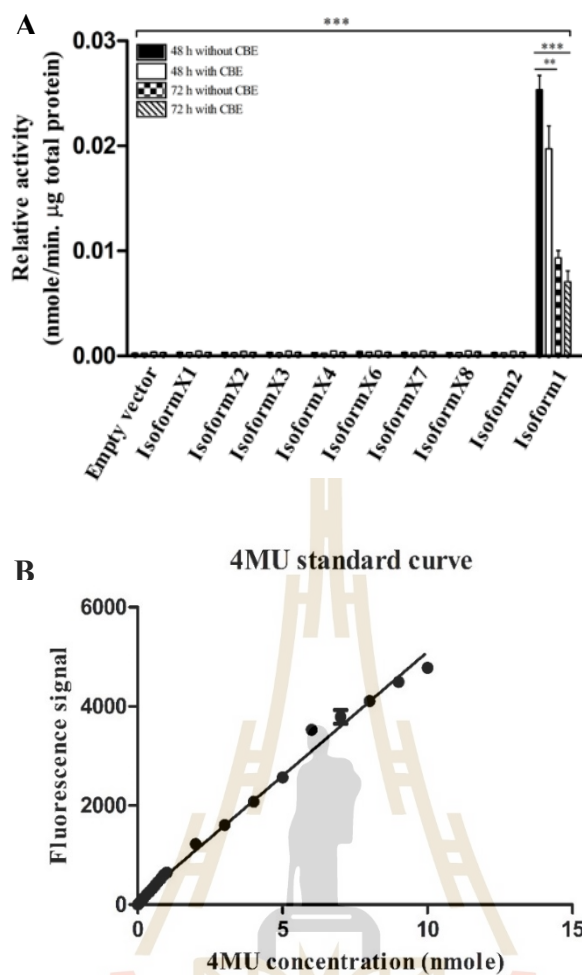


**Figure 4.8** Effect of expression of 9 human GBA2 isoforms on enzyme activity in transfected COS-7 cells. (A) shows human GBA2 *in vitro* activity in cell extracts, while (B) shows the standard curve of 4MU product. Data are expressed as mean of three independent replicates  $\pm$  SD,  $p < 0.01$  and  $p < 0.05$ . The difference alphabets were considered as the statistically significant.

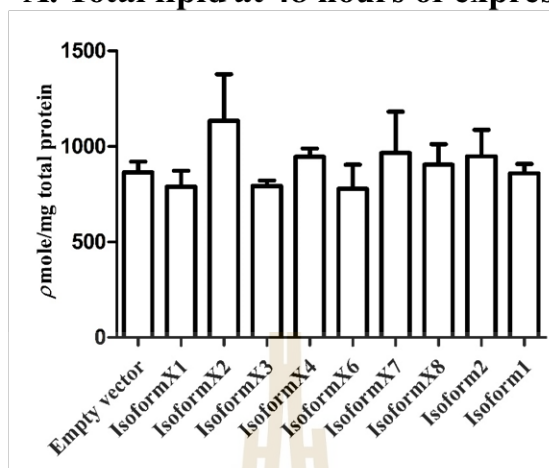
#### **4.5 Sphingolipid species levels affected by overexpression of human GBA2 isoforms in transfected COS-7 cells**

The above results confirmed that GBA2 isoform 1 expressed in COS-7 cells can hydrolyze the synthetic 4MUG substrate, while other isoforms show no or low activity with this substrate. However, it does not indicate whether human GBA2 isoform 1 or the other isoforms can act on natural glucosylceramide substrates in the cells. Indeed, many previous studies have shown sphingolipid profiles from diseases or GBA2 mutation expression in cells and a Gaucher mouse model (Raju, Schonauer et al., 2015, Boutin, Sun et al., 2016, Hamler, Brignol et al., 2017). However, they not yet reveal the effects of GBA2 overexpression on lipid profiles, including sphingolipid, glycerophospholipid and glycerolipid profiles or the effect from the different GBA2 isoforms. Firstly, total lipid of 48- and 72-hour expression conditions were measured and analyzed, as shown in Figure 4.9. The results suggest that the overexpression of all GBA2 isoforms had no major effect on the total amount of lipids, indicating that the lipid level was kept consistent in the cells. Since GBA2 act as on sphingolipids, monitoring the effects of the isoforms on sphingolipid substrates and products should be more sensitive. Therefore, the sphingolipid levels in COS-7 cells expressing the isoforms were determined by shotgun mass spectrometry. Total sphingolipid was analyzed along with 3 different sphingolipid subclasses, including ceramide, hexosylceramide and sphingomyelin, which were measured at both 48 and 72 hours, as shown in Figure 4.10 and Figure 4.11. Increases in ceramide and sphingomyelin and a decrease in hexosylceramides were seen, but only the increase in ceramide was statistically significant upon GBA2 isoform 1 overexpression. GBA2 overexpression may increase ceramide by hydrolyzing glucosylceramide to ceramide and glucose, as well as by

GBA2 transglucosylation activity, which can promote the transfer of glucosyl-moieties from GlcCer to cholesterol (Marques, Mirzaian et al., 2016).

Heat maps of the sphingolipid concentration Z-scores in cells expressing GBA2 isoforms at 48 and 72 hours are shown in Figure 4.12 and Figure 4.13. The species analyzed include ceramides (Cer) with long chain fatty acid or base (total number of carbons in the ceramide: C32-42), hexosylceramides (HexCer) with long chain fatty acid or base C38-42, and sphingomyelins (SM) with long chains (C32-44). Interestingly, clustering of the cell extracts based on their sphingolipid compositions identified GBA2 isoform 1 as the out group, which would be expected if it is the only isoform with significant activity on the sphingolipids. In the extract from cells transformed with isoform 1, hexosylceramide CerG1(d34:1), CerG1(d42:2), CerG1(d40:1) and CerG1(d42:1) show low concentrations (low Z-scores), while ceramides Cer d34:1, d40:1, d42:1 and d42:2 were found at high levels relative to the other conditions. In contrast, the levels of CerG1(d38:2), CerG2(d34:1), CerG2(42:1) and CerG2(42:2) were similar to or slightly higher than control upon overexpression of GBA2 isoform 1, suggesting that they may be galactosylceramides, which are not likely to be hydrolyzed by GBA2, or other hexosylceramides not hydrolyzed by GBA2. Previous studies, shown only glucosylceramide, but not galactosylceramide accumulation in GBA2-knockout mice (Raju, Schonauer et al., 2015).

### A. Total lipid at 48 hours of expression



### B. Total lipid at 72 hours of expression

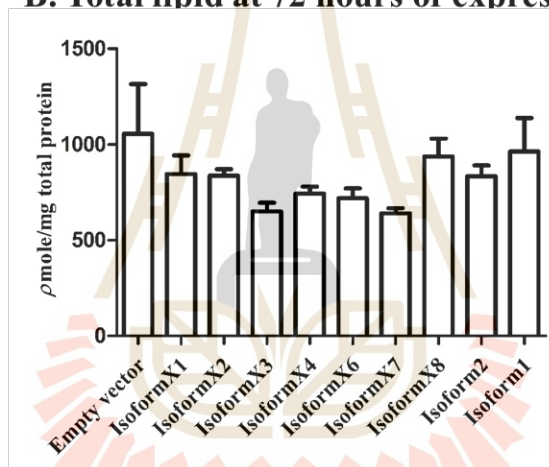


**Figure 4.9** Profiles of total lipid, including phosphoglycerol lipids, glycerol lipids and sphingolipids in COS-7-cells transfected with the 9 human GBA2 isoforms. Extracts at (A) 48 hours (B) 72 hours incubation time are expressed as bar graphs. Data are expressed as mean of three independent replicates  $\pm$  SD, \* $p < 0.05$ .

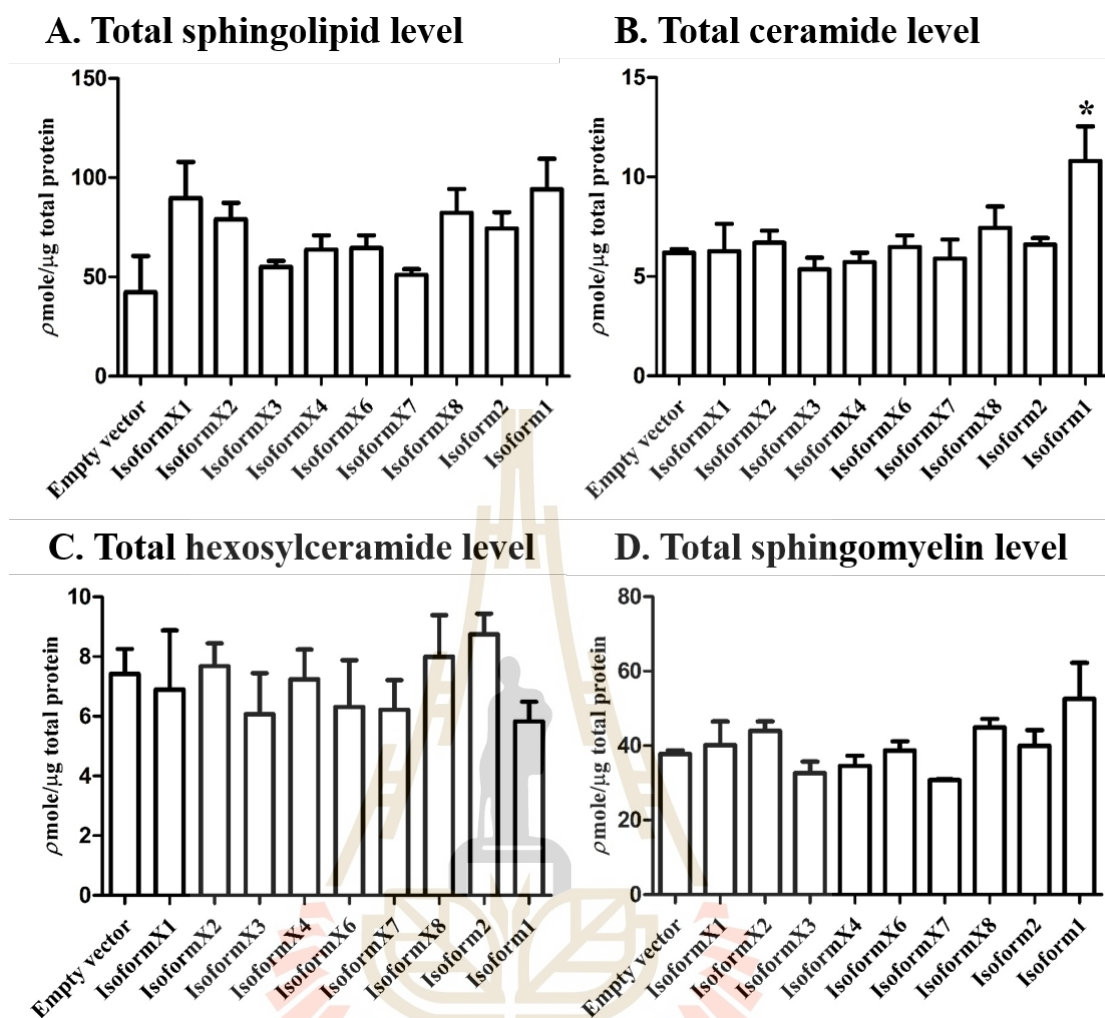


**Figure 4.10** Profiles of total sphingolipids, ceramides, hexosylceramides and sphingomyelins in COS-7 cells transfected with the 9 human GBA2 isoforms at 48 hours incubation time. Data are expressed as mean of three independent replicates  $\pm$  SD, \* $p < 0.05$ .

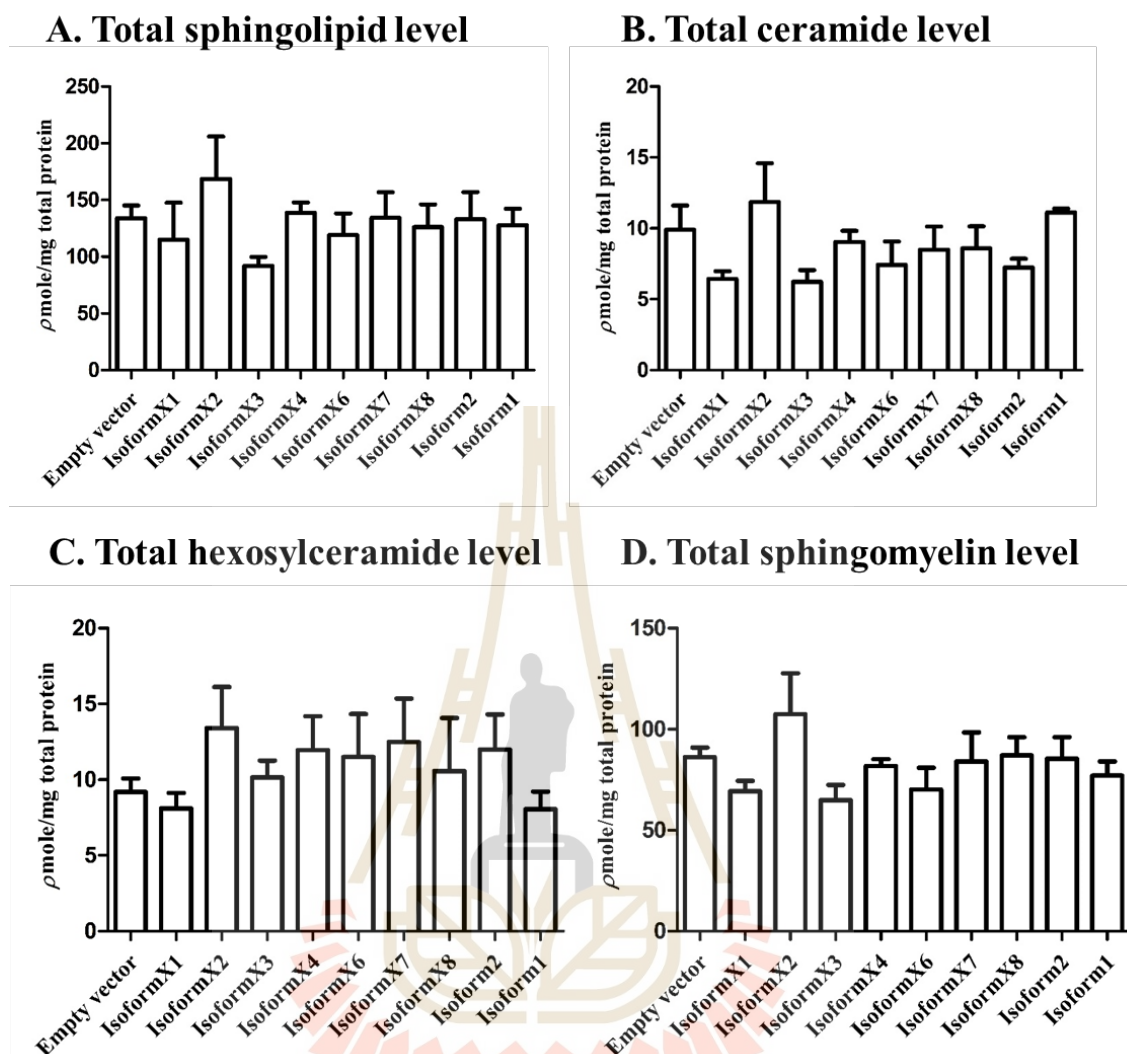


**Figure 4.11** Profiles of total sphingolipids, ceramides, hexosylceramides and sphingomyelins in COS-7-cells transfected with the 9 human GBA2 isoforms after 72 hours incubation time. Data are expressed as mean of three independent replicates  $\pm$  SD, \* $p < 0.05$ .

It appears that GBA2 isoform 1 strongly hydrolyzes GlcCer to release Cer and glucose, resulting in lower hexosylceramide levels (though not significantly lower) and higher free ceramide levels, while other isoforms did not significantly affect these levels, as emphasized by combining all species of each lipid class. Thus, the Figure 12 and 13

heat maps identified sphingolipid species that are likely to be GBA2 substrates and products, based on their increased or decreased levels upon expression of GBA2 isoform 1. These were combined, as were the sphingomyelins to give total levels in Figure 4.14. Combining these levels showed a significant increase in ceramides (Figure 4.14(A)) and decrease in the hexosylceramides (Figure 4.14(B)), but the changes in SM levels were not significant (Figure 4.14(C)). SM has been identified as a core component of the cell membrane, so its level may be controlled by other factors and not significantly affected by the increase in ceramides upon GBA2 overexpression, given the experimental error. This result corresponds to a previous result in which no significant difference in sphingomyelin levels was observed between knockout and wild type GBA2 in mice sperm (Raju, Schonauer et al., 2015). Ceramides with carbon chains (carbons:double bonds) 34:1, 36:1, 40:1, 40:2, 42:1, 42:2 and 42:3 (Figure 4.14(A) and Figure 4.15(A)), as well as hexosylceramides with ceramides 34:1, 40:1, 42:1, and 42:2 (Figure 4.15(B) and Figure 4.15(B)) were detected. SM species 36:2, 40:1, 40:2, 41:1, 41:2, 42:1, 42:2, 42:3, 44:2 and 44:3 were detected (Figure 4.14(C) and Figure 4.15(C)), as shown in the bar graph. In contrast to isoform 1, the other isoforms expressed 48 hours did not induce significant changes in cellular sphingolipid levels (Figure 4.14), so the structural changes noted to cause loss of activity on the synthetic substrate, MUG, also appear to cause loss of activity on the detected glucosylceramides. Thus, these results confirmed that GBA2 isoform 1 is likely the only active isoform, as well as indicating that HexCer 34:1, 40:1, 42:1 and 42:2 all appear to be human GBA2 substrates. Effect of incubation time contribute to the sphingolipid level.

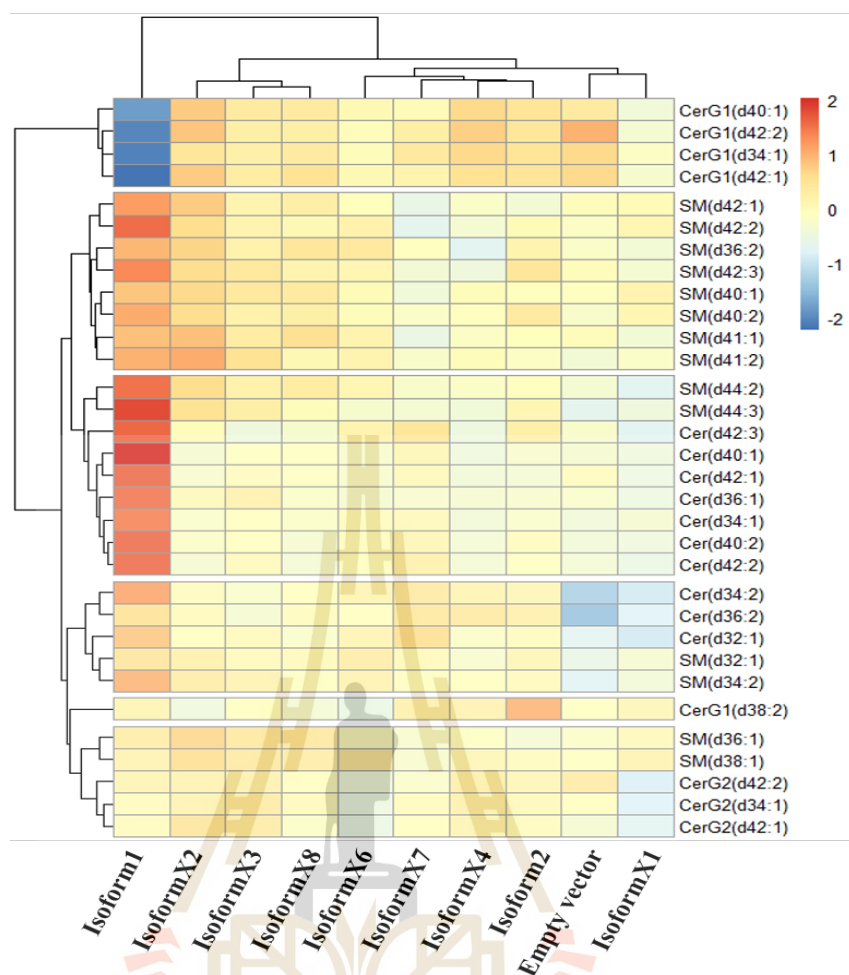


**Figure 4.12** Heat map diagram of profiles of sphingolipid, ceramides, hexosylceramide and sphingomyelin in COS-7 cells transfected with the 9 human GBA2 isoforms 48 hours after transfection. The heat map illustrates comprehensive quantifications of sphingolipid in cells expressing the human GBA2 isoforms and controls at 48 h after transfection, while the cluster diagrams illustrate the similarities of the patterns. All values are expressed as Z-score as described in methodology part 3.7.3. Values are color-coded from blue (decrease in lipid species, 0 to -2) to red (increase on lipid species, 0 to 2).

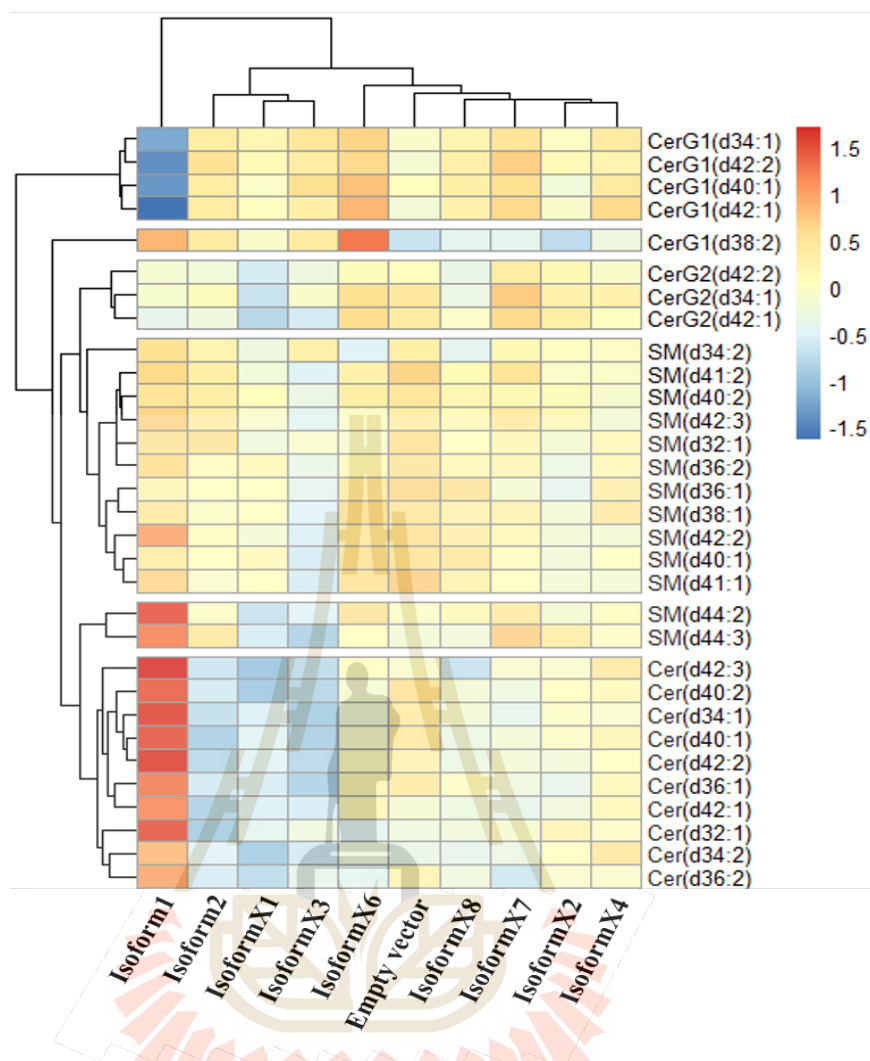


**Figure 4.13** Heat map diagram of profiles of sphingolipid, ceramides, hexosylceramide and sphingomyelin in COS-7-cells transfected with the 9 human GBA2 isoforms, at 72 h after transfection. The heat map illustrates comprehensive relative quantifications of sphingolipid in cells expressing the human GBA2 isoforms and controls, while the cluster diagrams illustrate the similarities of the patterns. All values are expressed as Z-score, as described in Figure 4.12.

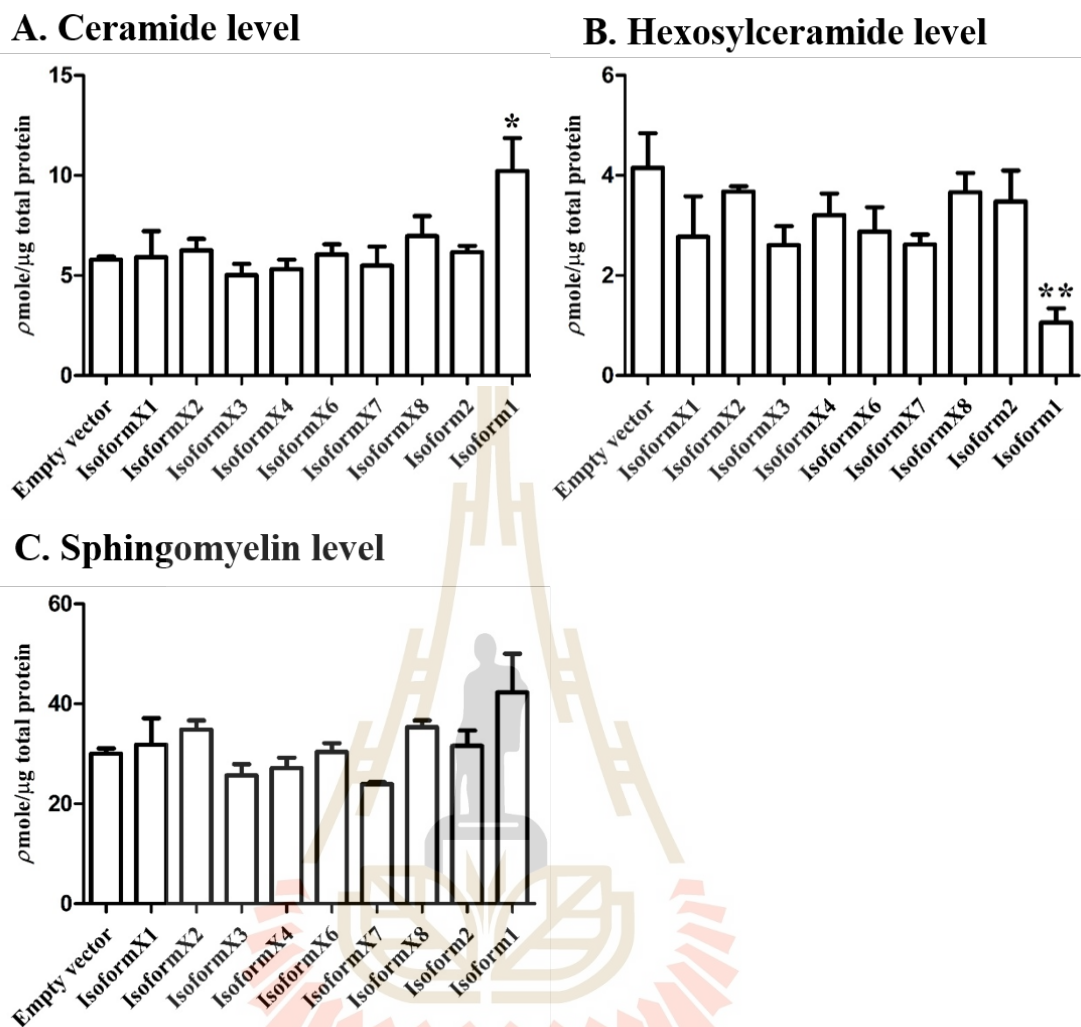


**Figure 4.14** Amounts of ceramides, hexosylceramide and sphingomyelin detected in all extracts of COS-7 cells transfected with the 9 human GBA2 isoforms at 48 hours. (A) Ceramide (including 34:1, 36:1, 40:1, 40:2, 42:1, 42:2 and 42:3), (B) Hexosylceramide (including 34:1, 40:1, 42:1 and 42:2), and (C) Sphingomyelin (including 36:2, 40:1, 40:2, 41:1, 41:2, 42:1, 42:2, 42:3, 44:2 and 44:3). Data are expressed as mean of three independent replicates  $\pm$  SD, \* $p < 0.05$  and \*\* $p < 0.01$ .

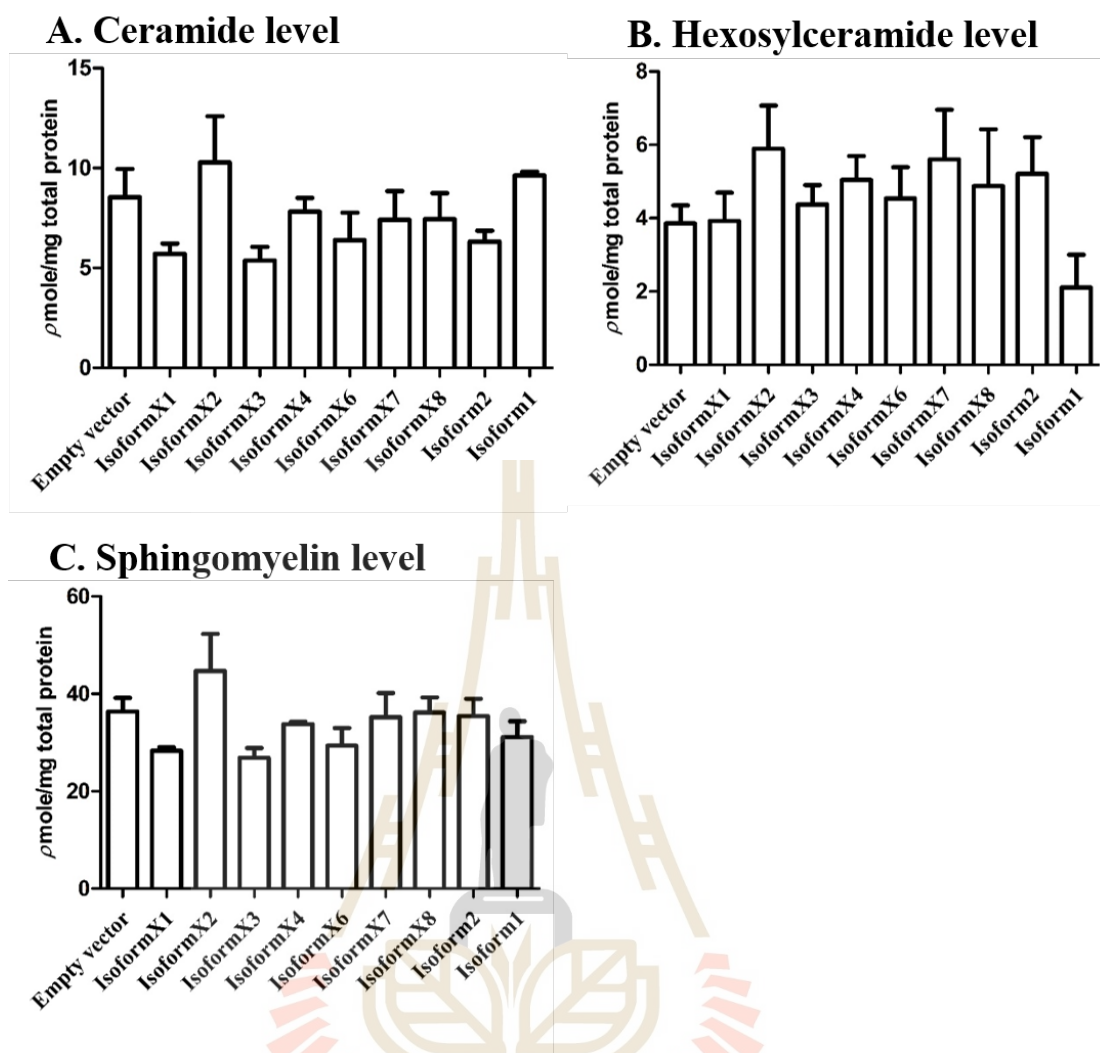


**Figure 4.15** Amounts of ceramides, hexosylceramide and sphingomyelin detected in all extracts of COS-7-cells transfected with the human GBA2 9 isoforms at 72 hours. (A) Ceramide (34:1, 36:1, 40:1, 40:2, 42:1, 42:2 and 42:3), (B) Hexosylceramides (34:1, 40:1, 42:1 and 42:2), and (C) Sphingomyelins (36:2, 40:1, 40:2, 41:1, 41:2, 42:1, 42:2, 42:3, 44:2 and 44:3). Data are expressed as mean of three independent replicates  $\pm$  SD, \* $p < 0.05$ .

## 4.6 Sphingolipid ratios and the direction of sphingolipid flow

To generate a more sensitive parameter for the movement of ceramides from glucosylceramides to other species upon overexpression of GBA2, the ratio of Cer to HexCer and SM to HexCer were calculated. Levels of sphingolipids with the same carbon chain (ceramide), including HexCer and Cer (d34:1, d40:1, d42:1 and d42:2), and SM (only d40:1 d42:1 and d42:2, since d34:1 was not detected in 48 hours and 72 hours, while d42:1 was not detected in 72 hours) in cell extracts from 48 and 72 hours after transfection were evaluated. The expression of human GBA2 isoform 1 in COS-7 cells resulted in increased ratios of Cer to HexCer (d34:1, d40:1, d42:1 and d42:2) in 48-hour extracts, while expression of the other isoforms did not significantly change these ratios, compared to the empty-vector control, as seen in Figure 4.16(A). While the same general pattern was seen in extracts from 72 hours after transfection, the levels were much more variable, leading less significant differences, as shown in Figure 4.17(A). The ratio of SM to HexCer (40:1, 42:1 and 42:2) was also significantly higher in GBA2 isoform 1-transfected COS-7 cells, compared to other isoforms and control at 48 h (Figure 4.18(A)), while only 40:1, and 42: were significant at 72 hours. This evidence suggests that GBA2 activity contributes to the conversion of sphingolipid from GlcCer to Cer, and that some of the released Cer may be converted to SM. Since a GBA2 isoform could act on one or a subset of the glucosylceramide species, the change of intracellular sphingolipid ratio was analyzed for each ceramide/hexosylceramide pair, including HexCer to Cer (d34:1) in Figure 4.16(B), HexCer to Cer (d40:1) in Figure 4.16(C), HexCer to Cer (42:1) in Figure 4.16(D), and HexCer to Cer (d42:2) in Figure 4.16(E). The ratios of Cer to HexCer were increased in extracts of cells transfected with GBA2 isoform 1, but not the other isoforms, 48 hours after transfection. This confirms that each of these pairs

represents a GBA2 isoform 1 substrate and product, while the other isoforms show no obvious activity toward them. Again, a similar pattern was seen at 72 hours, but the high variation meant the differences were not significant, as shown in Figure 4.17. In order to investigate the movement of sphingolipid from hexosylceramide to sphingomyelin, the ratio between sphingomyelin to hexosylceramide and sphingomyelin to ceramides were analyzed with different conditions, including total ceramide, total sphingomyelin, individual sphingomyelin and individual ceramide ratios of sphingomyelin to ceramide. Results demonstrated that sphingomyelin to hexosylceramide ratios were significantly different by isoform1 compared to empty vector control and other conditions as shown in Figure 4.18 and 4.19, while sphingomyelin to ceramide ratios were no significantly different with all conditions as shown in Figure 4.20 and 4.21, suggesting that remaining ceramide might be used for synthesis other sphingolipid like sphingosine, ceramide kinase, hexosylceramide instead of sphingomyelin, while ceramides were generated by hydrolysis of hexosylceramide shown relevant for sphingomyelin synthesis.

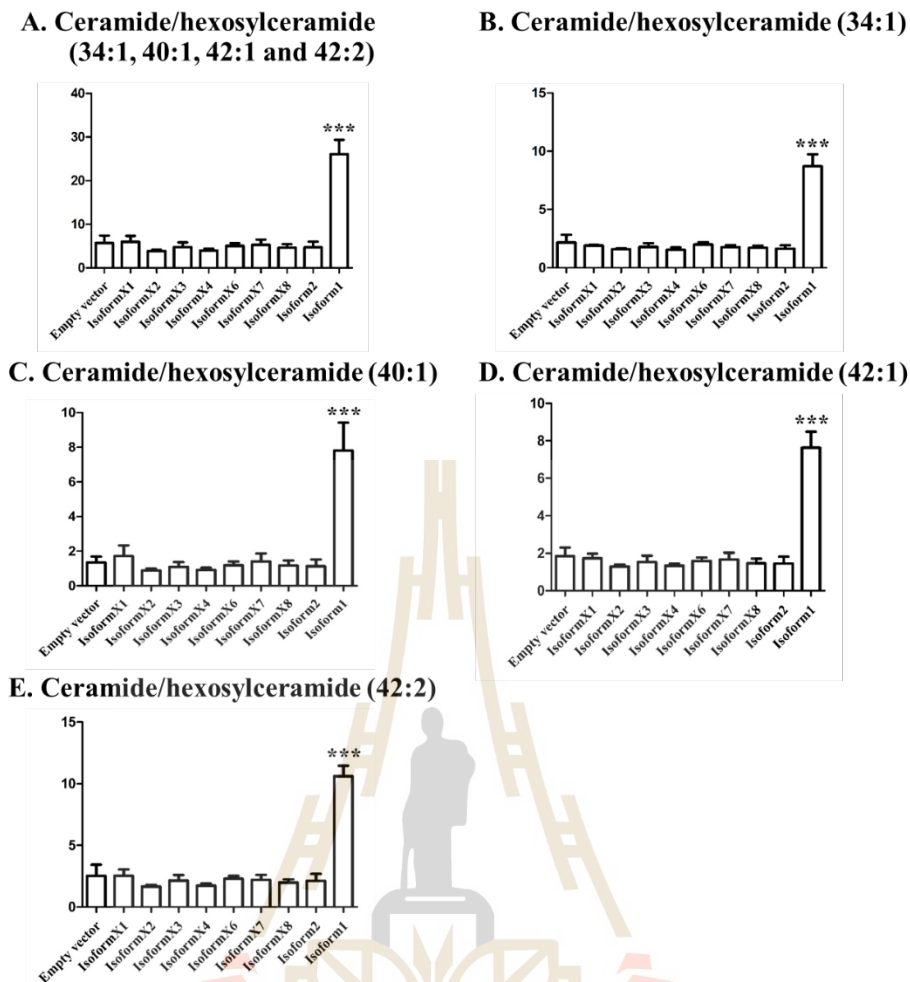


**Figure 4.16** Effect of GBA2 isoforms on ceramide/hexosylceramide ratios of specific ceramide species 48 hours after transfection. (A) Ceramide/hexosylceramide ratios (combined d34:1, d40:1, d42:1 and d42:2). The individual ceramide/hexosylceramide ratios for d34:1, d40:1 d42:1 and d42:2 are shown in (B) (C) (D) and (E), respectively. COS-7-cells were transfected with expression vectors for human GBA2 isoforms and incubated for 48 hours. Cells were harvested, lipids extracted, and then subjected to shotgun mass spectroscopy analysis. Data are expressed as mean of three independent replicates  $\pm$  SD, \*\*\* $p < 0.01$ .

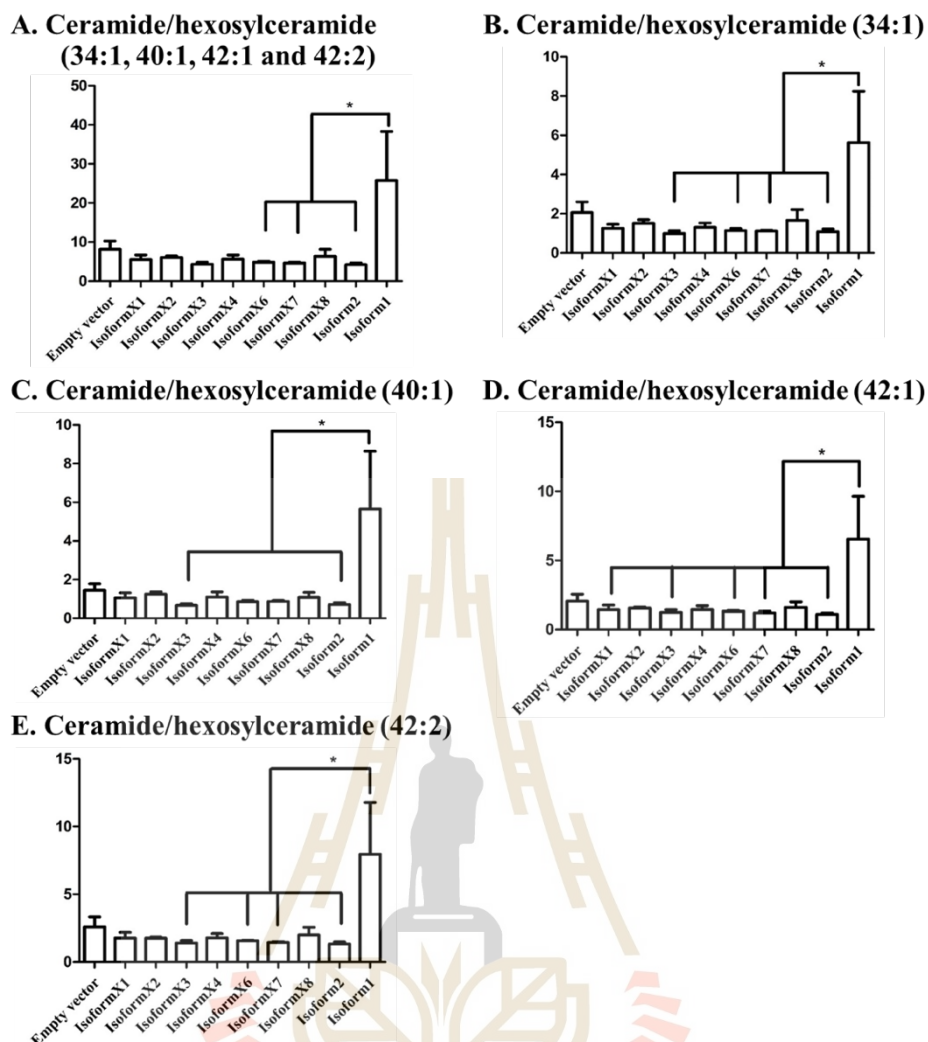
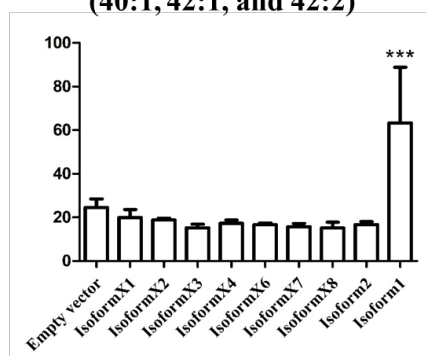
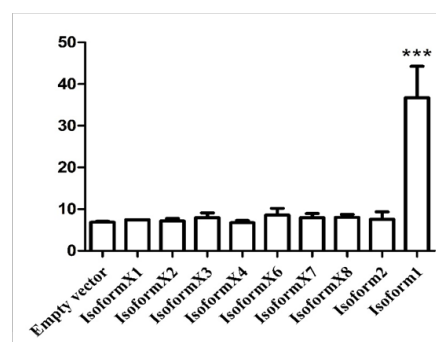


**Figure 4.17** Effect of GBA2 isoforms on ceramide/hexosylceramide ratios of specific ceramide species 72 hours after transfection (A) Ceramide/hexosylceramide ratios (combined d34:1, d40:1, d42:1 and d42:2). The individual ceramide/hexosylceramide ratios for d34:1, d40:1, d42:1 and d42:2 are shown in (B) (C) (D) and (E), respectively. COS-7-cells were transfected with expression vectors for human GBA2 isoforms and incubated for 48 hours. Cells were harvested, lipids extracted, and then subjected to shotgun mass spectroscopy analysis. Data are expressed as mean of three independent replicates  $\pm$  SD, \* $p < 0.05$ .

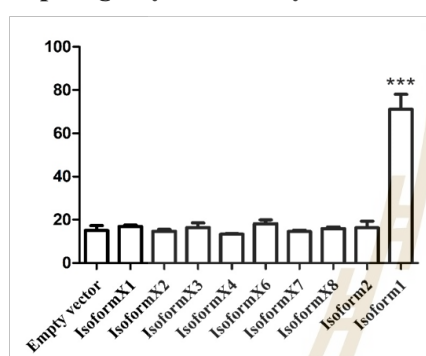
**A. Sphingomyelin/hexosylceramide (40:1, 42:1, and 42:2)**



**B. Sphingomyelin/hexosylceramide (40:1)**



**C. Sphingomyelin/hexosylceramide (42:1)**



**D. Sphingomyelin/hexosylceramide (42:2)**

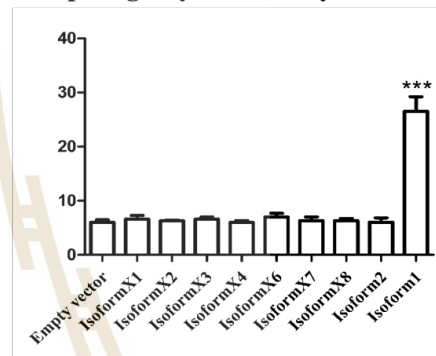
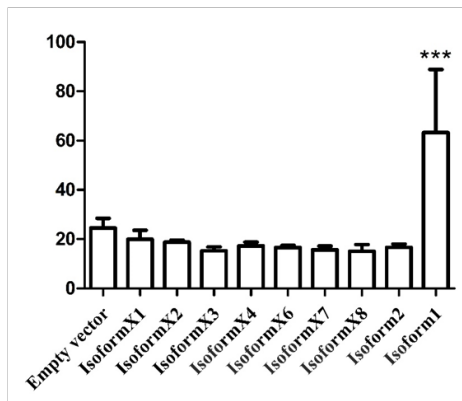
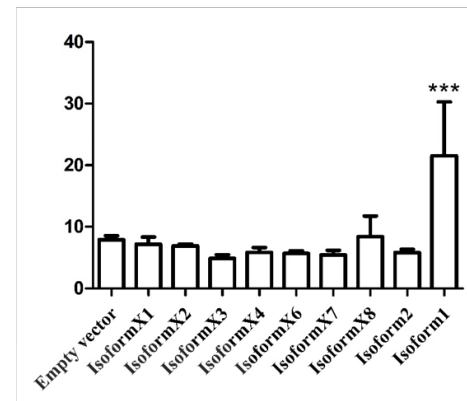


**Figure 4.18** Effect of GBA2 isoforms on sphingomyelin/hexosylceramide ratios of specific ceramide species 48 hours after transfection (A) sphingomyelin/hexosylceramide ratios (combined d40:1, d42:1 and d42:2). The sphingomyelin/hexosylceramide ratios d40:1, d42:1 and d42:2 are shown in (B) (C) and (D), respectively. COS-7-cells were transfected with expression vectors for human GBA2 isoforms and incubated for 48 hours. Cells were harvested, lipids extracted, and then subjected to shotgun mass spectroscopy analysis. Data are expressed as mean of three independent replicates  $\pm$  SD, \*\*\* $p$ <0.01.

**A. Sphingomyelin/hexosylceramide (40:1 and 42:2)**



**B. Sphingomyelin/hexosylceramid (40:1)**



**C. Sphingomyelin/hexosylceramide (42:2)**

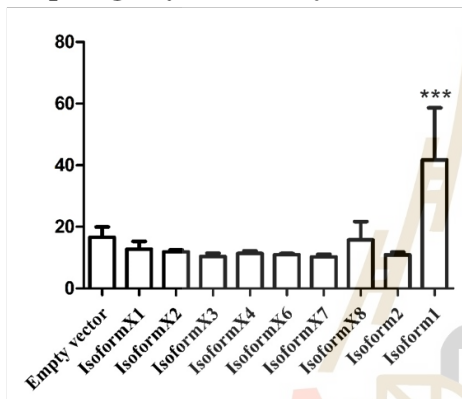


**Figure 4.19** Effect of GBA2 isoforms on sphingomyelin/hexosylceramide ratios of specific ceramide species 72 hours after transfection (A) sphingomyelin/hexosylceramide ratios (combined d40:1, and d42:2). The sphingomyelin/hexosylceramide ratios d40:1, and d42:2 are shown in (B) and (C), respectively. COS-7-cells were transfected with expression vectors for human GBA2 isoforms and incubated for 48 hours. Cells were harvested, lipids extracted, and then subjected to shotgun mass spectroscopy analysis. Data are expressed as mean of three independent replicates  $\pm$  SD, \*\*\* $p < 0.01$ .

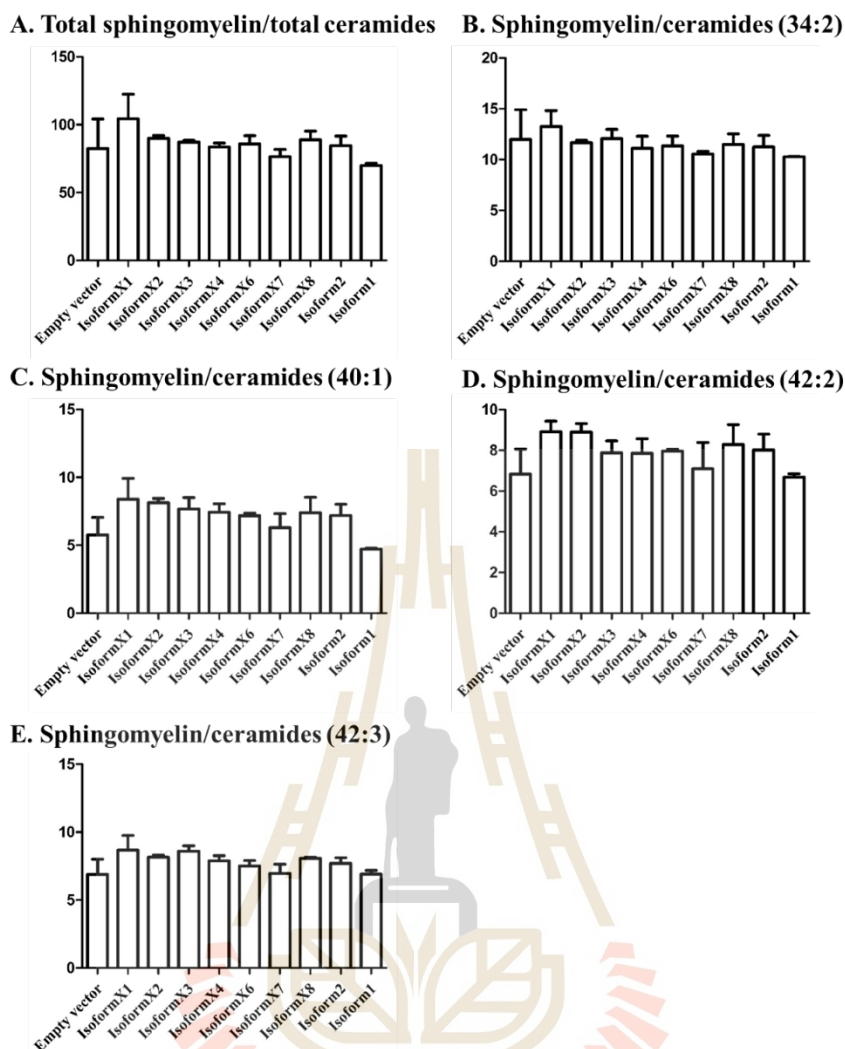


**Figure 4.20** Effect of GBA2 isoforms on sphingomyelin/ceramide ratios of specific lipid species Sphingolipid ratio in 48 hours (A) total sphingomyelin/total ceramide, B. sphingomyelin/hexosylceramide (d34:2) and sphingomyelin/ceramide d40:1, d42:2 and d42:3 were shown in (C) (D) and (E), respectively. COS-7 cells were transfected with human GBA2 isoforms and incubated for 48 hours. Cells were harvested, lipids extracted, and then subjected to shot gun mass spectroscopy analysis for quantification of the level of sphingolipid. Data are expressed as mean of three independent replicates  $\pm$  SD, \* $p < 0.05$ .

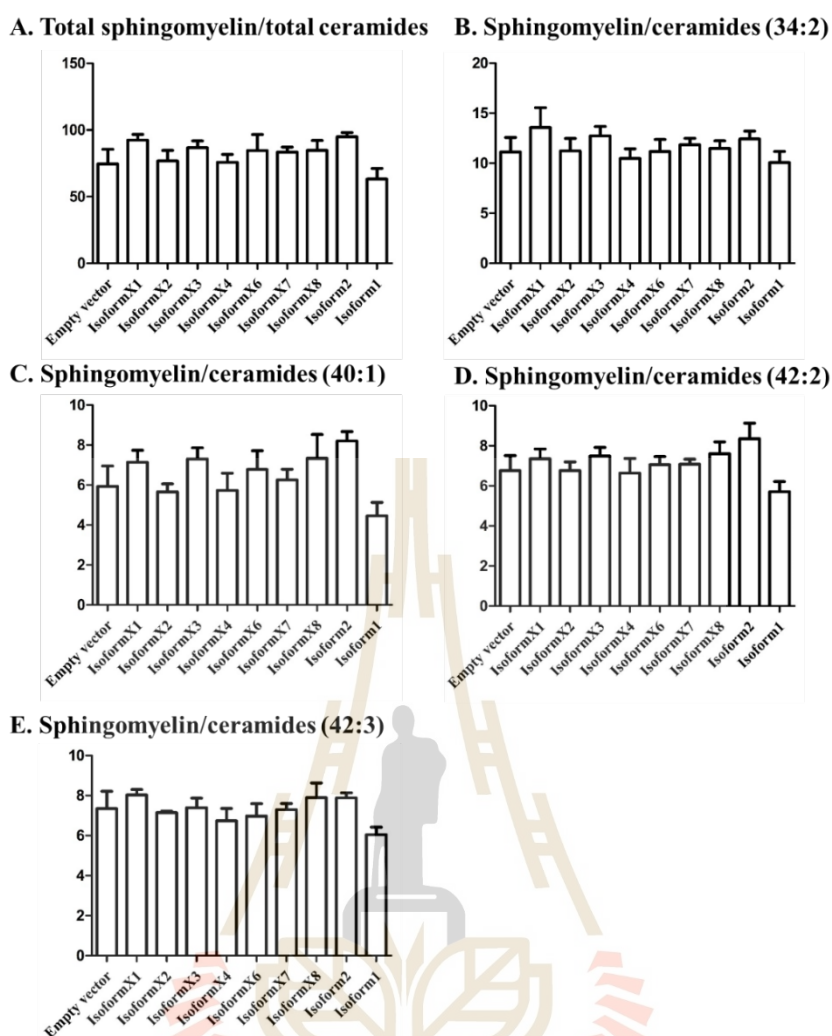
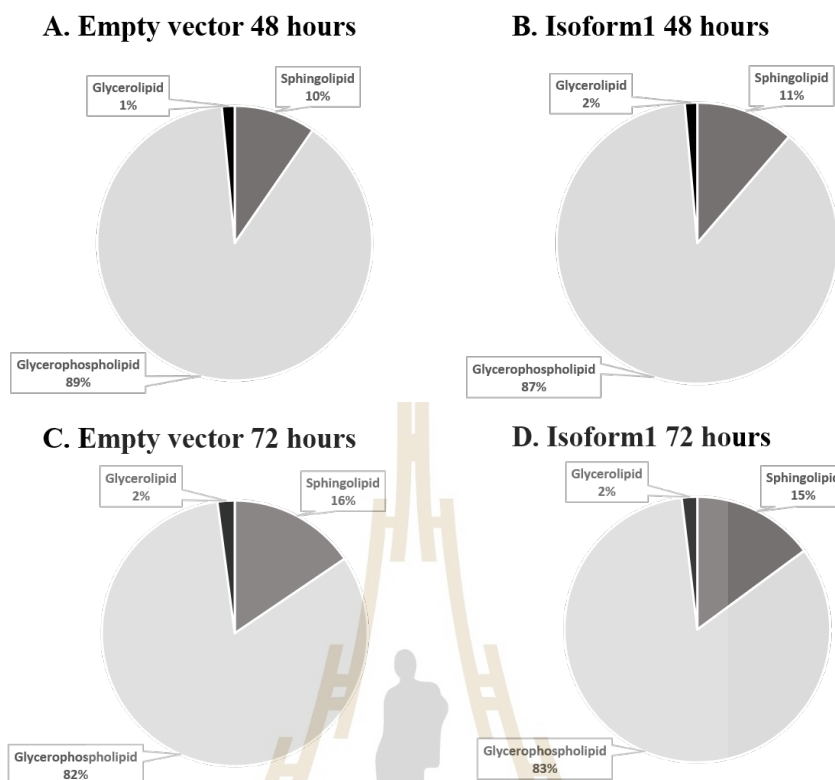


**Figure 4.21** Effect of GBA2 isoforms on sphingomyelin/ ceramide ratios of specific ceramide species at 72 hours. (A) total sphingomyelin/ total ceramide, (B) sphingomyelin/ hexosylceramide (34:2) and sphingomyelin/ ceramide d40: 1, d42: 2 and d42:3 were shown in (C) (D) and (E) respectively. COS-7-cells were transfected with human GBA2 isoforms and incubated for 72 hours. Cells were harvested, lipids extracted, and then subjected to shot gun mass spectroscopy analysis for quantification of the levels of sphingolipids. Data are expressed as mean of three independent replicates  $\pm$  SD, \* $p$ <0.05.

#### 4.7 Lipid classes in cells

To investigate whether GBA2 expression changed the relative levels of lipid classes in the cells, which might affect cellular processes, total lipid amounts in the 3 lipid classes were compared, as shown in Figure 4.22. The pie charts look similar trend with lipid component in the human colorectal cancer LIM1215 cell line, which shown 3 lipid classes including glycerophospholipids, glycerolipids and sphingolipids (Lydic, Townsend et al., 2015).

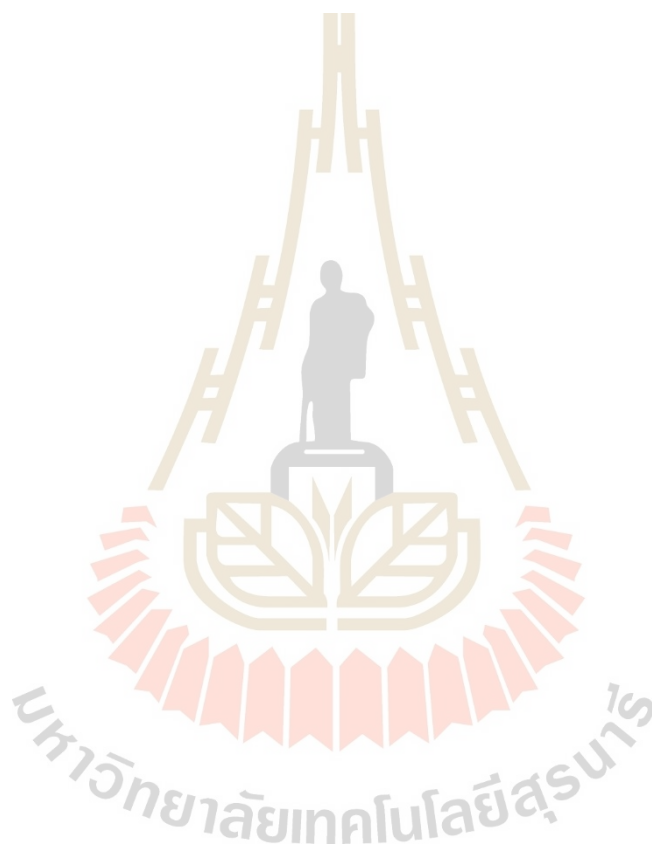




**Figure 4.22** Representation total of 3 lipid classes, sphingolipids, glycerophospholipids and glycerolipids, in COS-7 cells transfected with the human GBA2 isoform 1. (A) and (B) total lipids in 3 classes of lipid species in cells transfected with empty vector and GBA2 isoform 1, respectively, 48 hours after transfection. (C) and (D) total lipids in 3 classes of lipid species in cells transfected with empty vector and GBA2 isoform 1 72 hours after transfection.

The lipid distribution in 3 different lipid classes, including total sphingolipid, total glycerophospholipid and total glycerolipid of cells transfected for 48 hours and 72 hours is shown in Figure 4.23. The two most abundant lipid species in each lipid classes are labeled in extracts from 48 and 72 hours. SM (d42:2 was the sphingolipid with the highest concentrations in extracts of cells transformed with the empty vector and those

transformed with GBA2 isoform 1, consistent with SM being the most abundant sphingolipid in the cell. Moreover, PC and DG were found in the highest amounts for the glycerophospholipid and glycerolipid classes, respectively, as shown in Figure 4.23(B) to 4.23(E).



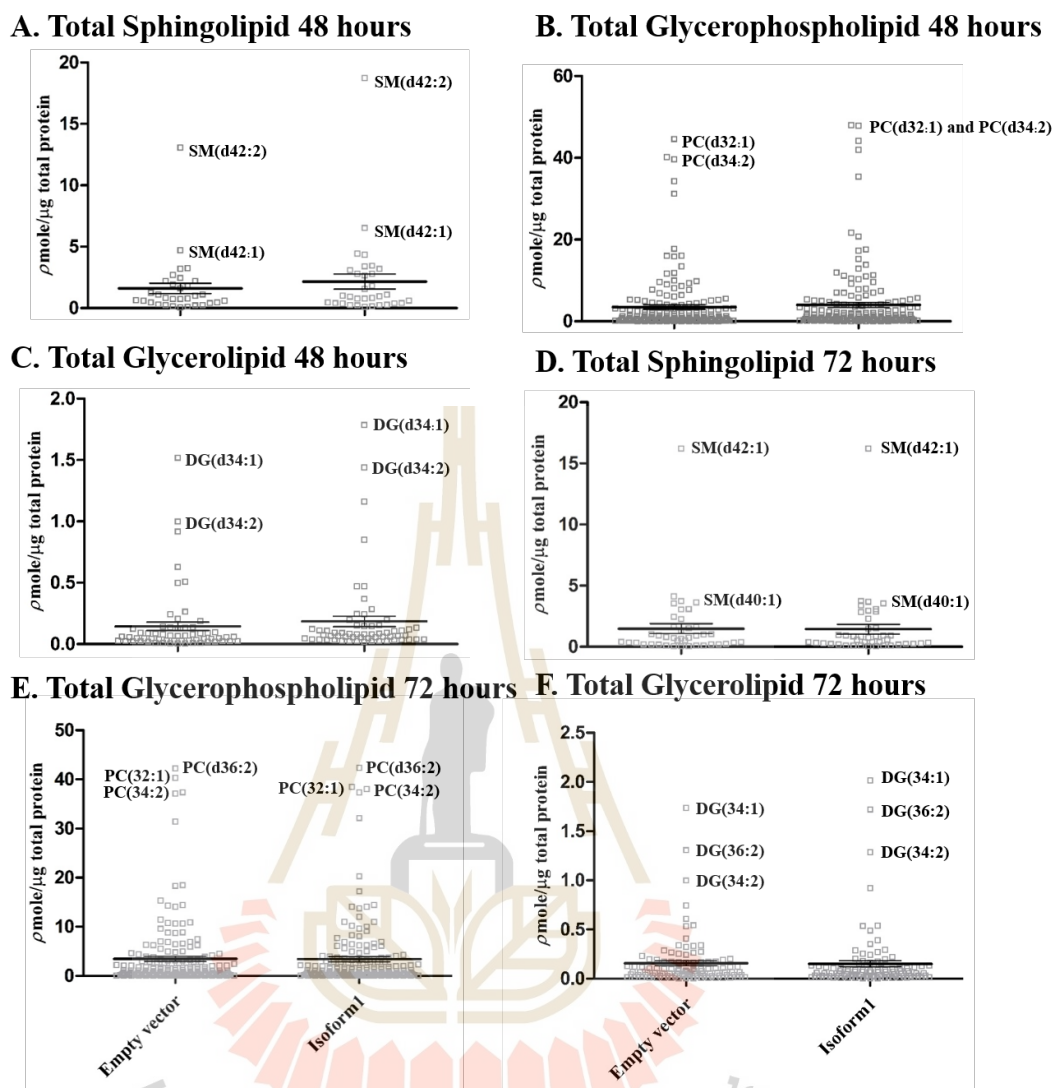
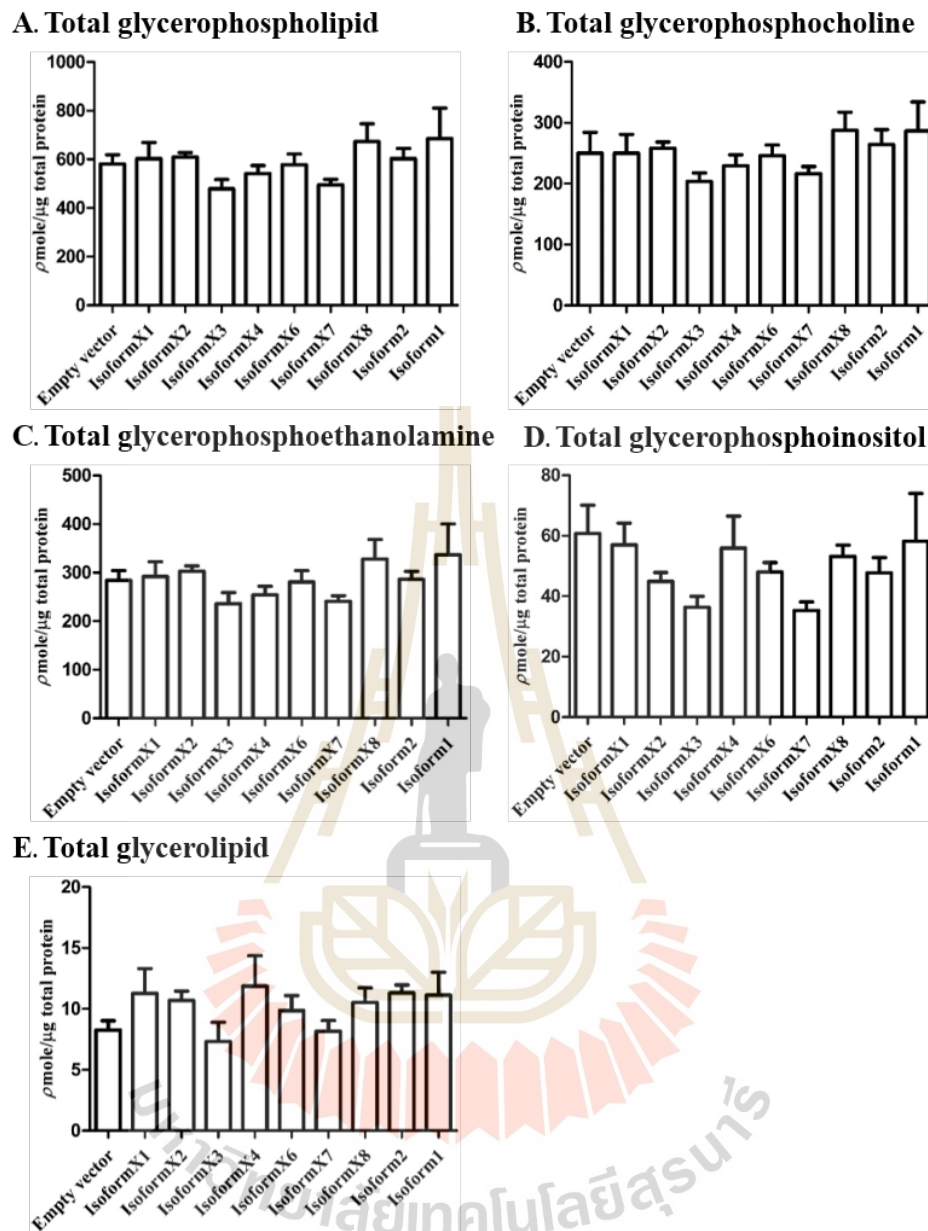


**Figure 4.23** The lipid distribution of 3 lipid classes. (A) Levels of all detected species of sphingolipid after 48 hours of transfection, (B) Levels of all detected species of glycerophospholipid after 48 hours of transfection, (C) Levels of all detected species of glycerolipid after 48 hours of transfection, (D) Sphingolipid species at 72 hours after transfection, (E) Glycerophospholipid species at 72 hours after transfection, (F) Glycerolipid species at 72 hours after transfection.

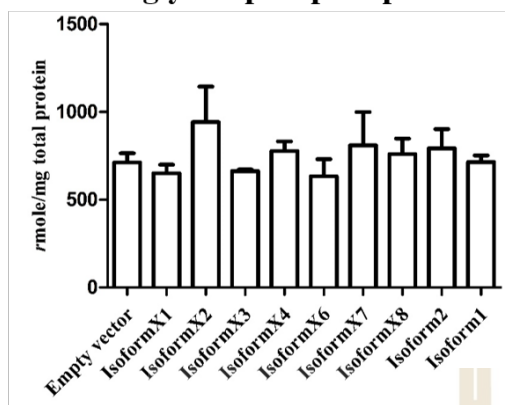
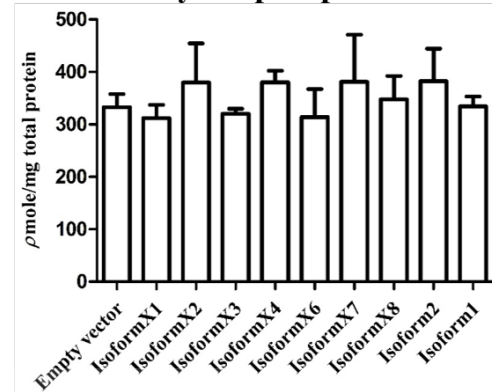
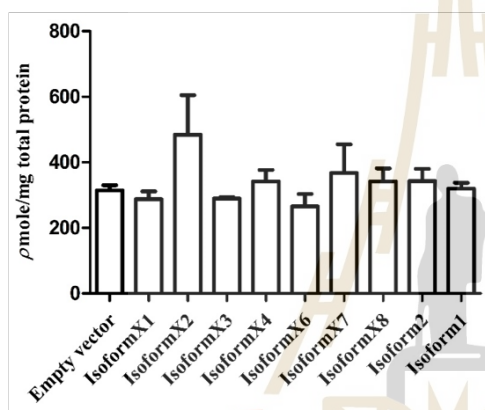
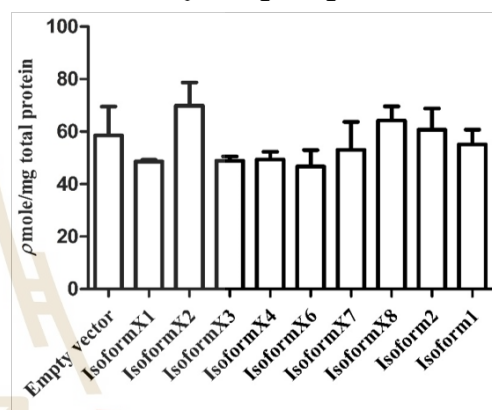
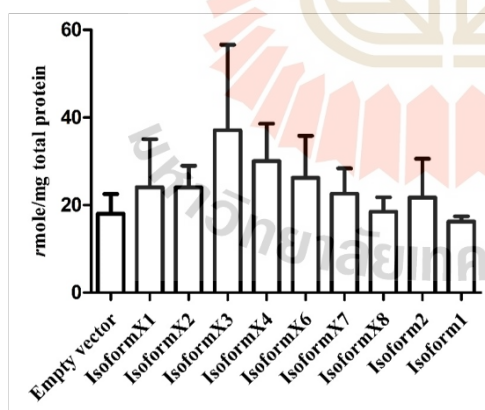
In order to see whether the lipids aside from sphingolipids remained constant in the cells, the levels of major glycerophospholipids and glycerolipid were analyzed in

cells at 48 hours after transfection, as shown in Figure 4.24, as well as at 72 hours after transfection, as shown in Figure 4.25. The results suggest no significant difference in total glycerolphospholipids or glycerolipids or the individual major glycerophospholipids glycerophosphocholine, glycerophosphoethanolamine, or glycerophosphoinositol. This suggests that overexpression of GBA2 isoforms did not disrupt the overall lipid homeostasis needed to continue the cell processes.





**Figure 4.24** The total glycerophospholipid and glycerolipid levels in cell extracts at 48 hours after transfection. Data are expressed as mean of three independent replicates  $\pm$  SD, \* $p < 0.05$ .

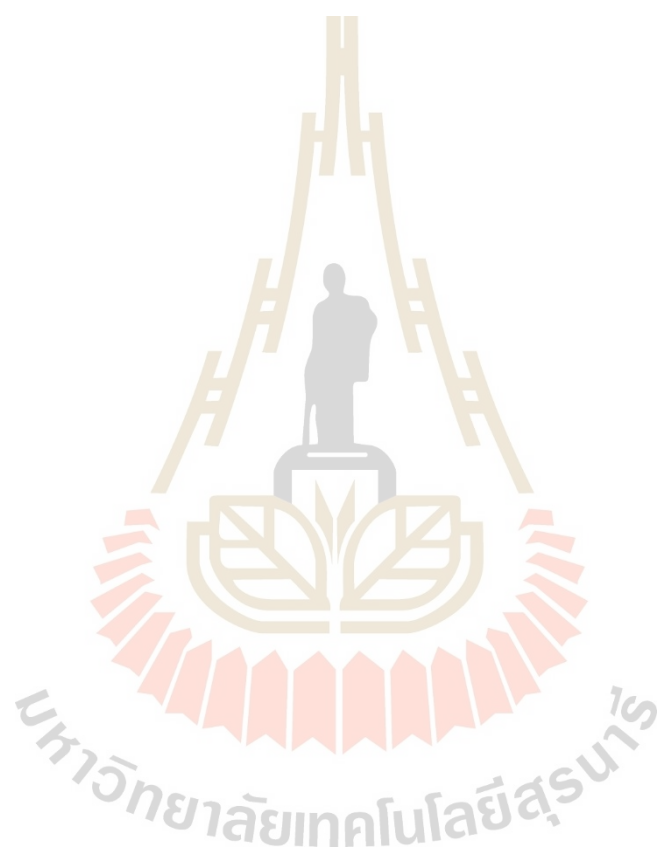
**A. Total glycerophospholipid****B. Total Glycerophosphocholine****C. Total Glycerophosphoethanolamine****D. Total Glycerophosphoinositol****E. Total Glycerolipid**

**Figure 4.25** The total glycerophospholipid and glycerolipid levels in cell extracts at 72 hours after transfection. Data are expressed as mean of three independent replicates  $\pm$  SD, \* $p < 0.05$ .

#### 4.8 Interconnectivity of sphingolipid metabolism affected by GBA2

There are interconnections between sphingolipid, glycerolipid and glycerophospholipid metabolism. From the results described above, GBA2 isoform 1 can hydrolyze GlcCer to release Cer as an immediate lipid product. Then, the subsequent action of ceramidase, ceramide kinase, and SM synthase may potentially convert the ceramide to sphingosine, C1P, and SM, respectively. Since DAG may be generated from glycerophosphocholine (phosphatidylcholine, PC) by moving the phosphocholine group from PC to Cer, this sphingolipid conversion may be connected to that of glycerophospholipid to glycerolipid. Thus, the ratio between total DAG to PC at 48 and 72 hours after transfection with GBA2 were explored in Figure 4.26 and Figure 4.27. The ratios of DAG to PC with lipid bases of 34:1, 40:2, 40:3, 40:5 and 40:6 show increases, as would be expected if phosphocholine is transferred from PC to Cer to make SM, thereby producing DAG, but the increases were not statistically significant. That maybe because all lipid isoforms do not contribute to this cross-talk or their levels are not strongly affected by it. To investigate whether PC with specific fatty acyl chain lengths are converted to DG, the ratios between pairs of DG/PC with the same fatty acid masses were compared in Figure 4.26(B)-(F) of Figure 4.26 and Figure 4.27. Although nearly all showed the same trend, only ratios DAG to PC with a fatty acyl component of 34:1 at 48 hours and that with a fatty acyl component of 40:3 at 72 hours after transfection with GBA2 isoform 1 were significantly different compared to empty vector at  $p < 0.05$ . Thus, this result suggests that PC 34:1 can provide the choline group to ceramide to generate to sphingomyelin, thereby converting PC 34:1 to DAG 34:1. While the ratio for 40:3 DAG to PC was not clearly changed at 48 hours, it appeared significantly increased by GBA2

at 72 hours. Thus, these studies can suggest that altering the levels of sphingolipids can cause changes in phosphoglycerolipid and glycerolipid levels as well.



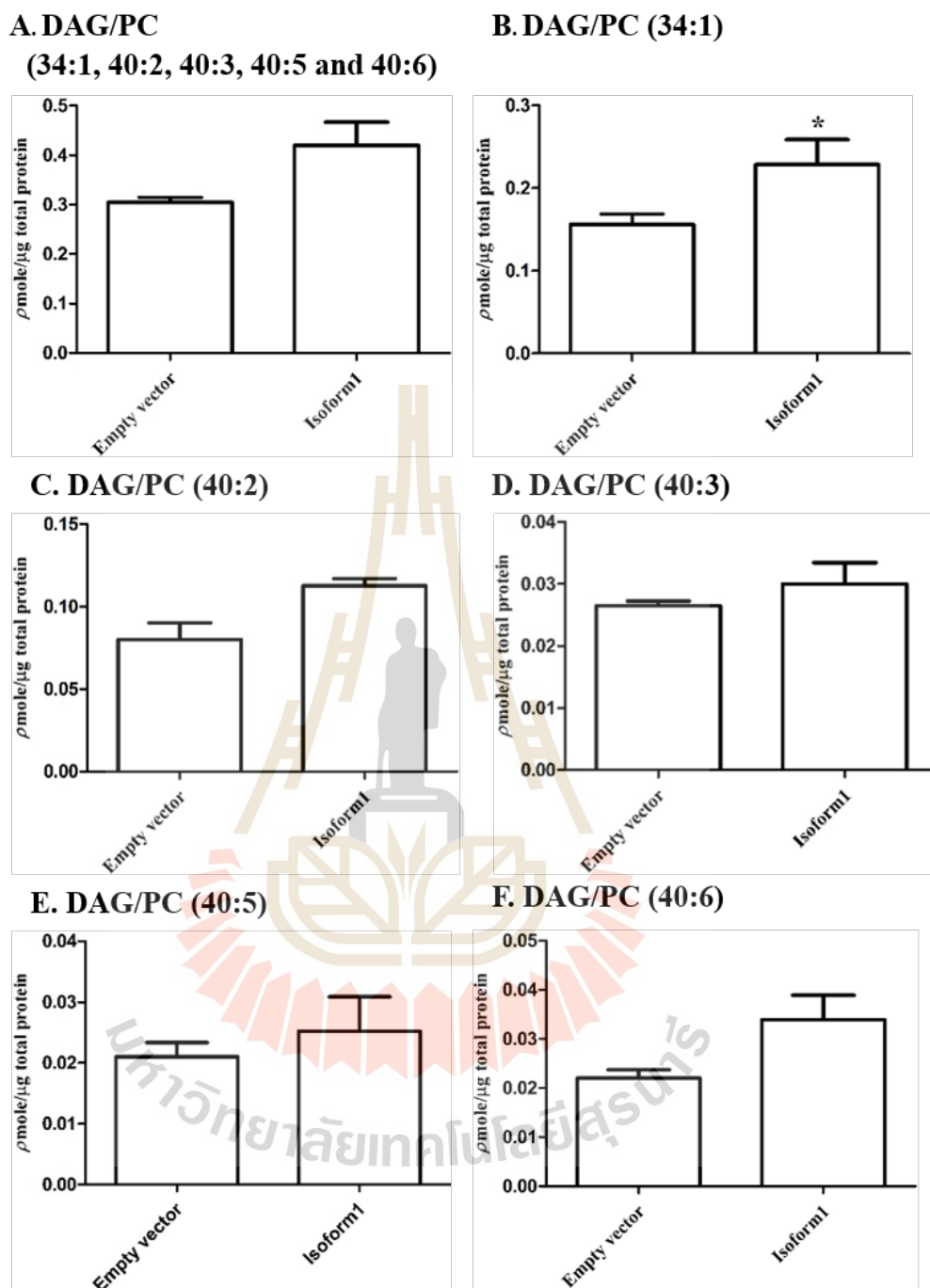


**Figure 4.26** The changes of DAG to PC ratios upon expression of GBA2 48 hours.

Data are expressed as mean of three independent replicates  $\pm$  SD, \* $p < 0.05$ .

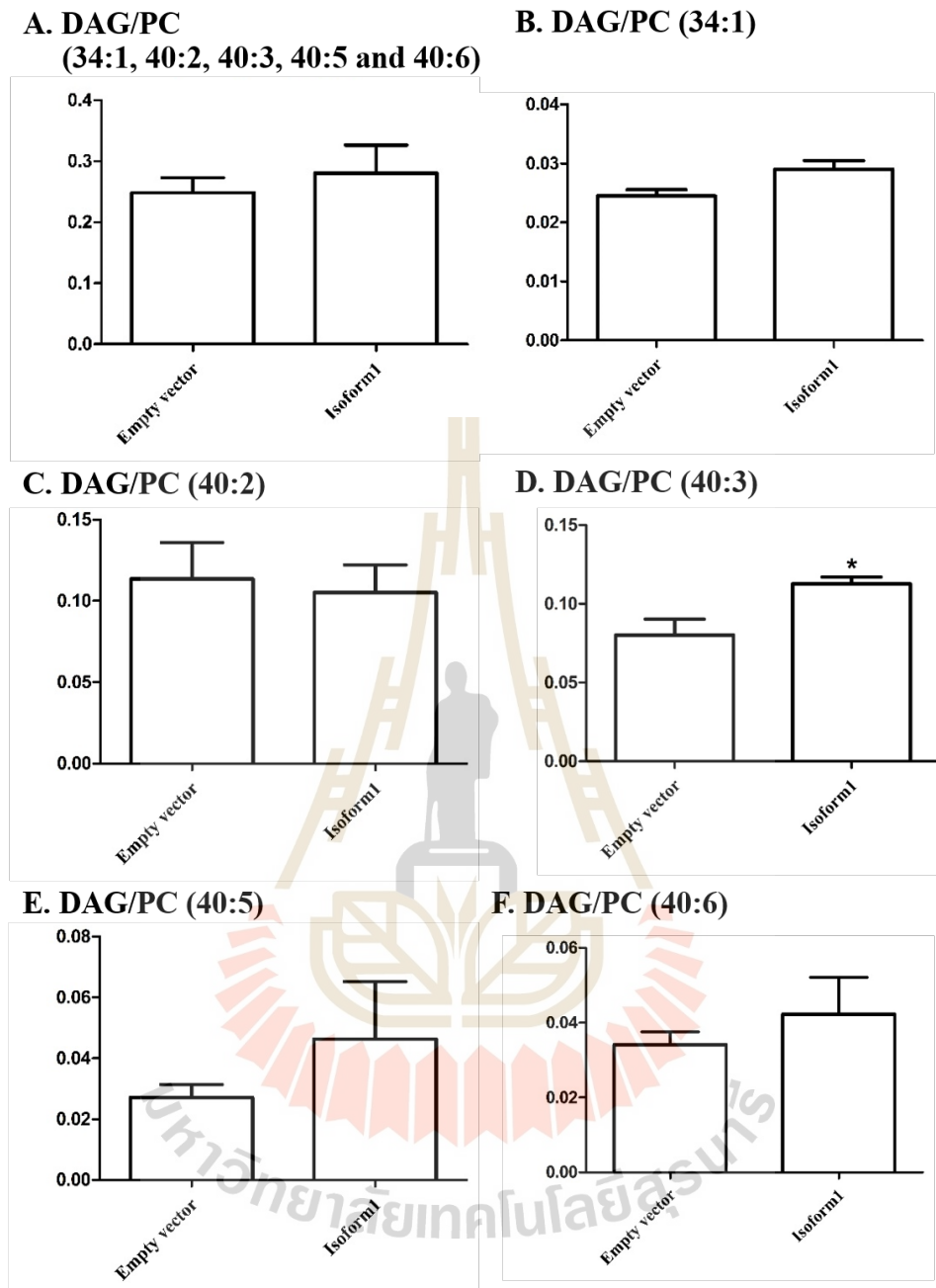


**Figure 4.27** The changes of DAG to PC ratios upon expression of GBA2 72 hour.

Data are expressed as mean of three independent replicates  $\pm$  SD, \* $p < 0.05$ .

#### 4.9 Sequence analysis of novel *GBA* mutation

Recent study by Teeratorn Pulkes et al revealed the 5 novel *GBA* mutation in Thai Parkinson's Disease (PD) patients, including 1275C>A (N386K), 1399C>T (P428S), 1309delG, IVS9+3G>C and IVS10-9\_10GT>AG. 4 *GBA* mutation and 1 wild type protein sequences were aligned, as shown in Figure 4.28. The alignment illustrates that 1309delG causes a frame shift mutation to generate the truncated protein that loses 92 amino acid at the C-terminal end, which is strong evidence that 1309delG is a deleterious mutation that can cause *GBA* deficiency via loss of function. On the other hand, N386K and P428S cause amino acid substitutions, which might reduce the enzyme activity. Moreover, IVS9+3G>C and IVS10-9\_10GT>AG are also mutations that may cause *GBA* deficiency and loss the function, although they occur in introns. It can set the hypothesis that IVS9+3G>C and IVS10-9\_10GT>AG promote alternative splicing to cause the possible truncated protein and thereby loss of *GBA* function in the cell. In addition, our samples study included *GBA* mutation IVS2+1G>A, which destroys the 5' splice site for intron 2, resulting in aberrant splicing that skips exon 2. Skipping exon 2 might affect the protein localization, since it encodes much of the secretory signal sequence of *GBA* protein, which is necessary for it to localize in the lysosome (Van meel, Bos et al., 2019). The predicted signal peptide of *GBA* wild type was compared to *GBA* carrying 1309delG as shown in Figure 4.2

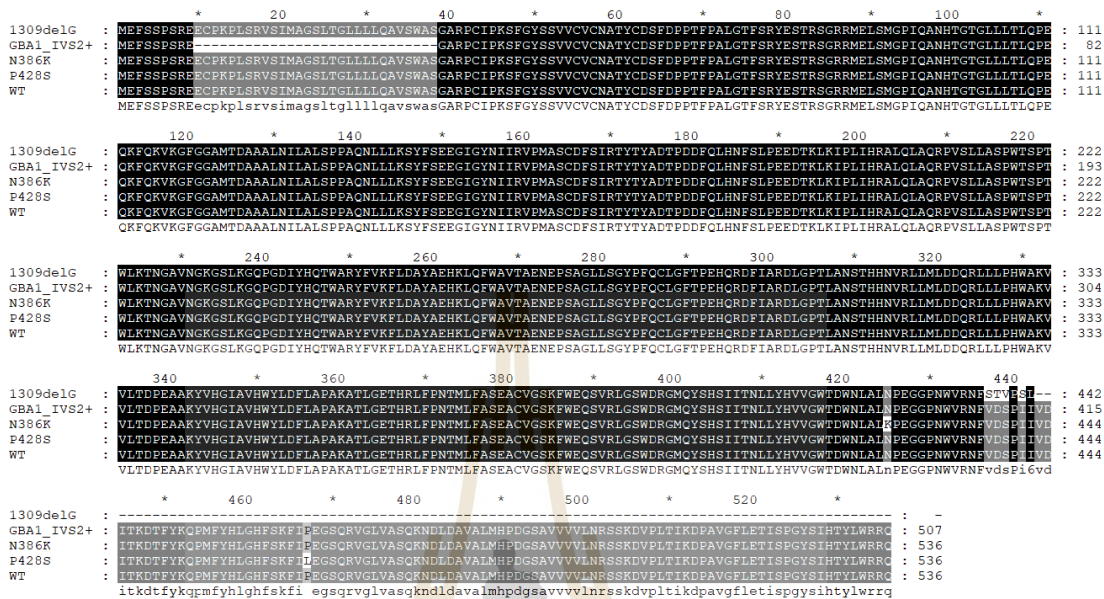


**Figure 4.28** Amino acid sequence alignment of human *GBA* mutation, compared to *GBA* wild type.





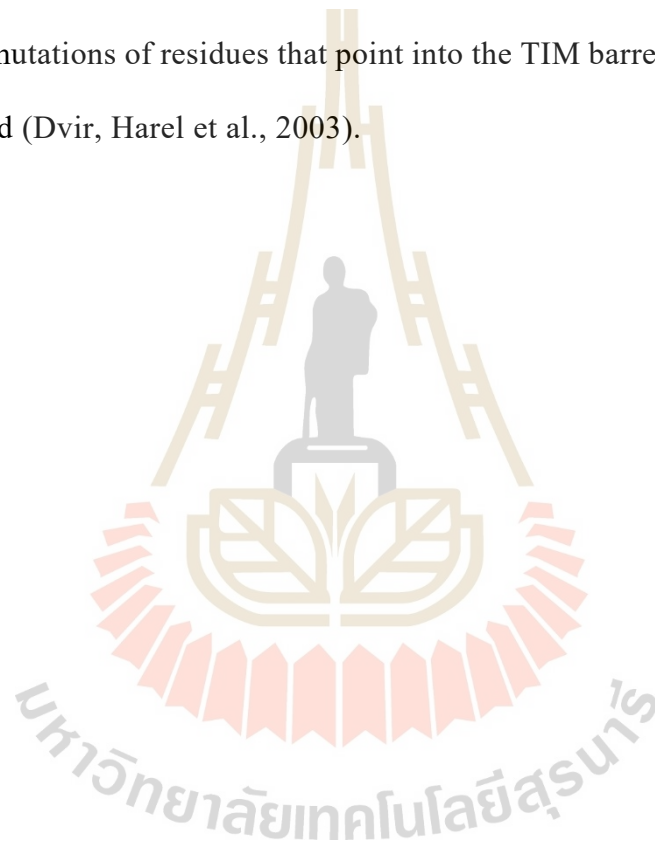
#### 4.10 Structure analysis of human *GBA* mutations

Homology modeling was used to build the protein structural models from the mutated amino acid sequences based on the X-ray crystal structure of human GBA (1OGS) solved by Dvir and colleagues (Dvir, Harel et al., 2003) to make their effects easier to visualize. The structural model shows what part of the protein is missing or where does the amino acid substitution occur to suggest what effect it might have.

In order to understand the structural and functional effects of the mutations, the mutated GBA protein sequences were used to predict their protein structure by SWISS-MODEL, including 1309delG, 1275C>A (N386K), and 1399C>T (P428S), as shown in Figure 4.30 and Figure 4.31. However, the exact effects of IVS9+3G>C and IVS10-9\_10GT>AG on mRNA splicing and the final protein sequence are not known, so the homology models could not be generated. The predicted structures were very similar to the human GBA structure on which they were based and suggested explanations for the effect of disease causing GBA mutants on the protein structure and activity.

As shown in the alignment in Figure 4.28, the amino acid substitution N386K changes from asparagine to lysine and P428S changes from proline to serine in the C-terminal part of GBA, while 1309delG causes loss of a part starting from I445, thereby losing about 94 amino acid at the C-terminus of GBA. According to structure (Figures 4.30 and 4.31), the parts of the structures missing in truncated proteins resulting from the 1309delG, IVS9+3G>C and IVS10-9\_10GT>AG mutations are critical for GBA structure and function, so the truncations are causes of the GBA dysfunction. For the 1275C>A (N386K), and 1399C>T (P428S) are amino acid substitution, which can supports the idea that these mutations may contribute to reduce enzyme activity. GBA carrying 1275C>A (N386K) was changed

from asparagine, a polar uncharged sidechain, to lysine, a positively charged amino acid, as shown in Figure 4.30. Asparagine provides hydrogen bond interaction between N386 to N92 (Figure 4.30(B)), although 4.8 Å is too long for a hydrogen bond that due to the position error. Lysine provide the positive charge at the side chain that might form an interaction with E388 as a negative charge, which is located near K386 (Figure 4.30(C)). N386K is linked to the longest  $\alpha$ -helix (helix 7), in which several other deleterious mutations of residues that point into the TIM barrel, such as N370, have been reported (Dvir, Harel et al., 2003).



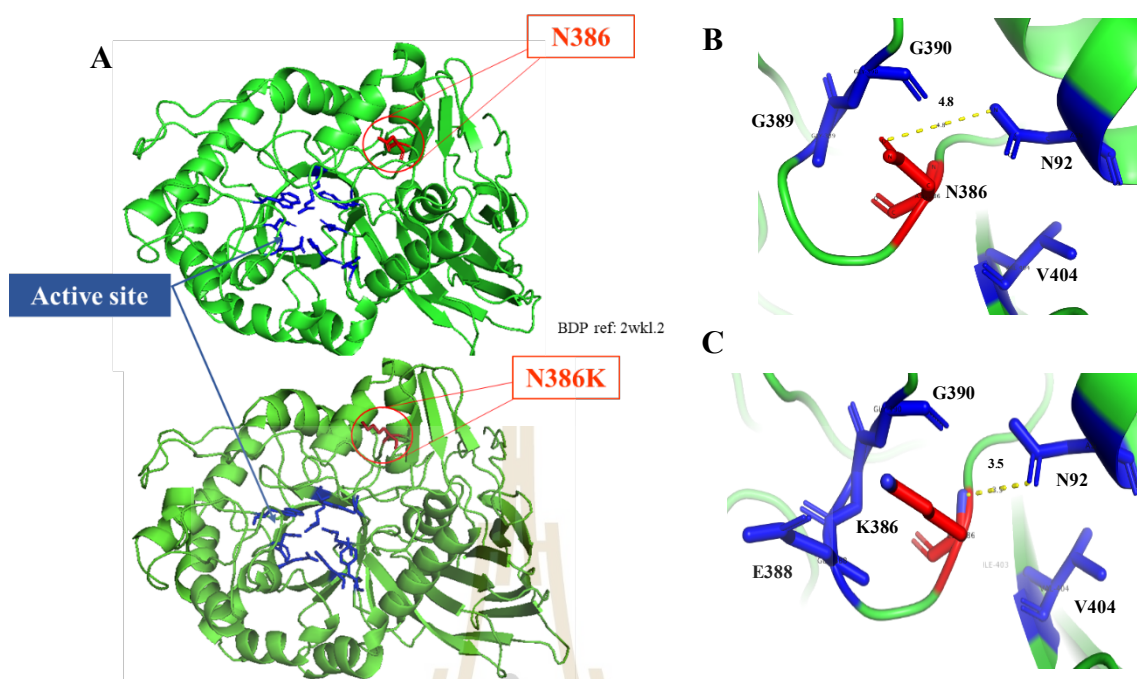


**Figure 4.30** A homology model of the human GBA mutation N386K based on the X-ray crystal structure (PDB code 2wkl.2). (A) GBA wild type (top) and GBA carrying N386K (bottom). N386 is shown in stick representation and highlighted in red color. (B) Close-up view showing N386 is located at a loop linked to G389 and G390, N386 trend to interact with N92 by hydrogen bonding with N of N92 to O of N386. (C) Close-up of the mutated residue K386, which is highlighted in red color, located at a loop linked to G389 and G390, K386 trend interact with N92 by hydrogen bonding with N of N92 to O of N386 with length 3.5 Å.

The P428S mutation is near the TIM barrel and a separate immunoglobulin-like domain on which L444 is located (Dvir, Harel et al., 2003) (Figure 4.4(A)). Changing proline to serine decreases the rigidity of the main chain and adds a polar uncharged side chain. Thus, changing from proline to serine provide participate in hydrogen bonds

with other amino acid, such as S431 (3.1 Å) but R170 (5.5 Å) is too long for the hydrogen bond interaction (Figure 4.31(B)) as well as promote low rigidity of a loop. In addition, P428S mutation is located near a L444 as commonly mutated position that found in Thai population (Pulkes, Choubtum et al., 2014), which is in the TIM barrel domain and a separate immunoglobulin-like domain area, suggesting that this mutation might has relevant to residues interaction effect like L444P or has similar effect compared to L444P mutation.



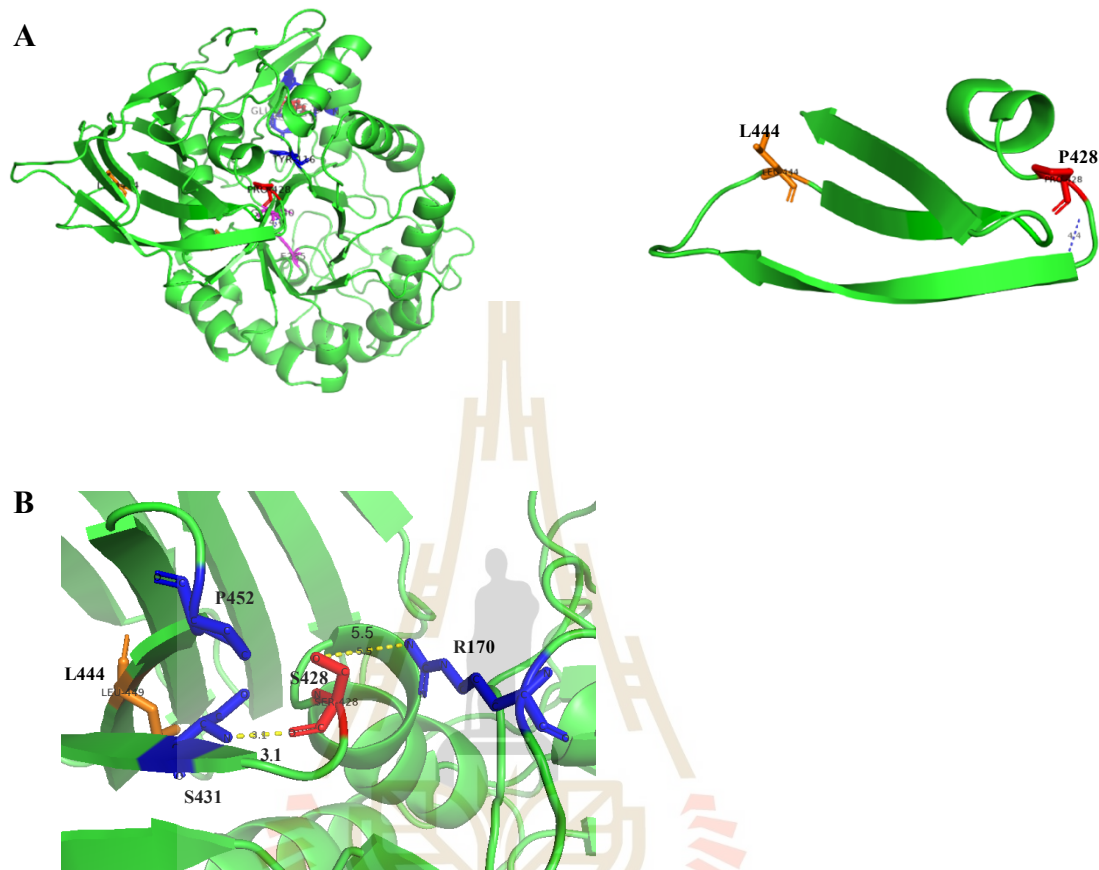


**Figure 4.31** A homology model human GBA mutation P428S based on the X-ray crystal structure (PDB code 2wk1.2). (A) P428 is shown located near the TIM barrel domain and a separate immunoglobulin-like domain on which L444 is located. (B) P428S may result in hydrogen bond interactions between S428 and R170 and S431.

For the GBA carrying 1309delG is a critical frame-shift mutation causing GBA deficiency via loss of function. It results in a truncated protein that lost 94 amino acid, as shown in Figure 4.32. The lost part contained a part of the TIM barrel and a separate non-catalytic immunoglobulin-like domain that is important to regulate activity or has

a structural role (Dvir, Harel et al., 2003), suggesting that this mutation caused GBA dysfunction.

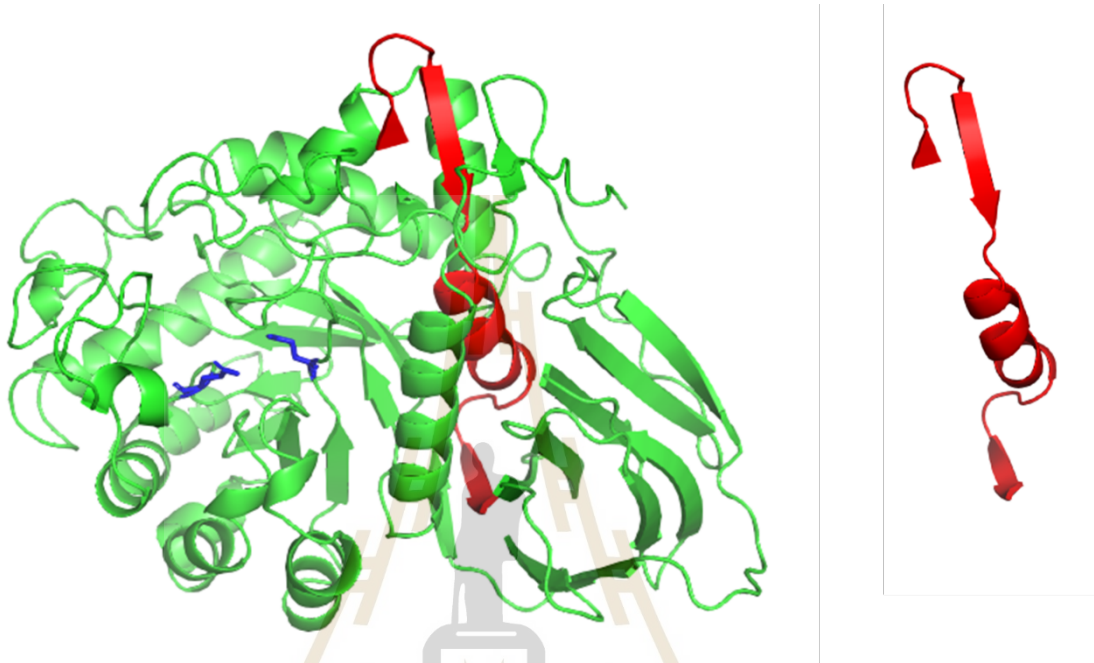


**Figure 4.32** A homology model human GBA mutation (1309delG) based on the X-ray crystal structure (PDB code 2wkl.2) showing that the part (red color) lost in the mutation was a part of the TIM barrel domain and the immunoglobulin-like domain that is important to regulate or structural role for this non-catalytic domain as well as the active-site residues (E235 and E340) are shown in blue color.

#### 4.11 Activity of human *GBA* and *Parkin* mutation

In order to confirm which *GBA* mutations contribute to enzyme dysfunction and whether they have an effect on the overall level of activity in the heterozygous state found in Parkinson's Disease, *GBA* activity against the fluorescent substrate 4-methylumbelliferyl  $\beta$ -D-glucoside (4MUG) was measured in Parkinson's patient fibroblast extracts. The fibroblast lines tested included one each with the five *GBA* mutations (1275C>A (N386K), 1309delG, IVS2+1G>A and IVS11-9,10 GT>AG), two with *Parkin* mutations (Het ex8 del and M1T/ne-), and five without known mutations from PD patients and three from healthy controls. We found that the levels of activity in fibroblasts with the *GBA* mutations 1309delG (fibroblast line HF6), IVS11-9,10 GT>AG (HF14) and the unknown mutation line HF7 were significantly lower than the healthy control lines HF16 and HF17, and other mutations, as shown in Figure 4.33. However, only the HF14 and HF7 lines had activity significantly below the HF19 normal control fibroblast cell line and the HF11 *GBA* mutation cell line. The *GBA* activity can provide the evidence that truncated protein may reduce enzyme activity, since 1309delG (in HF6) and IVS11-9,10 GT>AG (HF14) are truncations, but given the high variability in the control fibroblast cell lines and heterozygous nature of the mutations, it is not reasonable to draw too many conclusions. For the lines with *Parkin* mutation and others without known mutations, the activity was not significantly different compared to healthy controls. Therefore, these *Parkin* mutations do not appear to affect  $\beta$ -glucosidase activity much. However, this evidence only shows activity in extracts on nonnative substrate, so our further study measured the natural substrate and product sphingolipids in the cells.

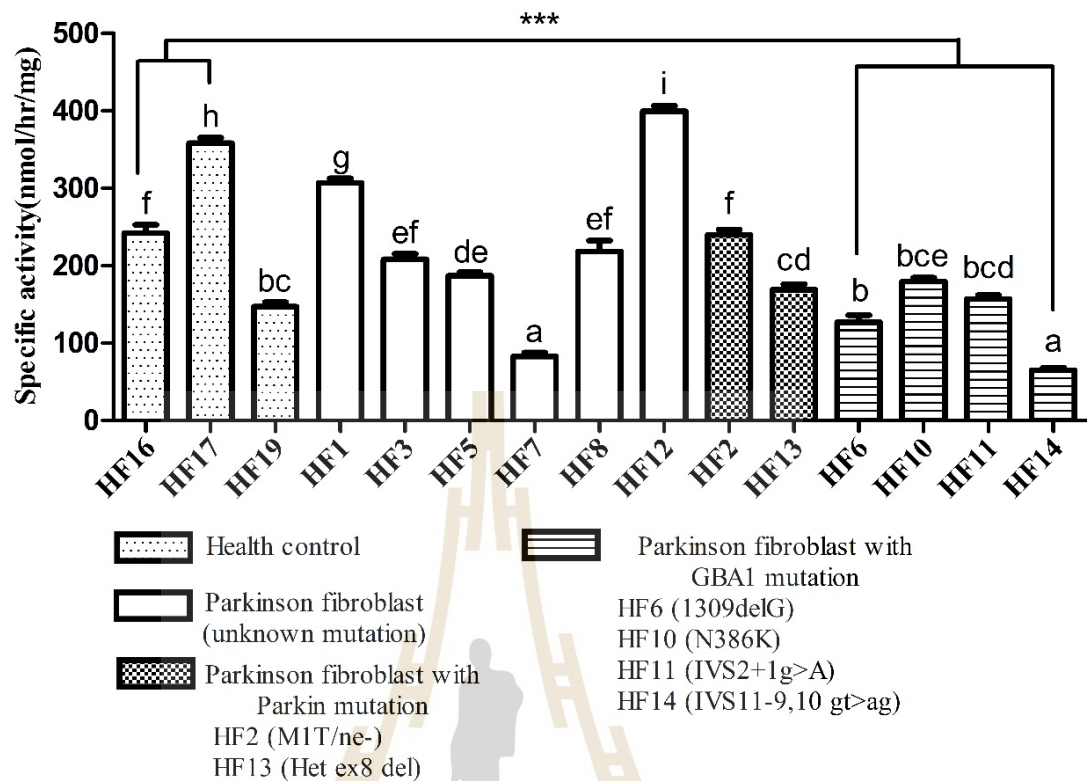


**Figure 4.33** GBA enzyme activity in Parkinson's patient fibroblasts with *GBA* and *Parkin* mutations. Data are expressed as mean of three independent replicates  $\pm$  SD, \* $p < 0.05$  and \*\*\* $p < 0.01$ . The difference alphabets were considered as the statistically significant.

## 4.12 Sphingolipid species levels in fibroblasts with *GBA* or *Parkin* mutations

Fibroblasts with *GBA* base pair substitution mutations generally had lower activity to hydrolyze the synthetic 4MUG substrate than those with frame shift mutations. However, it does not indicate whether heterozygous *GBA* mutations and *Parkin* mutations affect natural sphingolipid substrates in the cells. Therefore, the lipid levels in Parkinson's patient fibroblasts were determined by shotgun mass spectrometry. Total lipid and 3 different lipid classes, including sphingolipids, glycerophospholipids and glycerolipids, are shown in Figure 4.34. The total lipid and total sphingolipid were not significantly different, while glycerolipid appeared to be significantly different between HF10 (N386K (1275C>A)) and the three healthy controls. Thus, we can give the hypothesis that *GBA* mutations might affect the glycerolipid level in the cell suggesting the interconnectivity between the 3 lipid classes. In addition, sterol lipid was shown similar trend with glycerolipid (HF10) as shown in Figure 4.35. However, since we only had 1 fibroblast line with this mutation and it had relatively high *GBA* activity *in vitro*, the significance should not be overstated. In this study we would like to focus on the sphingolipid class, because *GBA* activity could directly affect the level of glucosylceramide, which acts as the *GBA* natural substrate in the cell. By the way, I expect that the reasons why total lipid was not significantly different is because cells try to keep lipid levels consistent in the cell to provide membranes structure and other lipid functions. In order to see whether the proportions of the 3 lipid classes were consistent or varied between representative fibroblast samples, including healthy controls, PD without known mutations, and PD with *GBA* and *Parkin* mutations, proportions were represented in pie charts in Figure 4.36. As expected, glycerophospholipid was the most abundant lipid class in the cell, followed by sphingolipid,

sterol lipid and glycerolipid. There are not significantly differences in proportions of these classes between fibroblast lines.

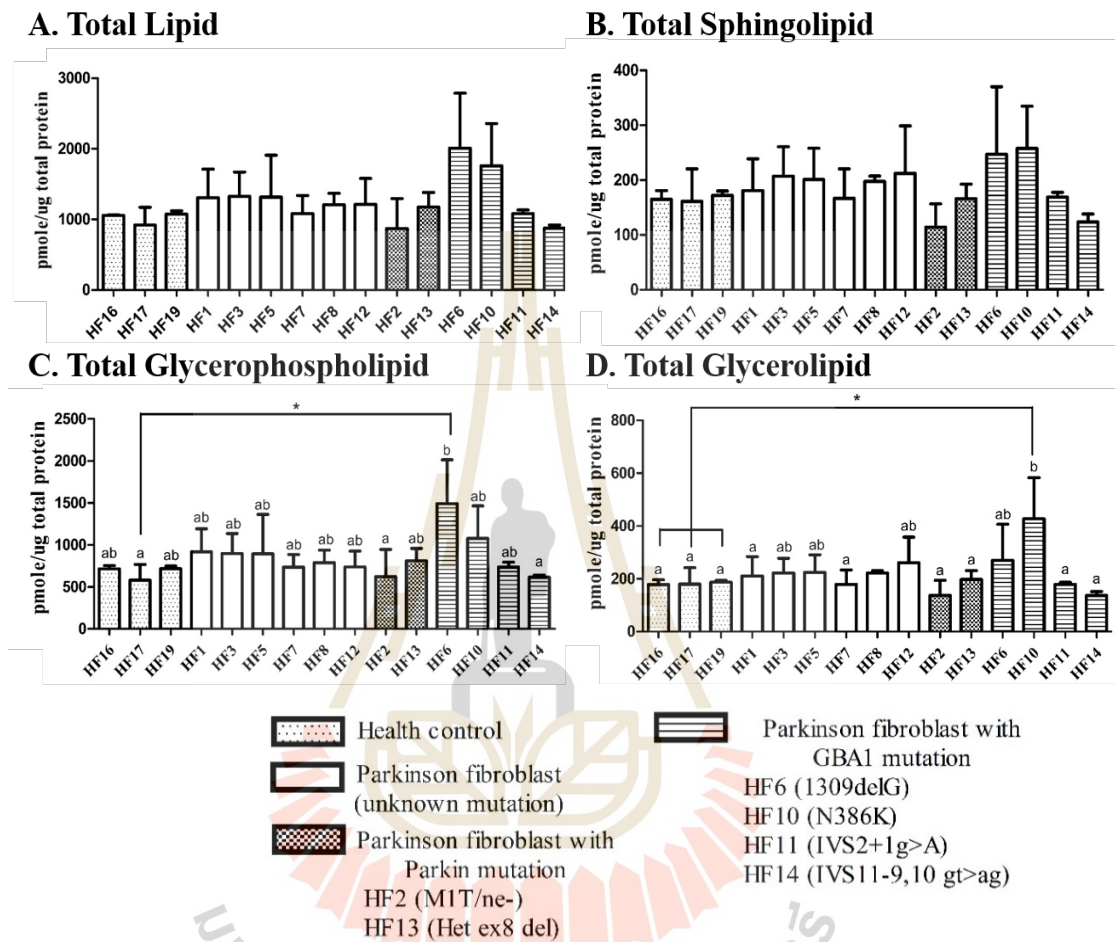


**Figure 4.34** Profiles of total lipid (A), total sphingolipid (B), total glycerophospholipid (C) and total glycerolipid (D) in Parkinson's patient fibroblast with *GBA* and *Parkin* mutations. Data are expressed as mean of three independent replicates  $\pm$  SD, \*  $p < 0.05$  and \*\*\*  $p < 0.01$ . The difference alphabets were considered as the statistically significant.

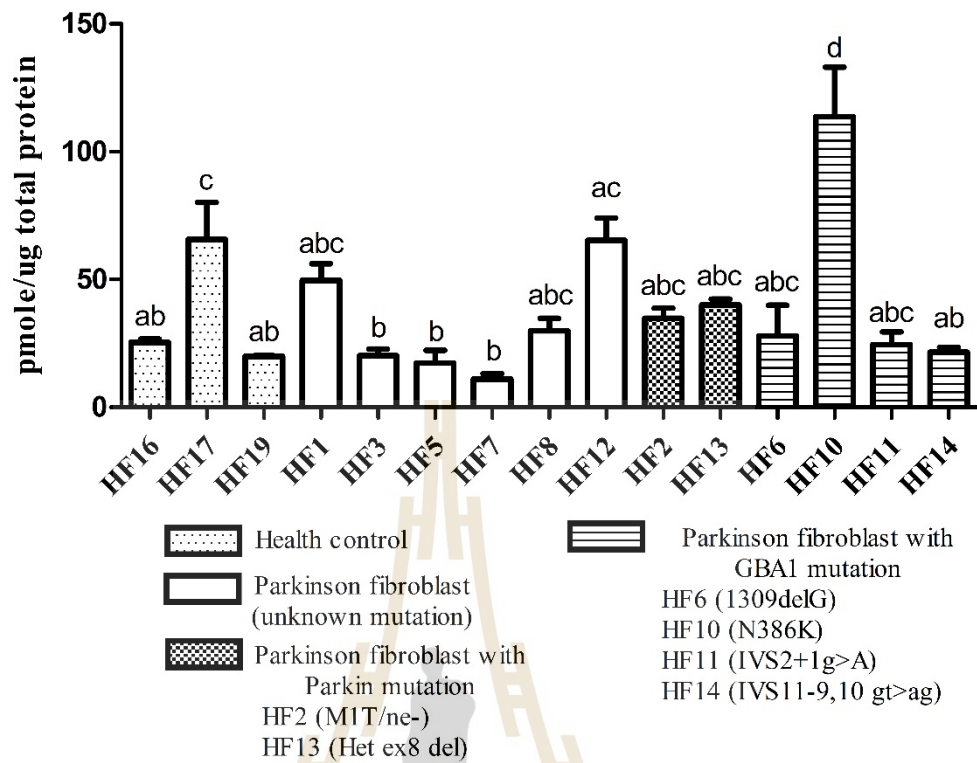


**Figure 4.35** Profiles of sterol lipid in Parkinson's patient fibroblast with *GBA* and *Parkin* mutations. Data are expressed as mean of three independent replicates  $\pm$  SD, \* $p < 0.05$  and \*\*\* $p < 0.01$ . The difference alphabets were considered as the statistically significant.

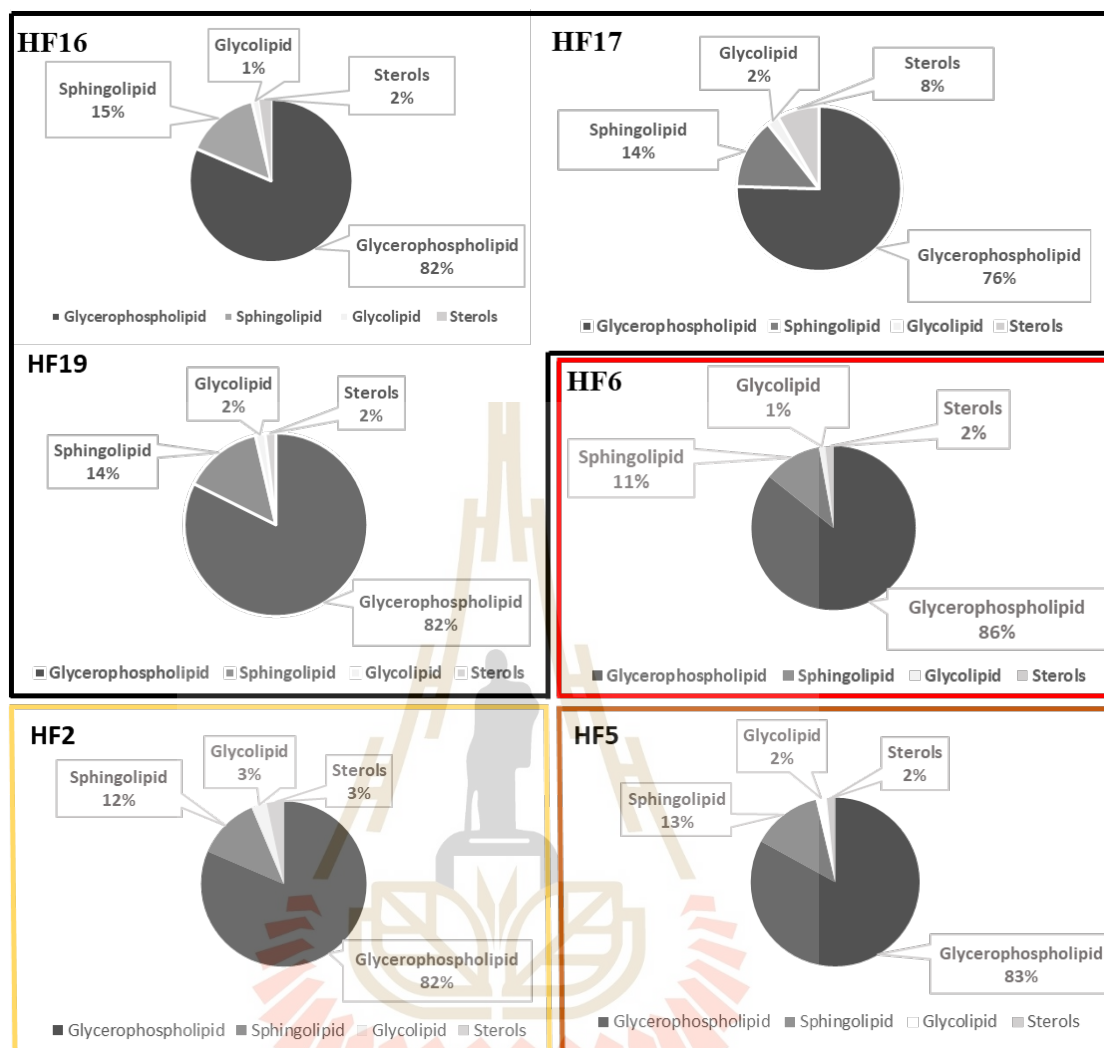


**Figure 4.36** Proportions of 3 lipid classes shown as pie charts. The representative samples include healthy control (HF16), (HF17) and (HF19), *GBA* mutation (HF6), *Parkin* mutation (HF2) and unknown mutation (HF5).

A heat map of the sphingolipid concentration Z-scores in the different fibroblast cell line extracts is shown in Figure 4.37. It shows those sphingolipids detected in all conditions, including ceramides (Cer) with combined fatty acids and base (total number of carbons in the ceramide) of C34-42, hexosylceramides (HexCer) with combined fatty acid and base chain lengths of C34-42, and sphingomyelins (SM) with combined chain lengths

of 32-44 carbons. Interestingly, clustering of the cell extracts based on their sphingolipid compositions did not cluster lines with GBA mutations together, but did cluster HF6, HF3, HF1 and HF10 together, which include *GBA*, *Parkin* and unknown mutation. However, only HF6 was remarkable in apparently having high levels of some HexCer, which would be expected if GBA level was low. HF6 (1309del1G) showed high concentrations (high Z-scores for hexosylceramide CerG1(d34:1), CerG1(d42:1), and CerG2(d42:1)). This is consistent with this GBA mutation causing a frameshift to eliminate a significant part of the protein so the enzyme loses the ability to hydrolyzes GlcCer, resulting in higher hexosylceramide and second species with the same molecular weight as CerG1(d42:1) like CerG2(d42:1). This apparently results in an increase in total HexCer for H6 compared to controls, while no significant difference was seen in ceramide and sphingomyelin levels, as shown in Figure 4.38. For the ceramide, it would be generated from *de novo* synthesis and other recycling pathways in the sphingolipid metabolism, and the cells need to keep the ceramide levels constant, because it is the core sphingolipid to generate other sphingolipid species. Furthermore, SM has been identified as a core component of the cell membrane, so its level may be controlled by other factors and not affected much by hexosylceramide level upon the mutation. For HF10 (1275C>A (N386K)), it appears to slightly reduce GBA activity, due to the change from Asn to Lys at the position 386. However, the mutation was heterozygous and the GBA activity from the other allele may be higher due to induction or some other factors.

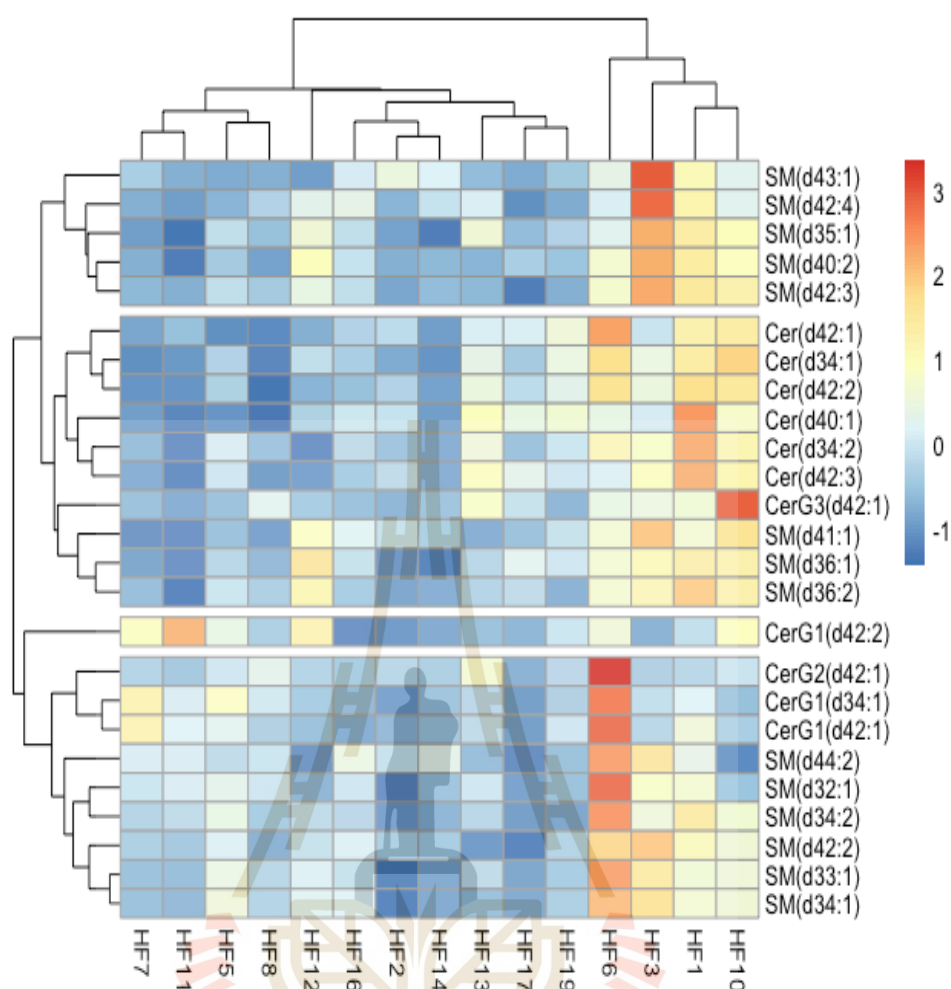


**Figure 4.37** Heat map diagram of profiles of the sphingolipids ceramides, hexosylceramides and sphingomyelins in Parkinson's disease patient fibroblasts carrying *GBA*, *Parkin* and unknown mutations. The heat map illustrates comprehensive quantifications of relative levels of sphingolipid species in the cell extracts, while the cluster maps illustrate the similarities of the patterns. All values are expressed as Z-score values and are color-coded from blue (below average amounts of lipid species) to red (above average amounts of lipid species).

For the other mutations that generate the truncated protein like IVS2+1G>A (HF11) and IVS11-9,10 GT>AG (HF14), Z-scores for HexCer were low, so no block in their hydrolysis was obvious. Thus, we hypothesize that these mutations can promote

the cell to induce the other allele or use the other ways to hydrolyze glucosylceramide in the cell. Since the cells have heterozygous GBA mutations, the dysfunction is in 1 allele, but the other allele still produces active GBA, resulting in these cells being able to hydrolyze glucosylceramide.

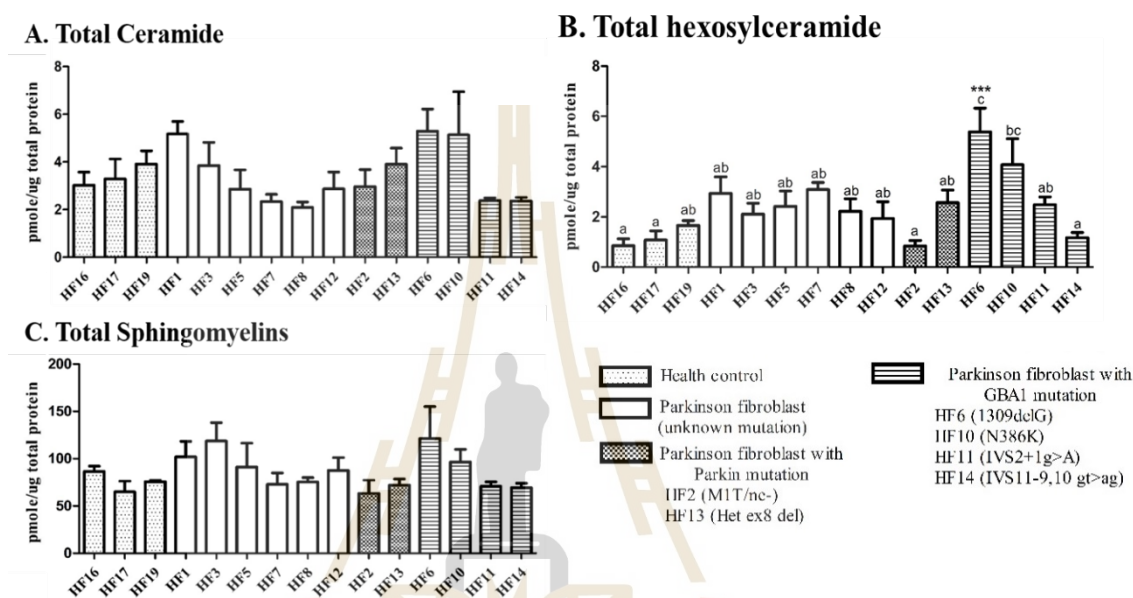


**Figure 4.38** Profiles of total ceramides, hexosylceramide and sphingomyelin, which are shown in the heat map in Parkinson's patient fibroblasts. (A) Total Ceramide (B) Total Hexosylceramide, and (C) Total sphingomyelins, expressed as a bar graph. Data are expressed as mean of three independent replicates  $\pm$  SD, \* $p < 0.05$  and \*\*\* $p < 0.01$ . The difference alphabets were considered as the statistically significant. In order to compare the changes related to the conversion of glucosylceramide to ceramide more closely, sphingolipids with the same carbon chain length and degree of desaturation of ceramide, hexosylceramide and sphingomyelin that were detected in each sample were compared. Hexosylceramide and ceramide with carbon chains of 34:1, 42:1 and 42:2 were detected in all samples, as shown in Figure 4.39(A) and 4.39(B), while among these only sphingomyelin with carbon chains of 34:1 and 42:2 were detected, as shown

in Figure 4.39(C). The result demonstrates that hexosylceramide was significantly higher in HF6 than in the healthy controls, and tended to be higher in the other GBA mutants as well, except for HF14. However, ceramide and sphingomyelins were not significantly different in HF6 and other GBA mutations compared to the other fibroblast lines.



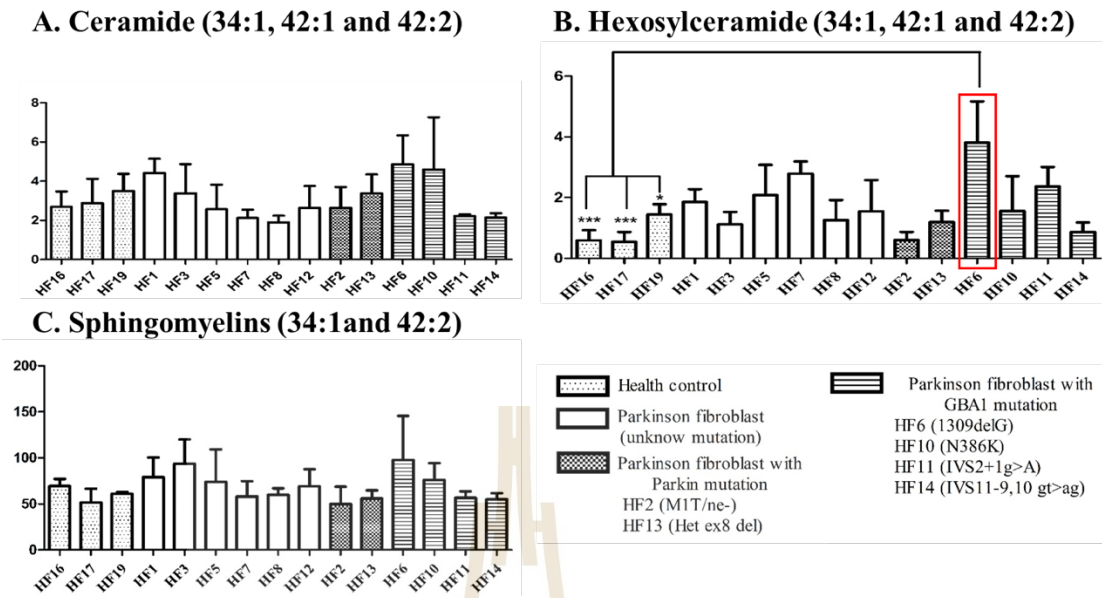


**Figure 4.39** Profiles of totals of ceramides, hexosylceramides and sphingomyelins, detected in all control Parkinson's patient fibroblasts with common ceramide carbon chain lengths and saturation. (A) Ceramide (34:1, 42:1 and 42:2) (B) Hexosylceramide (34:1, 42:1 and 42:2), and sphingomyelins (34:1 and 42:2), expressed as bar graphs. Data are expressed as mean of three independent replicates  $\pm$  SD, \* $p < 0.05$  and \*\*\* $p < 0.01$ . The difference alphabets were considered as the statistically significant.

### 4.13 Sphingolipid ratio control the direction of sphingolipid connectivity

To generate a more sensitive parameter for the movement of sphingolipid affected by *GBA* and *Parkin* mutation, the ratio of total Cer to total HexCer and total SM to total HexCer were calculated as shown in Figure 4.40 and Figure 4.41. In Figure 4.40, the *GBA* mutations, including HF6 (1309delG), HF10 (N386K) and HF11 (IVS2+1g>A) were significantly different, compared to 2 out of 3 healthy controls for total Cer to HexCer, but the HF19 control was not significantly different, while SM to HexCer found that HF6, HF10, HF11 and HF13 (Het ex8 del) were different compared to only 1 healthy control, suggesting that nothing was very significantly changed, considering the variation in normal human fibroblasts.

In order to detect the action of *GBA* on glucosylceramides with a specific carbon chain (length and number of double bonds), detected sphingolipids with the same carbon chain mass were used to calculate their ratios. As noted above, these included Cer and HexCer d34:1, d42:1, and d42:2, but d42:1 was not detected for SM, so only 34:1 and 42:2 were the same carbon chains that could be compared with HexCer and SM. The ratio of Cer to HexCer (d34:1, d42:1, and d42:2) was significantly decreased compared to healthy control HF16 and HF17, while SM to HexCer (d34:1 and d42:2) was significantly decreased compared to only 1 healthy control, HF 17, as shown in Figures 4.40(B) and 4.41(B), respectively.

Since a *GBA* could act more effectively on one or a subset of the glucosylceramide species, the change of intracellular sphingolipid ratio was analyzed for each ceramide/hexosylceramide pair, including Cer to HexCer (d34:1) in Figure 4.40(C), Cer to HexCer (d42:1) in Figure 4.40(D), HexCer to Cer (d42:2) in Figure 4.40(E). The ratios of Cer to HexCer were decreased for HF6 (1309delG) and HF11

(IVS2+1g>A), as well as unknown mutation HF5, HF7 and HF8, compared to 1-2 healthy control, suggesting that GBA mutation might affect to the sphingolipid level, but the variation in the control fibroblasts makes it difficult to be certain without more samples.

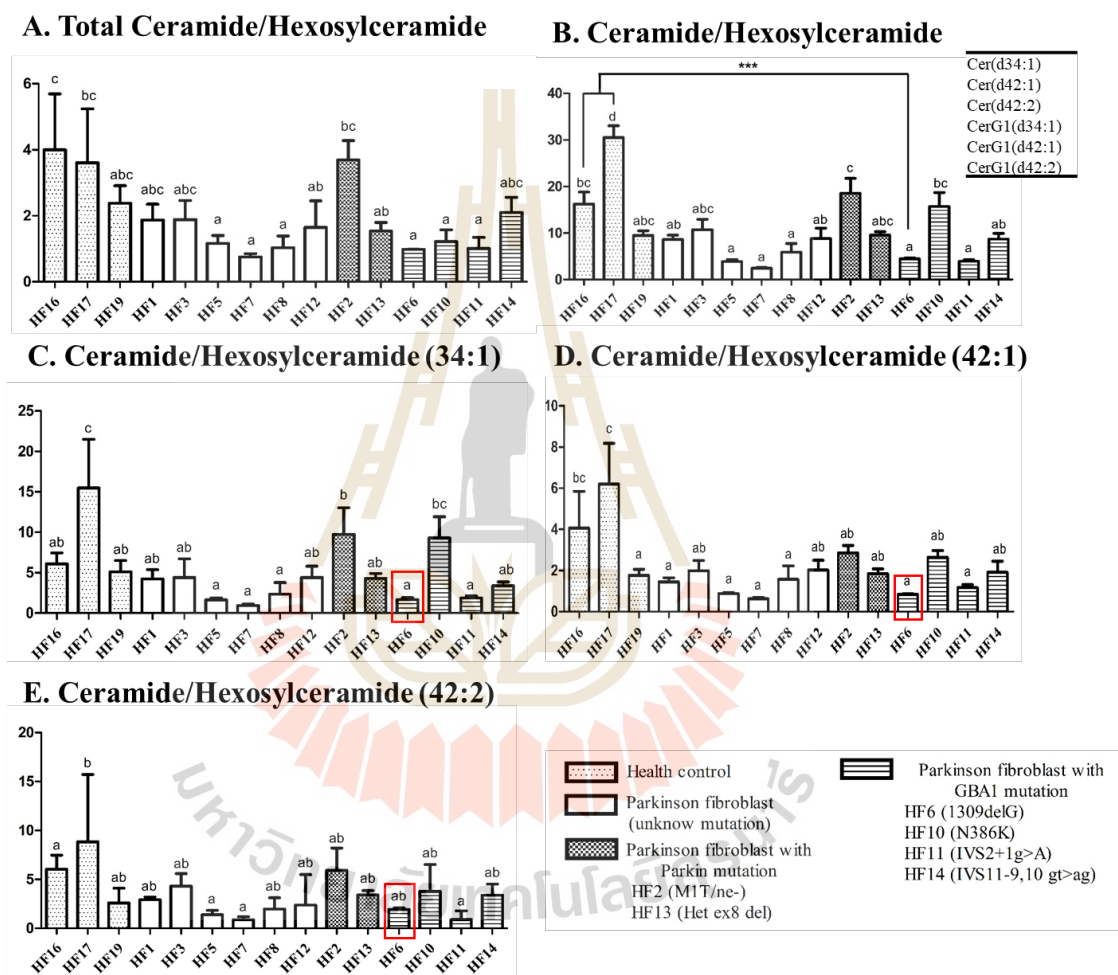


**Figure 4.40** Effect of *GBA* and *Parkin* on ceramide/hexosylceramide ratios of specific lipid species. (A) total ceramide/hexosylceramide, (B) ceramide/hexosylceramide (d34:1, d42:1 and d42:2) and ceramide/hexosylceramide for the individual ceramide forms d34:1, d42:1 and d42:2 are shown in (C) (D) and (E), respectively. Data are expressed as mean of three independent replicates  $\pm$  SD, \* $p$ <0.05 and \*\*\* $p$ <0.01. The difference alphabets were considered as the statistically significant.

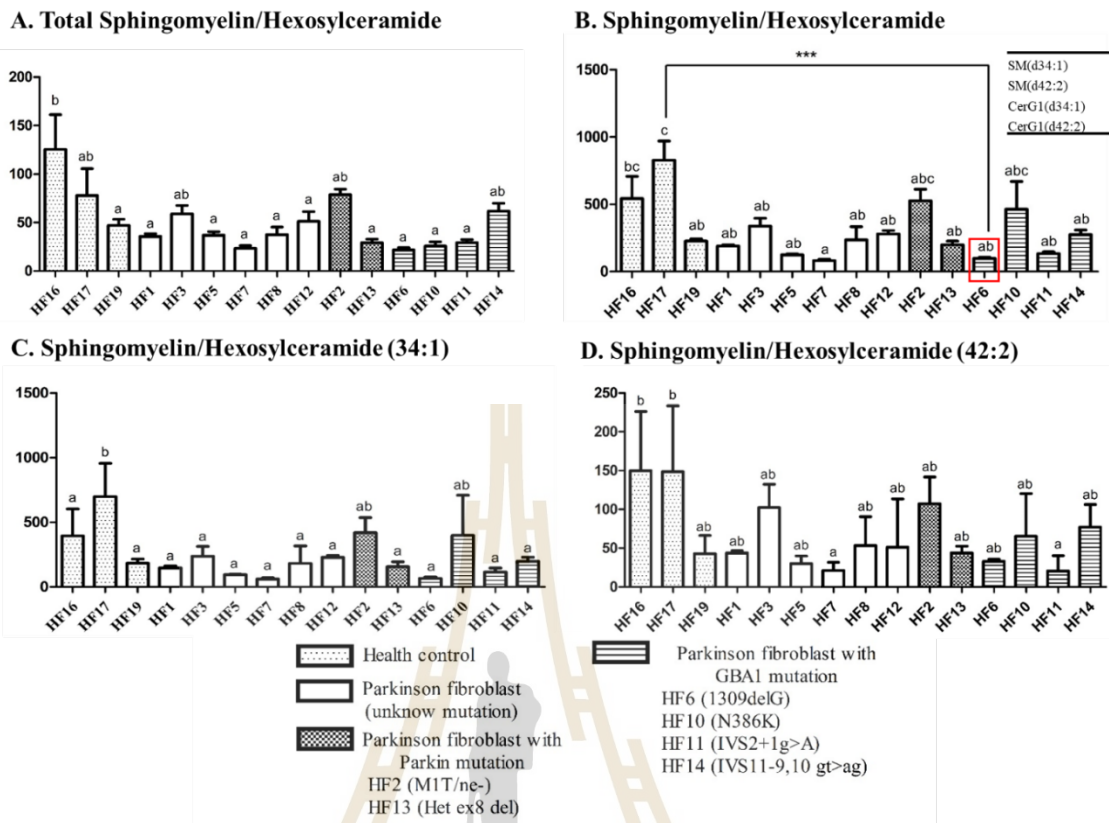


**Figure 4.41** Effect of *GBA*, *Parkin*, and unknown mutations on sphingomyelin/hexosylceramide ratios of specific lipid species. (A) Total sphingomyelin/hexosylceramide, (B) sphingomyelin/hexosylceramide (d34:1 and d42:2) and sphingomyelin/hexosylceramide d34:1 and d42:2 individually are shown in (C) and (D), respectively. Cells were harvested, lipids extracted, and then subjected to shotgun mass spectroscopy analysis for quantification of the level of sphingolipid. Data are expressed as mean of three independent replicates  $\pm$  SD, \*  $p < 0.05$  and \*\*\*  $p < 0.01$ . The difference alphabets were considered as the statistically significant.

#### 4.14 Correlation of sphingolipid ratio and its activity

In order to see whether there is a significant relationship between the sphingolipid movement and the activity, in the patient's fibroblasts, the sphingolipid ratios were plotted against the activity. Healthy controls HF16, HF17 HF19 and GBA mutations HF6 (1309delG), HF10 (N386), HF11 (IVS2+1g>A) and HF14 (IVS11-9,10 GT>AG) were used to calculate the correlation with its activity.

The result shows that Ceramide to hexosylceramide ratios, including carbon long chain 34:1, 42:1 and 42:2 present the correlation with the activity, with  $R^2 = 0.43, 0.81$  and  $0.78$ , respectively. Thus, when only healthy controls and GBA mutations were analyzed, there was a reasonable correlation between the activity and ratios of ceramide to hexosylceramide. Due to the high variation, this correlation did not hold when all Parkinson's disease fibroblast lines were included (data not shown). It seems likely that we would need a much larger number of samples to verify this correlation in general.

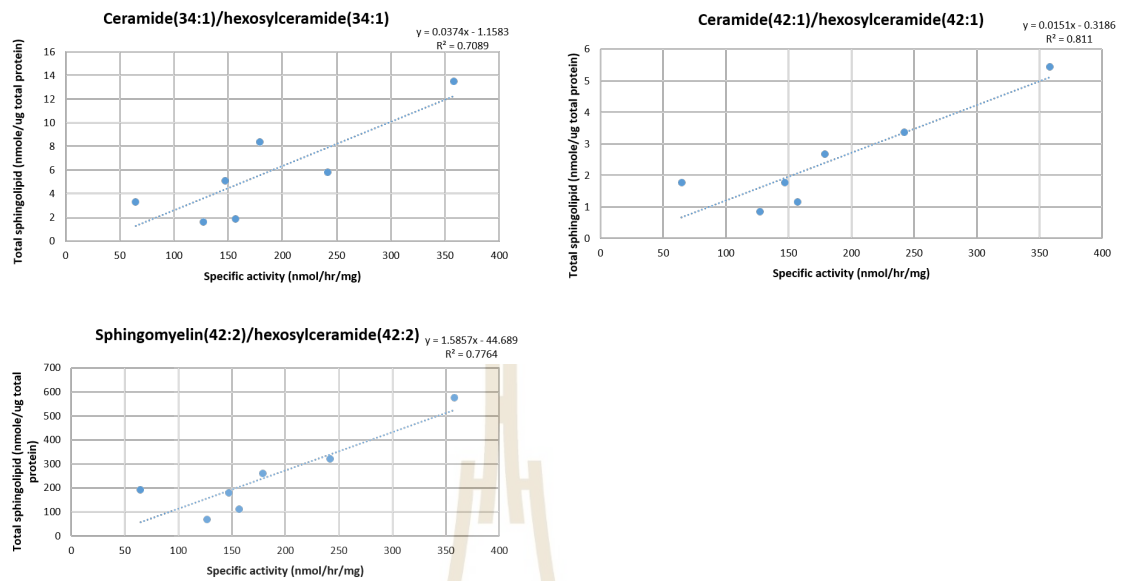


**Figure 4.42** The correlation of ceramide/hexosylceramide ratio with its activity, in healthy control fibroblast lines HF16, HF17, HF19 and GBA mutation fibroblast lines HF6, HF10, HF11 and HF14. The  $R^2$  correlation coefficients were calculated.

## CHAPTER V

### CONCLUSION

The human GBA2 isoforms were analyzed to visualize the predicted structures and functionality of the 9 predicted GBA2 isoforms that cover most of the gene and do not contain other start codons before their putative start codons. After concluding that these 9 isoforms could possibly produce functional proteins, the corresponding cDNA were expressed in COS-7 cells. Because GBA2 isoform 1 and GBA2 isoformX1 differ only by the insertion of 6 amino acid residues in the N-terminal domain of isoform X1, while other GBA2 isoforms were missing amino acid segments compared to isoform1, thus we hypothesized that GBA2 isoform 1 and GBA2 isoformX1 were going to be active isoforms, but the other isoforms may or may not be active.

1. The human GBA2 isoforms genes were synthesized and were successfully expressed in COS-7 cells. The cells were harvested at 48 and 72 hours incubation time, then expression was confirmed by qRT-PCR and western blotting analysis. The RNA expression at 48 hours was significantly higher than 72 hours. When GBA2 isoform protein levels were identified by western blotting analysis using anti-GBA2 and anti-FLAG-tag antibodies, the significantly differences of total protein

2. Concentration was shown between non-transfection condition and other isoforms as shown in both 48 and 72 hours conditions. All the GBA2 isoforms band were present at both times and were significantly different compared to the control.

3. When GBA2 activity on 4MUG synthetic substrate was measured, only GBA2 isoform 1 hydrolyzed the substrate as well as incubation time affected the enzyme activity because of RNA level caused by transient transfection. This result confirmed that adding and missing of amino acid significantly affected the GBA2 isoforms activity. Interestingly, GBA2 isoformX1 is not the active structure, despite only having small difference of adding 6 amino acids in the N-terminal domain compared to isoform1.

4. The effect of GBA2 overexpression in COS-7 cells on total lipids, total sphingolipids total glycerophospholipids, total glycerolipids, as well as total lipid species with different carbon chain lengths in 3 different lipid classes were identified.

4.1 Total lipid, total sphingolipid, total hexosylceramide, total sphingomyelin, total glycerosphospholipid, total glycerophosphocholine, total glycerophosphoethanolamine, total glycerphosphoinositol and total glycerolipid levels of 48 and 72 hours were not significantly different with all conditions, so GBA2 overexpression did not disrupt overall lipid homeostasis. In contrast, the total ceramide level in extracts of cells overexpressing isoform1 at 48 hours after transfection was significantly increased, but at 72 hours it was not significantly different. In contrast, the total hexosylceramide level was significantly decreased at 48 hours, but at 72 hours it was not significantly different. Thus, No significant differences were seen with other isoforms. This result supports the concept that GBA2 isoform 1 was only active isoform that

can contribute to the total ceramide level by releasing hydrolyzing the glucosylceramide to release ceramide and glucose.

4.2 The sphingolipid with different carbon chain lengths and degrees of saturation were identified as GBA2 substrates and products. According to the heat map, GBA2 isoform 1 had the lowest Z-scores for hexosylceramide d34:1, d40:1, d42:1 and d42:2 levels at both 48 and 72 hours, which confirmed that these were GBA2 substrates. However the levels of CerG1(d38:2), CerG2(d34:1), CerG2(d42:1) and CerG2(d42:2) were similar to or slightly higher than control upon overexpression of GBA2 isoform 1, suggesting that they may be galactosylceramides, which are not likely to be hydrolyzed by GBA2. Moreover, ceramide d34:1, d36:1, d40:1, d40:2, d42:1, d42:2 and d42:3 levels of GBA2 isoform 1 in 48 hours was significantly different, compared to the other isoforms and control, which confirms that ceramide levels were affected by GBA2 isoform 1 expression as the GBA2 product. However, sphingomyelin of 48 hours looks higher than other conditions, but the difference is not statistically significant. In contrast, sphingomyelin of 72 hours were not significantly different with all condition.

5. Sphingolipid ratios that may indicate the direction of sphingolipid flow and connectivity were also analyzed. The sphingolipids for which the same carbon chain length (carbon number) and unsaturation, including d34:1, d40:1, d42:1 and d42:2, was detected for both ceramide and hexosylceramide were used to calculate the ratio of ceramide to hexosylceramide. In the case of sphingomyelin to hexosylceramide those with chain lengths and double bonds of d40:1, d42:1 and d42:2 were analyzed. Only GBA2 isoform 1 was significantly different compared to other conditions and control

with higher ratios at 48 hours, while at 72 hours isoform1 was also not significantly different compared to some conditions. These confirm that hexosylceramide and ceramide with d34:1, d40:1, d42:1 and d42:2 lipids were likely to be the GBA2 substrate and product, respectively and the lipid levels tended to equilibrate to be more similar to control with increasing time. Moreover, some of the released ceramide may have been used in sphingomyelin synthesis by SM synthase, which also converts glycerophosphocholine to diacylglycerol in the process of SM synthesis.

6. Lipid distribution was observed to see which sphingolipid carbon chain length/ desaturation species are the most abundant, and which are affected by GBA2 isoform 1. Sphingomyelins d42:2 and d42:1 were the most abundant at both 48 and 72 hours, in extracts of cells transfected with empty vector and isoform1 as well. As PC and DG were noted as the most abundant in the cells as shown in 48 and 72 hours.

7. The levels of glycerolphospholipids and glycerol lipids were examined in COS-7 cells overexpressing GBA2 isoform 1, in order to identify connections between sphingolipid, glycerolphospholipid and glycerolipid. In order to confirm the effect of sphingomyelin involving with glycerophosphocholine (PC) and glycerolipid (DAG) level. The ratio between DAG to PC with fatty acyl chains with total carbons and double bonds of 34:1, 40:2, 40:3, 40:5 and 40:6 were analyzed. The ratio of DAG to PC 34:1 at 48 hours was shown as significantly different between empty vector and isoform1, compared to other conditions. In contrast, at 72 hours was shown as no significantly different with 34:1, while shown significantly different with 40:3. As mentioned above, 34:1 was mainly carbon number, contributed to GBA activity. Thus, this evidence provided that DAG to PC 34:1 significantly contribute to the ceramide and sphingomyelin level.

At this point, this study reveals the effect of missing and adding amino acid contribute to GBA2 isoforms activity as well as possible GBA2 substrates and products with different carbon chain lengths and numbers of double bonds. Moreover, the levels of SM, PC and DAG suggested a degree of interconnectivity between lipid classes in distributing the ceramide released from glucosylceramide by GBA2.

In order to understand the effect of *GBA* mutation to sphingolipid level in human fibroblast cells as well as contribution of *Parkin* mutation to GBA activity? Next result has provided the lipid profile of human fibroblast carrying *GBA* and *Parkin* mutation.

8. Five novel GBA mutations found in PD Thai patient, including 1275C>A (N386K), 1399C>T (P428S), 1309delG, IVS9+3G>C and IVS10-9\_10GT>AG were analyzed by homology modeling. In order to solve the question that do the heterozygous *GBA* mutations cause any decrease in activity and is it enough to affect the GlcCer and Cer levels in fibroblasts? Do other mutations like *Parkin* mutations have an affect on GBA activity in the cell as well? The structure homology modelling analysis showed the missing part of GBA (1309delG), which change V398 to S, followed by stop codon to truncate the protein. Thus, this mutant is likely to lose its ability to hydrolyze glucosylceramide, while GBA (N386K) point mutation might still be active to hydrolyze glucosylceramide.

9. The activity of human fibroblasts carrying *GBA* and *Parkin* were determined. The human fibroblast line carrying *GBA* (1309delG) and *GBA* (IVS11-9, 10 gt>ag) had significantly lower  $\beta$ -glucosidase activity than the control, which suggests that the truncated protein significantly affected the enzyme activity. The HF7 with no mutation detected in the *GBA* or *Parkin* genes also had significantly lower activity than control,

might suggested that HF17 carries a mutation in a gene that has a secondary affect on GBA activity.

10. The effects of *GBA* and *Parkin* mutations on total lipid, total sphingolipid total glycerophospholipid, and total glycerolipid, as well as specific lipid species with different carbon chain lengths and numbers of double bonds were explored. According to enzyme activity, GBA carrying 1309delG was significantly higher than controls in glycerophospholipid and glycerolipid, while no significant difference was seen in total lipid and total sphingolipid in all conditions. All conditions, 1-3% of the total lipids were glycerolipid, 12-15% were sphingolipid and 83-84% were glycerophospholipid.

10.1 The sphingolipid with different carbon chain lengths were identified as GBA substrates and products. According to the heat map, hexosylceramide level (34:1, 42:1 and 42:2) were shown the highest Z-score of GBA mutation (1309delG, HF6), while the corresponding ceramides are also high, so it might reflect that as much as the inability to hydrolyze them. In contrast, GBA mutation (IVS11-9 10 gt>ag, HF14) had lower activity, but did not show the similar changes in the heat map. In addition, ceramide and sphingomyelin levels of all condition were not significantly different, compared to the healthy control. Thus, these results suggested that the glucosylceramides accumulation in the cell might be more relevant by caused *GBA* (1309delG) mutation.

10.2 The sphingolipid with different carbon long chains were identified. Hexosylceramide with 34:1 42:1 and 42:2 contribute to GBA substrate, which show significantly higher than healthy control, which suggested that at least 3 GBA mutation, including 1309delG, IVS11-9, 10 gt>ag, and N386K would

have lost ability to hydrolyzed glucosylceramide. However, the heterozygous and the other allele might be expressed more highly to compensate.

11. Sphingolipid ratio control the direction of sphingolipid connectivity was identified. The highlight sphingolipid with different carbon long chain including 34:1, 42:1 and 42:2 were made for the ratio between ceramide to hexosylceramide as well as sphingolipid to hexosylceramide with 34:1, and 42:1 According to previous result, human fibroblast carrying at least 3 mutations shown the significantly lowest ability to hydrolyzed glucosylceramide to release ceramide with all carbon long chain as well as contribute to the sphingomyelin synthesis to reduce the sphingomyelin level. However, it can't confirm that this evidence significantly affected by *GBA* mutation because of heterozygous active alleles might be expressed, then it acted as the active enzyme as well as it was the reason to give high variation on in this result.

12. In order to see the activity correlated with sphingolipid, the correlation of sphingolipid ratio and its activity was identified. The correlation between sphingolipid ratios and activity was plotted. Healthy control fibroblast lines HF16, HF17 and HF19 and *GBA* mutation fibroblast lines HF6 (1309delG), HF10 (N386), HF11 (IVS2+1g>A) and HF14 (IVS11-9,10 GT>AG) were included. For these samples, the ceramide to hexosylceramide ratios, including carbon chain types 34:1, 42:1 and 42:2 showed a correlation with  $R^2 = 0.4289, 0.811$  and  $0.7764$ , respectively.

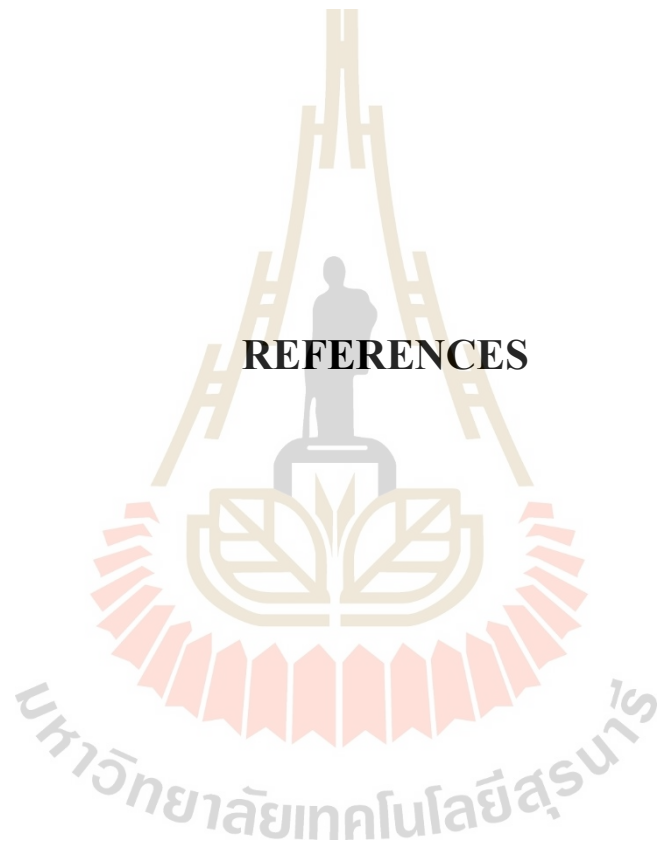
At this point, the study has revealed the relation of sphingolipid profiles with *GBA* and *Parkin* mutation. *GBA* (1309delG) was identified as the main effect to glucosylceramide accumulation in the cell as well as 34:1, 42:1 and 42:2 of hexosylceramide was identified as the carbon chain lengths most affecting, suggesting they might be *GBA* substrates. Therefore, we would like to make a final summary that

the 34:1, 42:1 and 42:2 of carbon long of glucosylceramide, ceramide, sphingomyelin might be responsible to sphingolipid metabolism with 3 sphingolipid species for GBA sphingolipid metabolism in COS-7 cells system as well as *GBA* mutations were contributed to sphingolipid metabolism in human fibroblast cells.

#### Suggestion

1. In order to study *GBA* and *Parkin* mutation affect to sphingolipid profiles, a larger sample size is needed to generate more confident in statistical analysis.
2. Some Parkinson's disease patient fibroblast lines without a known mutation showed an interesting result, in terms of GBA activity, thus trying to find an unknown mutation in this line by genome sequencing is of interest.

## REFERENCES



## REFERENCES

- Abdul-Hammed, M., Breiden, B., Schwarzmann, G., and Sandhoff, K. (2017). Lipids regulate the hydrolysis of membrane bound glucosylceramide by lysosomal  $\beta$ -glucocerebrosidase. **Journal of lipid research**. 58(3): 563-577.
- Adam, M., Ardinger, H., Pagon, R., Wallace, S., Bean, L., Stephens, K., and Amemiya, A. Gaucher Disease--GeneReviews®.
- Aerts, J. M., Kuo, C.-L., Lelieveld, L. T., Boer, D. E., van der Lienden, M. J., Overkleeft, H. S., and Artola, M. (2019). Glycosphingolipids and lysosomal storage disorders as illustrated by gaucher disease. **Current Opinion in Chemical Biology**. 53: 204-215.
- Bartke, N., and Hannun, Y. A. (2009). Bioactive sphingolipids: metabolism and function. **Journal of lipid research**. 50(Supplement): S91-S96.
- Bdira, F. B., Artola, M., Overkleeft, H. S., Ubbink, M., and Aerts, J. M. (2018). Distinguishing the differences in  $\beta$ - glycosylceramidase folds, dynamics, and actions informs therapeutic uses. **Journal of lipid research**. 59(12): 2262-2276.
- Blanksby, S. J., and Mitchell, T. W. (2010). Advances in mass spectrometry for lipidomics. **Annual Review of Analytical Chemistry**. 3: 433-465.

- Boot, R. G., Verhoek, M., Donker-Koopman, W., Strijland, A., van Marle, J., Overkleeft, H. S., and Aerts, J. M. (2007). Identification of the non-lysosomal glucosylceramidase as  $\beta$ -glucosidase 2. **Journal of Biological Chemistry**. 282(2): 1305-1312.
- Breitbart, R. E., Andreadis, A., and Nadal-Ginard, B. (1987). Alternative splicing: a ubiquitous mechanism for the generation of multiple protein isoforms from single genes. **Annual review of biochemistry**. 56(1): 467-495.
- Cairns, J. R. K., and Esen, A. (2010).  $\beta$ -Glucosidases. **Cellular and Molecular Life Sciences**. 67(20): 3389-3405.
- Charoenwattanasatien, R., Pengthaisong, S., Breen, I., Mutoh, R., Sansenya, S., Hua, Y., and Tanaka, H. (2016). Bacterial  $\beta$ -glucosidase reveals the structural and functional basis of genetic defects in human glucocerebrosidase 2 (GBA2). **ACS chemical biology**. 11(7): 1891-1900.
- Fahy, E., Cotter, D., Sud, M., and Subramaniam, S. (2011). Lipid classification, structures and tools. **Biochimica et Biophysica Acta (BBA)-Molecular and Cell Biology of Lipids**. 1811(11): 637-647.
- Ferraz, M. J., Kallemeijn, W. W., Mirzaian, M., Moro, D. H., Marques, A., Wisse, P., and Aerts, J. (2014). Gaucher disease and Fabry disease: new markers and insights in pathophysiology for two distinct glycosphingolipidoses. **Biochimica et Biophysica Acta (BBA)-Molecular and Cell Biology of Lipids**. 1841(5): 811-825.
- Fuller, M., Szer, J., Stark, S., and Fletcher, J. M. (2015). Rapid, single-phase extraction of glucosylsphingosine from plasma: A universal screening and monitoring tool. **Clinica Chimica Acta**. 450: 6-10.

- Hamler, R., Brignol, N., Clark, S. W., Morrison, S., Dungan, L. B., Chang, H. H., and Benjamin, E. R. (2017). Glucosylceramide and glucosylsphingosine quantitation by liquid chromatography-tandem mass spectrometry to enable in vivo preclinical studies of neuronopathic Gaucher disease. **Analytical chemistry**. 89(16): 8288-8295.
- Han, X. (2016). Lipidomics for studying metabolism. **Nature Reviews Endocrinology**. 12(11): 668.
- Han, X., and Gross, R. W. (2003). Global analyses of cellular lipidomes directly from crude extracts of biological samples by ESI mass spectrometry a bridge to lipidomics. **Journal of lipid research**. 44(6): 1071-1079.
- Han, X., Yang, K., and Gross, R. W. (2012). Multi-dimensional mass spectrometry-based shotgun lipidomics and novel strategies for lipidomic analyses. **Mass spectrometry reviews**. 31(1): 134-178.
- Hannun, Y. A., and Obeid, L. M. (2008). Principles of bioactive lipid signalling: lessons from sphingolipids. **Nature reviews Molecular cell biology**. 9(2): 139-150.
- Haugarvoll, K., Johansson, S., Rodriguez, C. E., Boman, H., Haukanes, B. I., Bruland, O., and Telstad, W. (2017). GBA2 mutations cause a Marinesco-Sjogren-like syndrome. **Genetic and Biochemical Studies**. 10(3): 250-269
- Hruska, K. S., LaMarca, M. E., Scott, C. R., and Sidransky, E. (2008). Gaucher disease: mutation and polymorphism spectrum in the glucocerebrosidase gene (GBA). **Human mutation**. 29(5). 567-583.
- Kallemeijn, W. W., Witte, M. D., Voorn-Brouwer, T. M., Walvoort, M. T., Li, K.-Y., Codée, J. D., and Aerts, J. M. (2014). A sensitive gel-based method combining distinct cyclophellitol-based probes for the identification of acid/base residues in

- human retaining  $\beta$ -glucosidases. **Journal of Biological Chemistry**. 289(51): 35351-35362.
- Kishimoto, K. , Urade, R. , Ogawa, T. , and Moriyama, T. (2001) . Nondestructive quantification of neutral lipids by thin-layer chromatography and laser-fluorescent scanning: suitable methods for “lipidome” analysis. **Biochemical and biophysical research communications**. 281(3): 657-662.
- Lombard, V., Golaconda Ramulu, H., Drula, E., Coutinho, P. M., and Henrissat, B. (2014). The carbohydrate- active enzymes database ( CAZy) in 2013. **Nucleic acids research**. 42(D1): D490-D495.
- Lozano, M. n. M. , Hovis, J. S. , Moss III, F. R. , and Boxer, S. G. (2016). Dynamic reorganization and correlation among lipid raft components. **Journal of the American Chemical Society**. 138(31): 9996-10001.
- Maceyka, M. , and Spiegel, S. (2014). Sphingolipid metabolites in inflammatory disease. **Nature**. 510(7503): 58-67.
- Marques, A. R., Aten, J., Ottenhoff, R., van Roomen, C. P., Moro, D. H., Claessen, N., and Mirzaian, M. (2015) . Reducing GBA2 activity ameliorates neuropathology in Niemann-Pick type C mice. **PloS one**. 10(8): 110-121
- Marques, A. R., Mirzaian, M., Akiyama, H., Wisse, P., Ferraz, M. J., Gaspar, P., and Alfonso, P. (2016). Glucosylated cholesterol in mammalian cells and tissues: formation and degradation by multiple cellular  $\beta$ -glucosidases. **Journal of lipid research**. 57(3): 451-463.
- Martin, E. , Schüle, R. , Smets, K. , Rastetter, A. , Boukhris, A. , Loureiro, J. L. , and Wessner, M. (2013) . Loss of function of glucocerebrosidase GBA2 is

- responsible for motor neuron defects in hereditary spastic paraplegia. **The American Journal of Human Genetics**. 92(2): 238-244.
- Mistry, P. K., Liu, J., Sun, L., Chuang, W.-L., Yuen, T., Yang, R., and Keutzer, J. (2014). Glucocerebrosidase 2 gene deletion rescues type 1 Gaucher disease. **Proceedings of the National Academy of Sciences**. 111(13): 4934-4939.
- Ogretmen, B. (2018). Sphingolipid metabolism in cancer signalling and therapy. **Nature Reviews Cancer**. 18(1): 33.
- Ogretmen, B., and Hannun, Y. A. (2004). Biologically active sphingolipids in cancer pathogenesis and treatment. **Nature Reviews Cancer**. 4(8): 604-616.
- Pulkes, T., Choubtum, L., Chitphuk, S., Thakkinstian, A., Pongpakdee, S., Kulkantrakorn, K., and Boonkongchuen, P. (2014). Glucocerebrosidase mutations in Thai patients with Parkinson's disease. **Parkinsonism & related disorders**. 20(9): 986-991.
- Raju, D., Schonauer, S., Hamzeh, H., Flynn, K. C., Bradke, F., vom Dorp, K., and Poetsch, A. (2015). Accumulation of glucosylceramide in the absence of the beta-glucosidase GBA2 alters cytoskeletal dynamics. **PLoS genetics**. 11(3).
- Ramstedt, B., and Slotte, J. P. (1999). Interaction of cholesterol with sphingomyelins and acyl-chain-matched phosphatidylcholines: a comparative study of the effect of the chain length. **Biophysical journal**. 76(2): 908-915.
- Ridley, C. M., Thur, K. E., Shanahan, J., Thillaiappan, N. B., Shen, A., Uhl, K., and Platt, F. M. (2013).  $\beta$ -Glucosidase 2 (GBA2) activity and imino sugar pharmacology. **Journal of Biological Chemistry**. 288(36): 26052-26066.
- Romero, P. R., Zaidi, S., Fang, Y. Y., Uversky, V. N., Radivojac, P., Oldfield, C. J., and Obradovic, Z. (2006). Alternative splicing in concert with protein intrinsic

disorder enables increased functional diversity in multicellular organisms.

**Proceedings of the National Academy of Sciences.** 103(22): 8390-8395.

Sakamoto, W., Coant, N., Canals, D., Obeid, L. M., and Hannun, Y. A. (2018).

Functions of neutral ceramidase in the Golgi apparatus. **Journal of lipid research.** 59(11): 2116-2125.

Schonauer, S., Körschen, H. G., Penno, A., Rennhack, A., Breiden, B., Sandhoff, K.,

and Haberkant, P. (2017). Identification of a feedback loop involving  $\beta$ -glucosidase 2 and its product sphingosine sheds light on the molecular mechanisms in Gaucher disease. **Journal of Biological Chemistry.** 292(15): 6177-6189.

Scotti, M. M., and Swanson, M. S. (2016). RNA mis-splicing in disease. **Nature**

**Reviews Genetics.** (171): 19.

Siebert, M., Sidransky, E., and Westbroek, W. (2014). Glucocerebrosidase is shaking

up the synucleinopathies. **Brain.** 137(5): 1304-1322.

Stratil, A. n., Wagenknecht, D., Van Poucke, M., Kubíčková, S., Bartenschlager,

H., Musilová, P., and Peelman, L. J. (2004). Comparative and genetic analysis of the porcine glucocerebrosidase (GBA) gene. **Comparative**

**Biochemistry and Physiology Part B: Biochemistry and Molecular Biology.** 138(4): 377-383.

Sultana, S., Reichbauer, J., Schüle, R., Mochel, F., Synofzik, M., and van der Spoel, A.

C. (2015). Lack of enzyme activity in GBA2 mutants associated with hereditary spastic paraplegia/cerebellar ataxia (SPG46). **Biochemical and biophysical research communications.** 465(1): 35-40.

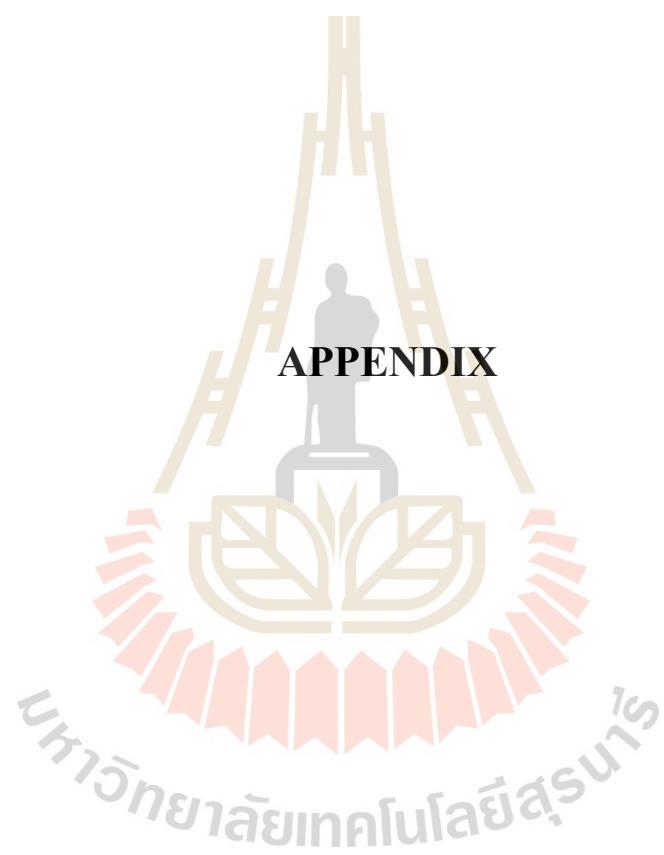
- Taguchi, Y. V., Liu, J., Ruan, J., Pacheco, J., Zhang, X., Abbasi, J., and Chandra, S. S. (2017). Glucosylsphingosine promotes  $\alpha$ -synuclein pathology in mutant GBA-associated Parkinson's disease. **Journal of Neuroscience**. 37(40): 9617-9631.
- Tracey, T. J., Steyn, F. J., Wolvetang, E. J., and Ngo, S. T. (2018). Neuronal lipid metabolism: multiple pathways driving functional outcomes in health and disease. **Frontiers in molecular neuroscience**. 11: 10.
- Van Cauwenberghe, C., Van Broeckhoven, C., and Sleegers, K. (2016). The genetic landscape of Alzheimer disease: clinical implications and perspectives. **Genetics in Medicine**. 18(5): 421-430.
- Vance, J. E., and Vance, D. E. (2008). **Biochemistry of lipids, lipoproteins and membranes**: Elsevier. 20(6): 100-115
- Watson, A. D. (2006). Lipidomics: a global approach to lipid analysis in biological systems. **Journal of lipid research**. 47(10): 2101.
- Woeste, M. A., and Wachten, D. (2017). The enigmatic role of GBA2 in controlling locomotor function. **Frontiers in molecular neuroscience**. 10: 386.
- Xiong, H. Y., Alipanahi, B., Lee, L. J., Bretschneider, H., Merico, D., Yuen, R. K., and Hughes, T. R. (2015). The human splicing code reveals new insights into the genetic determinants of disease. **Science**. 347(6218): 1254806.
- Yamaji, T., Kumagai, K., Tomishige, N., and Hanada, K. (2008). Two sphingolipid transfer proteins, CERT and FAPP2: their roles in sphingolipid metabolism. **IUBMB life**. 60(8): 511-518.
- Yildiz, Y., Hoffmann, P., Vom Dahl, S., Breiden, B., Sandhoff, R., Niederau, C., and Elstein, D. (2013). Functional and genetic characterization of the non-lysosomal

glucosylceramidase 2 as a modifier for Gaucher disease. **Orphanet journal of rare diseases**. 8(1): 151.

Yildiz, Y., Matern, H., Thompson, B., Allegood, J. C., Warren, R. L., Ramirez, D. M., and Russell, D. W. (2006). Mutation of  $\beta$ -glucosidase 2 causes glycolipid storage disease and impaired male fertility. **The Journal of clinical investigation**. 116(11): 2985-2994.

Yoshida, K., Furuya, S., Osuka, S., Mitoma, J., Shinoda, Y., Watanabe, M., and Itoharu, S. (2004). Targeted disruption of the mouse 3-phosphoglycerate dehydrogenase gene causes severe neurodevelopmental defects and results in embryonic lethality. **Journal of Biological Chemistry**. 279(5): 3573-3577.

Zhou, H., Summers, S. A., Birnbaum, M. J., and Pittman, R. N. (1998). Inhibition of Akt kinase by cell-permeable ceramide and its implications for ceramide-induced apoptosis. **Journal of Biological Chemistry**. 273(26): 16568-16575.



**APPENDIX**

มหาวิทยาลัยเทคโนโลยีสุรนารี

## APPENDIX

### ANTIBODY DESIGN AND ANTIBODY OPTIMIZATION

#### 1. Antibody design and homology modeling

Homology modeling of human GBA2 was used to identify antigenic sequences on the protein surface that are conserved in all human GBA2 isoforms. Genscript Corporation provided a list of peptide sequences from the human GBA2 sequence in order of predicted antigenicity. By observing the multiple sequence alignment (Results Figure 4.1) and homology model (Results Figure 4.2), 3 different sequences were selected, including the peptide antigen sequences injected into rabbits to produce the anti-GBA2-1, anti-GBA2-2 and anti-GBA2-3 antibodies, as shown in Table A1.

**Table A1** Antibody sequence for human GBA2 9 isoforms.

Type of antibody	Protein sequence
Anti GBA2-1	KSPEDSRPPKETDC
Anti GBA2-2	CGQLDSPTGQSTPTQ
Anti GBA2-3	CRRNVIPHDIGDPDD

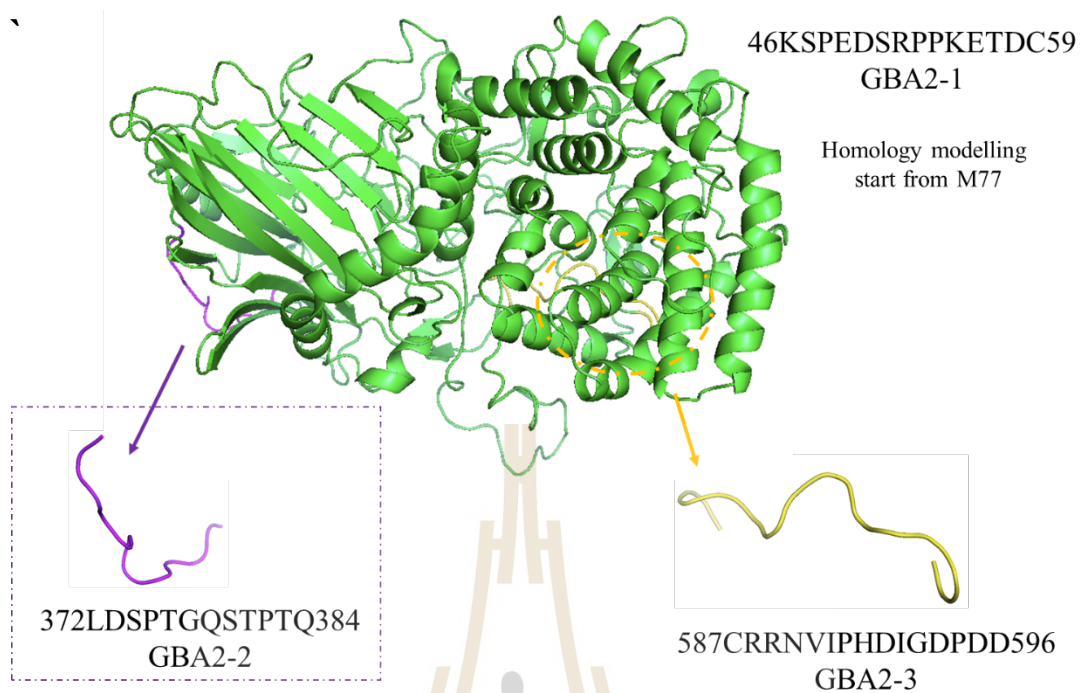


**Figure A1** The homology modeling of human GBA2 to show the position of 3 different antigen peptides in the predicted structure.

## 2. Antibody optimization

Peptide (antigen), pre-immune serum, and antibody solutions were prepared. Firstly, Peptide (antigen), bovine serum albumin (BSA), pre-immune serum, and anti-GBA2 antibody sera were dissolved in sterile water with final concentration 1 mg/mL. The peptide and BSA were diluted to 100, 40, 10, 4 and 1  $\mu\text{g/mL}$ . The anti-GBA2 antibodies were used at dilutions of 1:1000, 1:2000, 1:4000 and 1:8000 from the 1 mg/mL stock and a 1:1000 dilution of pre-immune serum was used. The nitrocellulose was cut and labeled, followed by spotting the peptide and BSA at 1  $\mu\text{L}$  5 times with each dilution. Then, the membranes were dried at room temperature for 15 minutes. Then, the protocol followed the western blotting method as described in 3.5.5 as well as anti-mouse/HRP (horse-radish-peroxidase-

conjugated) secondary antibody was used for anti-GBA2 at a dilution 1:2,000. The result show that the dilution of GBA2 antibody able to detect the lowest concentration of peptide antigen of 10  $\mu\text{g}/\text{mL}$  (50 ng protein in the spot), was the 1:200 dilution. Thus, the antibody dilution used was 1:200 for GBA2-2 and GBA2-3. The results are shown in Figure A2.



## CURRICULUM VITAE

<b>Name</b>	Mr. Peeranat Jatoorathawichot
<b>Date of Birth</b>	July 30, 1993
<b>Place of Birth</b>	Khon kaen
<b>Education</b>	
2016-Present	Master of Science in School of Chemistry, Institute of Science, Suranaree University of Technology, Nakhon Ratchasima
2012-2016	Bachelor of Science in School of Biology, Institute of Science, Suranaree University of Technology, Nakhon Ratchasima (1st class honors).
<b>Awards</b>	
2018	Outstanding Poster Award for the poster Expression of human glucosylceramidase 2 isoforms in COS-7 cells from the 1 <sup>st</sup> International Conference on Healthcare Science and
2019	Outstanding student poster presentation from the 14 <sup>th</sup> International Symposium of The Protein Society of Thailand 22- 23 July 2019, Bangkok, Thailand